EVALUATION OF TORSIONAL LOAD TRANSFER FOR DRILLED SHAFT FOUNDATIONS

Final Report

SPR 304-701

Oregon Department of Transportation

EVALUATION OF TORSIONAL LOAD TRANSFER FOR DRILLED SHAFT FOUNDATIONS

Final Report

SPR 304-701

by
Armin W. Stuedlein, PhD, P.E.
Andre R. Barbosa, PhD
and
Qiang Li

Oregon State University

for

Oregon Department of Transportation
Research Section
555 13th Street NE, Suite 1
Salem OR 97301

and

Federal Highway Administration
400 Seventh Street, SW
Washington, DC 20590-0003

May 2016

Technical Report Documentation Page

1. Report No. FHWA-OR-RD-16-14	2. Government Accession No.	3. Recipient's Catalog No.
4. Title and Subtitle Evaluation of Torsional Load Transfer for Drilled Shaft Foundations		5. Report Date -May 2016- 6. Performing Organization Code
7. Author(s) Armin Stuedlein, PhD, PE (OSU); Andre Barbosa, PhD (OSU), Qiang Li (Student, OSU)		8. Performing Organization Report No.
9. Performing Organization Name and Address Department of Biological and Ecological Engineering Oregon State University 116 Gilmore Hall Corvallis, Oregon 97331		10. Work Unit No. (TRAIS) 11. Contract or Grant No.
12. Sponsoring Agency Name and Address Oregon Dept. of Transportation Research Section and Federal Highway Admin. 555 13th Street NE, Suite 1 400 Seventh Street, SW Salem, OR 97301 Washington, DC 20590-0003		13. Type of Report and Period Covered Technical Report 14. Sponsoring Agency Code

15. Supplementary Notes

16. Abstract: Despite the prevalence of the use of drilled shafts for the support of traffic signal and signs along state highways, relatively little is known about the torsional load transfer between the structure and soil providing its support. A review of literature indicated that just three full-scale torsional loading test series have been conducted, and these did not report the observation of the torsional load transfer. To help address this gap in knowledge, two instrumented test shafts, which were designed to support signal pole type SM3 based on ODOT Standard Drawing TM653, were constructed to evaluate the torsional capacity and load transfer of these shafts at full-scale at the Oregon State University (OSU) Geotechnical Engineering Field Research Site (GEFRS).

Two shafts were constructed: one shaft designated as the torsion test drilled shaft with production base (TDS) was constructed using the dry method, whereas another shaft designated as the torsional drilled shaft with frictionless base (TDSFB) was constructed by placing bentonite chips the bottom of the cavity to create near-zero base shear condition. Monotonic, quasi-static and cyclic loading tests were performed using two hydraulic actuators and a displacement couple. The imposed rotation and corresponding torque was monitored using string-potentiometers and load cells, respectively. Embedded strain gages were installed on both test shafts over five depths to measure shear strains and reveal the load transfer of the drilled shafts in torsion. The torsional load transfer is back-calculated from the instrumentation data and described in detail.

Existing design procedures for predicting torsional capacity of drilled shafts were investigated. The CDOT Design Method and the Florida District 7 Method, both of which can treat layered cohesive and cohesionless soils, were selected to estimate the torsional capacities of the test shafts and compared with the test results. However, these design methods appeared to over- and under-predict the torsional capacity, respectively, indicating the need for the development of improved methods for assessing torsional capacity.

17. Key Words	18. Distribution Statement Copies available from NTIS, and online at http://www.oregon.gov/ODOT/TD/TP_RES/		
19. Security Classification (of this report) Unclassified	20. Security Classification (of this page) Unclassified	21. No. of Pages 159	22. Price

SI* (MODERN METRIC) CONVERSION FACTORS

APPROXIMATE CONVERSIONS TO SI UNITS

Symbol	When You Know	Multiply By	To Find	Symbol
		LENGTH		
in	inches	25.4	millimeters	mm
ft	feet	0.305	meters	m
yd	yards	0.914	meters	m
mi	miles	1.61	kilometers	km
		AREA		
in^2	square inches	645.2	millimeters squared	mm^2
ft^2	square feet	0.093	meters squared	m^2
yd^2	square yards	0.836	meters squared	m^2
ac	acres	0.405	hectares	ha
mi^2	square miles	2.59	kilometers squared	km^2
		VOLUME		
fl oz	fluid ounces	29.57	milliliters	ml
gal	gallons	3.785	liters	L
ft^3	cubic feet	0.028	meters cubed	m^3
yd^3	cubic yards	0.765	meters cubed	m^3
NOTE: Volumes greater than 1000 L shall be shown in m^3.				
		MASS		
oz	ounces	28.35	grams	g
lb	pounds	0.454	kilograms	kg
T	short tons (2000 lb)	0.907	megagrams	Mg
		TEMPERATURE (exact)		
°F	Fahrenheit	(F-32)/1.8	Celsius	°C

APPROXIMATE CONVERSIONS FROM SI UNITS

Symbol	When You Know	Multiply By	To Find	Symbol
		LENGTH		
mm	millimeters	0.039	inches	in
m	meters	3.28	feet	ft
m	meters	1.09	yards	yd
km	kilometers	0.621	miles	mi
		AREA		
mm^2	millimeters squared	0.0016	square inches	in^2
m^2	meters squared	10.764	square feet	ft^2
m^2	meters squared	1.196	square yards	yd^2
ha	hectares	2.47	acres	ac
km^2	kilometers squared	0.386	square miles	mi^2
		VOLUME		
ml	milliliters	0.034	fluid ounces	fl oz
L	liters	0.264	gallons	gal
m^3	meters cubed	35.315	cubic feet	ft^3
m^3	meters cubed	1.308	cubic yards	yd^3
		MASS		
g	grams	0.035	ounces	oz
kg	kilograms	2.205	pounds	lb
Mg	megagrams	1.102	short tons (2000 lb)	T
		TEMPERATURE (exact)		
°C	Celsius	1.8C+32	Fahrenheit	°F

*SI is the symbol for the International System of Measurement

ACKNOWLEDGEMENTS

The research team would like to extend thanks to the efforts of numerous individuals and organizations. This research was funded by Grant SPR 304-701 through the Oregon Department of Transportation. PLI Systems, Inc., of Hillsboro, OR, donated materials, equipment and labor to construct the test shafts. This support is greatly appreciated. The properties of fresh concrete were measured by David Rodriguez. James Batti provided technical assistance with data acquisition. Logistical support was provided by Jeff Gent. Thanks go to Scott Ashford, Dean of the College of Engineering, for lending use of the hydraulic actuators and string-potentiometers. The research team is grateful to the in-depth technical review and comments on this research project from Scott Jollo and Jan Six of the Oregon Department of Transportation. The researchers also wish to thank the students from Oregon State University: Tygh Gianella, Andrew Strahler, John Martin, Jacky Chen, and Drew Nielson for helping with the fabrication and instrumentation of the reinforcement cages.

DISCLAIMER

This document is disseminated under the sponsorship of the Oregon Department of Transportation and the United States Department of Transportation in the interest of information exchange. The State of Oregon and the United States Government assume no liability of its contents or use thereof.

The contents of this report reflect the view of the authors who are solely responsible for the facts and accuracy of the material presented. The contents do not necessarily reflect the official views of the Oregon Department of Transportation or the United States Department of Transportation.

The State of Oregon and the United States Government do not endorse products of manufacturers. Trademarks or manufacturers' names appear herein only because they are considered essential to the object of this document.

This report does not constitute a standard, specification, or regulation.

EXECUTIVE SUMMARY

Despite the prevalence of the use of drilled shafts for the support of traffic signal and signs along state highways, relatively little is known about the torsional load transfer between the structure and soil providing its support. A review of literature indicated that just three full-scale torsional loading test series have been conducted, and these did not report the observation of the torsional load transfer. To help address this gap in knowledge, two instrumented test shafts, which were designed to support signal pole type SM3 based on ODOT Standard Drawing TM653, were constructed to evaluate the torsional capacity and load transfer of these shafts at full-scale at the Oregon State University (OSU) Geotechnical Engineering Field Research Site (GEFRS).

Two shafts were constructed: one shaft designated as the torsion test drilled shaft with production base (TDS) was constructed using the dry method, whereas another shaft designated as the torsional drilled shaft with frictionless base (TDSFB) was constructed by placing bentonite chips the bottom of the cavity to create near-zero base shear condition. Monotonic, quasi-static and cyclic loading tests were performed using two hydraulic actuators and a displacement couple. The imposed rotation and corresponding torque was monitored using string-potentiometers and load cells, respectively. Embedded strain gages were installed on both test shafts over five depths to measure shear strains and reveal the load transfer of the drilled shafts in torsion. The torsional load transfer is back-calculated from the instrumentation data and described in detail.

Existing design procedures for predicting torsional capacity of drilled shafts were investigated. The CDOT Design Method and the Florida District 7 Method, both of which can treat layered cohesive and cohesionless soils, were selected to estimate the torsional capacities of the test shafts and compared with the test results. However, these design methods appeared to over- and under-predict the torsional capacity, respectively, indicating the need for the development of improved methods for assessing torsional capacity.

TABLE OF CONTENTS

LIST OF TABLES

LIST OF FIGURES

1.0 INTRODUCTION

Drilled shafts offer an excellent alternative for transferring superstructure loads to the soil and/or rock stratigraphy present below the ground surface, and are commonly used to support mast arm traffic sign and signal poles. The design of these drilled shafts must provide sufficient capacity to resist the maximum anticipated loads, including lateral and torsional loads, the latter of which generally results from wind gust loading or seismic loading on curved bridges. For example, wind storms impacted the coasts of Oregon and Washington in 2007, and produced a maximum recorded wind gust of 237 km/h *(Reiter 2008)*.

Despite the prevalent usage of drilled shafts to resist the anticipated loads, the understanding of the actual torsional resistance provided by drilled shafts is not well established. For example, the AASHTO (2001) Standard Specifications for Structural Supports for Highway Signs, Luminaires, and Traffic Signals requires that drilled shafts be designed to provide adequate resistance for torsional loads without providing specific design guidance for computing torsional resistance or allowable displacements (rotation). In other words, there is no accepted national standard for the sizing of drilled shafts to resist the design torsional load. This report describes research conducted to help understand the transfer of torsional loads to soil along the shaft-soil interface.

1.1 BACKGROUND

Broms and Silberman *(Broms and Silberman 1964)* performed various loading tests, including torsional loading, on model piles in cohesionless soils; they concluded torsional resistance was somewhat greater than that in uplift loading, and somewhat smaller than that in compressive loading. O'Neill *(O'Neill 1964)*, Poulos *(Poulos 1975)*, Randolph *(Randolph 1981)*, and Chow *(Chow 1985)* each present solutions to estimate the torque-twist relationship of deep foundations. However, these approaches rely on linear-elastic, homogenous soil conditions, and are not appropriate to model soils approaching the strength limit, where soil exhibits significant non-linearity. Tawfiq *(Tawfiq 2000)* reported the first and what may be the only full-scale torsional loading tests on drilled shafts in sands, and produced an analytical model that has not been verified. Separately, the Florida and Colorado DOTs have independently produced simplified approaches to estimate the ultimate torsional resistance of deep foundations under torsional loading, however, these approaches do not provide any guidance on the amount of displacement that may be anticipated upon reaching the strength limit *(Nusairat et al. 2004)*. Additionally, no field measurements have been reported to-date that address the contribution of base shear resistance at the bottom of the shaft to the total torsional resistance; owing to the large diameter of the drilled shafts supporting traffic signs and signals, base shear could provide a significant amount of torsional resistance.

1.2 OBJECTIVES OF THIS STUDY

The objectives of this research are to gain an understanding of the load transfer of axially-loaded drilled shafts in torsion and to evaluate existing methods used to design drilled shaft for torsional loading. Instrumented test shafts were constructed in order to evaluate the behavior of typical

drilled shafts with and without a “frictionless base” at the Oregon State University (OSU) Geotechnical Engineering Field Research Site (GEFRS). The torsional capacity and load transfer of these shafts were evaluated at full-scale. The results of this research were compared to the capacities calculated using existing methods. Recommendations are proposed regarding the appropriate use of design formulas to best estimate torsional resistance and rotation displacement behavior based on the test results.

1.3 ORGANIZATION OF THIS REPORT

This report documents a full-scale torsional loading test conducted at the field research site at Oregon State University. The document is divided into five (5) chapters.

Chapter 2 provides a literature review that describes previous studies on drilled shaft response in torsion. The discussion focuses on the available torsional loading tests on drilled shafts and analytical methods for estimating torsional capacity.

Chapter 3 presents the geotechnical explorations, including cone penetration tests (CPTs), standard penetration test (SPTs), and laboratory soil tests to establish the relevant soil properties.

Chapter 4 details the test shaft design, fabrication and instrumentation of the steel reinforcing cages, and the construction of the test shafts.

Chapter 5 presents the approaches used for processing the recorded data, and presents the torsional response of the test shafts under quasi-static torsional loading and cyclic loading. Several design methods were employed to estimate the torsional capacities for both shafts and were compared with the test results to help inform policy governing the design of traffic structures supported on drilled shafts in the State of Oregon.

2.0 LITERATURE REVIEW

2.1 OVERVIEW

This chapter presents a literature review of previous studies on the torsional response of drilled shafts. The availability of torsional loading test data was determined to be relatively limited. As described below in Section 2.2, the available torsional loading tests are categorized into three main types, including those on: (1) small-scale model piles and shafts at 1g, (2) small-scale, multi-g centrifuge shafts, and (3) full-scale shafts. Section 2.3 presents the existing analytical methods for estimating torsional capacity. The literature review concludes with a summary of the review, including the identification of areas where information available in the literature is limited.

2.2 TORSIONAL LOADING TESTS REPORTED IN THE LITERATURE

2.2.1 Torsional Loading Tests on Small-Size Model Piles and Drilled Shafts

Poulos *(Poulos 1975)* performed a series of torsional loading tests on four solid aluminum piles driven in Kaolin clay. The diameter and length of each pile were 25.4 mm and 502 mm, 25.4 mm and 254 mm, 19 mm and 527 mm, and 19 mm and 298 mm (corresponding to 1.0 in and 19.75 in, 1.0 in and 10 in, 0.75 in and 20.75 in, and 0.75 in and 11.75, respectively). All piles were driven into the soil to full embedment. The rotation of the test piles and applied torque were monitored. Relationship between the applied torque and rotation from test are shown as solid curves in Figure 2.1. Although all of the piles were rotated 2° (0.035 radians), Poulos *(Poulos 1975)* reported test results for smaller rotations. As shown in Figure 2.1, no definitive peak was observed for the torque-rotation curves.

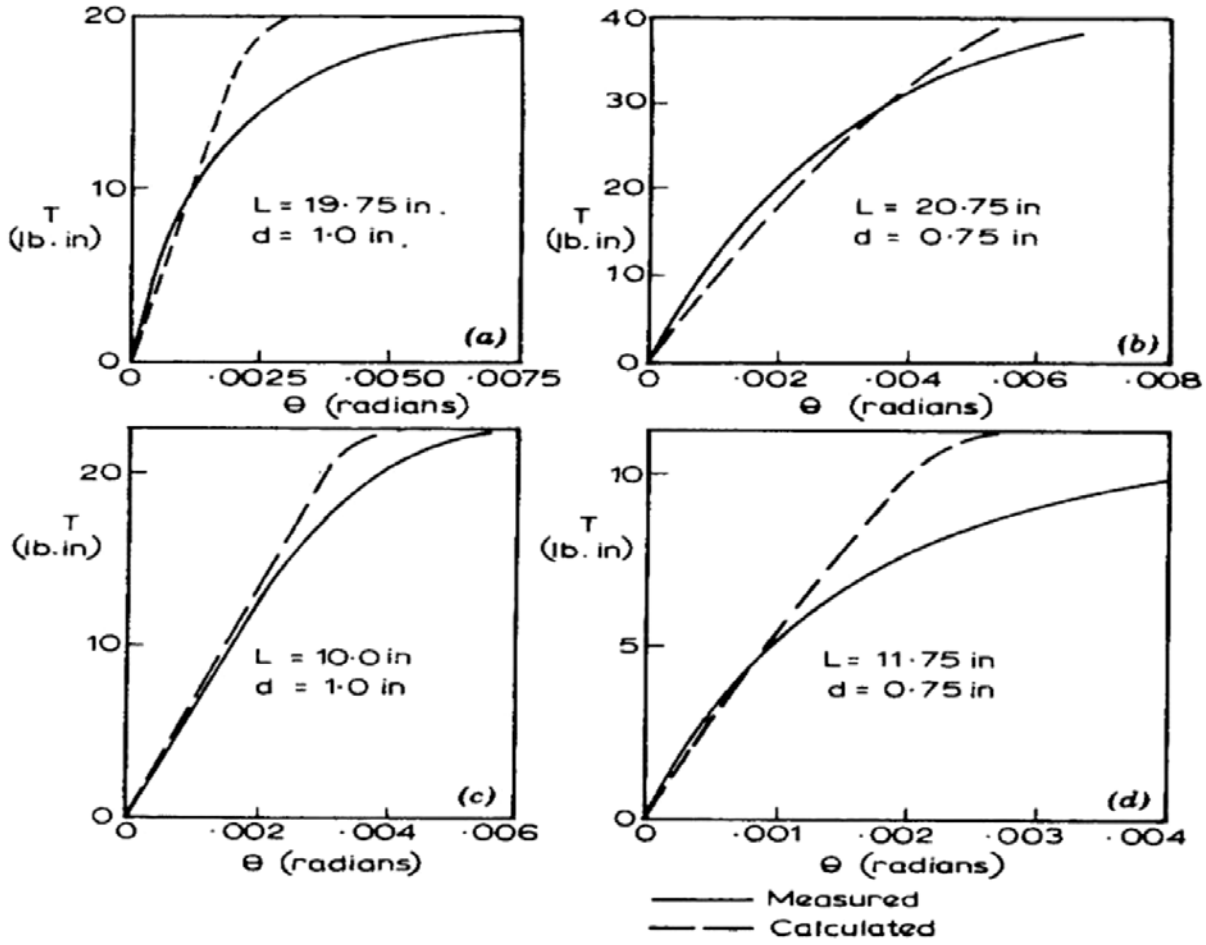

Figure 2.1: Relationship between torque and rotation *(Poulos 1975).* Note: 0.005 radians equals 0.29 degrees.

Dutt *(Dutt 1976)* and Dutt and O'Neill *(Dutt and O'Neill 1983)* performed torsional loading tests using two circular aluminum piles of 48 mm (1.9 in) external diameter and 2.5 mm (0.1 in) wall thickness and two square piles of 51 mm (2.0 in) outside dimensions and 3.2 mm (0.125 in) wall thickness. The total length of each pile was 1.7 m (5.5 ft) with 0.15 m (6 in) above ground surface, as shown in Figure 2.2. Owing to the focus on drilled shafts in this report, only the results of the test on the circular pile are summarized. As shown in Figure 2.3, one circular and square pile was installed by placing the air-dried sand around the piles. Both loose and dense sand conditions were considered. After the torsional loading tests on the model piles were concluded, the same model piles were removed and then driven at the places as shown in Figure 2.2, and torque applied so as to assess the differences in the torque-rotation response due to the construction method.

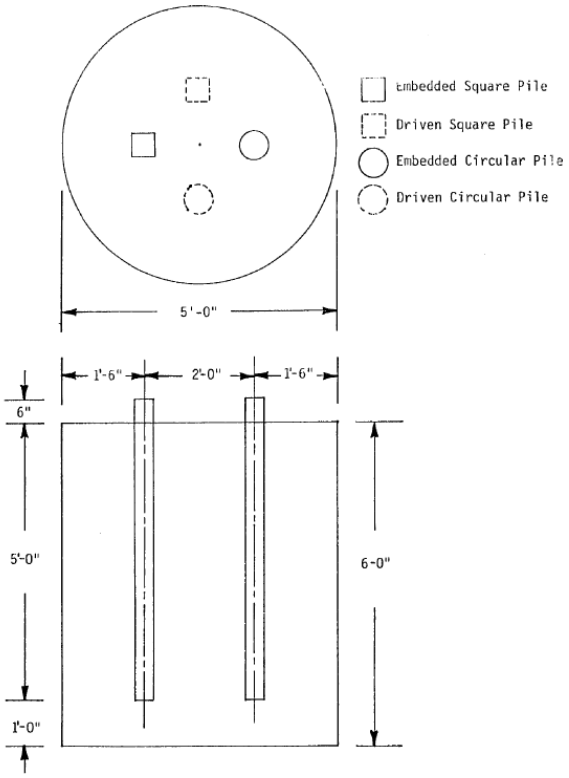

Figure 2.2: Layout of test piles *(Dutt 1976)*

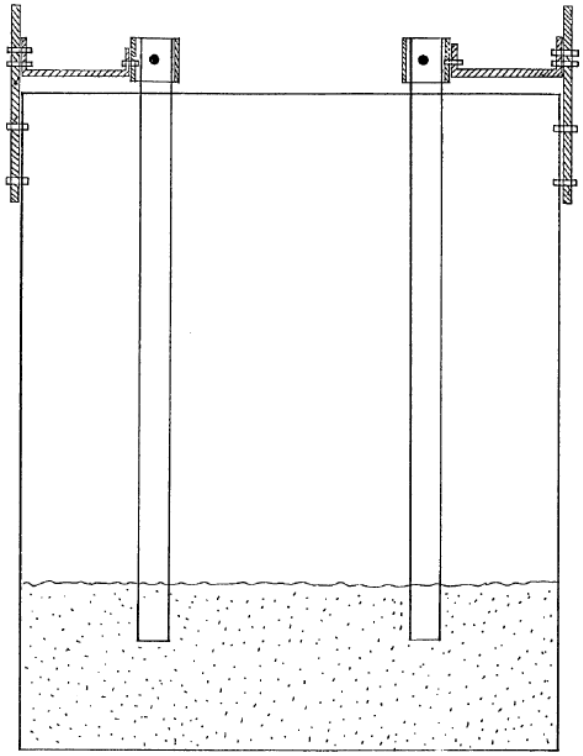

Figure 2.3: Installation of the first two piles *(Dutt 1976)*

Figure 2.4 and Table 2.1 summarize the physical characteristics of the sand used. Resistance strain gages were installed at four different elevations of the circular pile to measure the shear strains. However, valid data was only obtained from the pile that was embedded (as opposed to driven) in the dense sand. The relationship between torque and pile head twist (Figure 2.5) indicated that: (1) an increase of approximately four-fold in relative density from the loose to the dense state led to a less than a two-fold increase in the apparent pile head torque for the circular pile at failure, and (2) the torsional resistance for the driven pile was slightly larger than that for the embedded condition, which was due to the vibration-induced densification caused by driving. The torque distribution for circular pile embedded in dense sand is depicted in Figure 2.6. It indicates that the torsional resistance observed at a depth equal to 80 percent of its embedded length (~ 10 lb-in) was about 6 percent of the total available torsional resistance (~ 170 lb-in) at the rotation of 0.008 radians. It can be concluded that the torsional resistance offered by the base of the pile was insignificant, if not zero. Relationship between the torsion transfer and twist at different depths, as shown in Figure 2.7, were computed for circular pile embedded in dense sand. From this figure, the apparent ultimate torque transferred to the soil increased with depth, indicating the torque transferred to the soil is a function of the effective stresses.

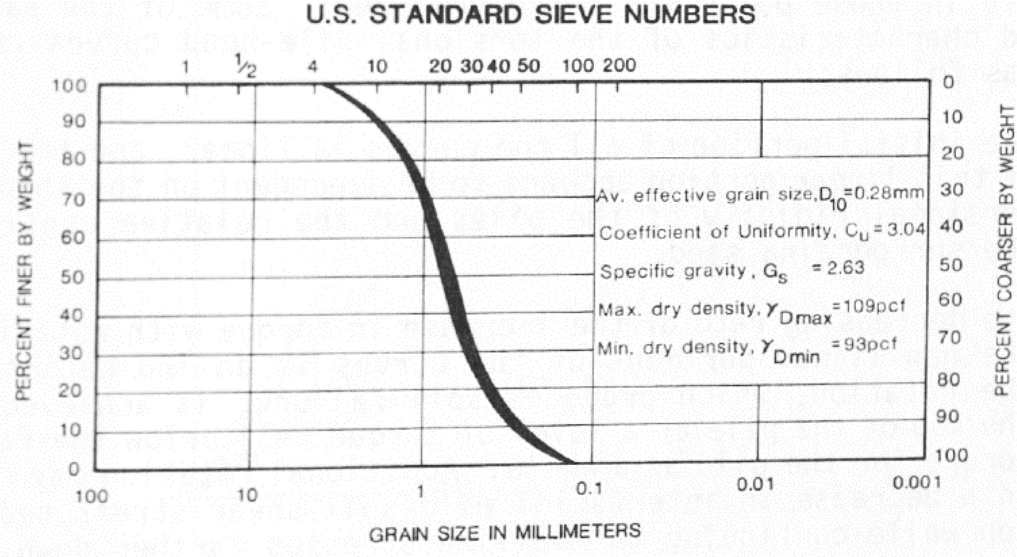

Figure 2.4: Physical properties of sands *(Dutt and O'Neill 1983)*

Table 2.1: Strength properties of test sands *(Dutt and O'Neill 1983)*

TRIAXIAL TEST		**DIRECT SHEAR TEST (Soil-Soil)**		**Direct Shear Test (Soil-Soft Aluminum)**	
Dry Density γ_D, pcf	Friction Angle Φ, Degrees	Dry Density γ_D, pcf	Friction Angle Φ, Degrees	Dry Density γ_D, pcf	Angle of Wall Friction Φ, Degrees
98.2	39.5	96.3	37.2	96.0	23.6
106.8	42.5	107.0	40.3	107.0	26.3

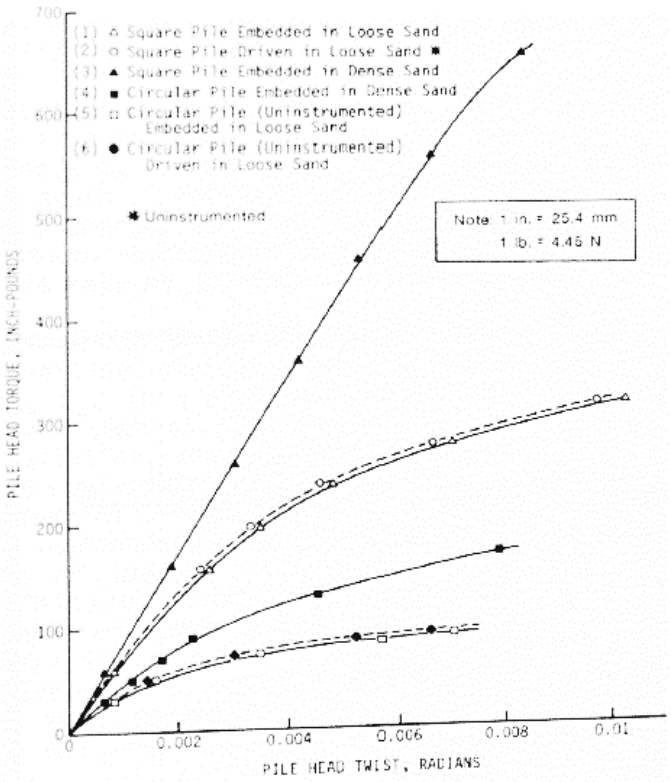

Figure 2.5: Pile-head torque-twist curves *(Dutt and O'Neill 1983)*

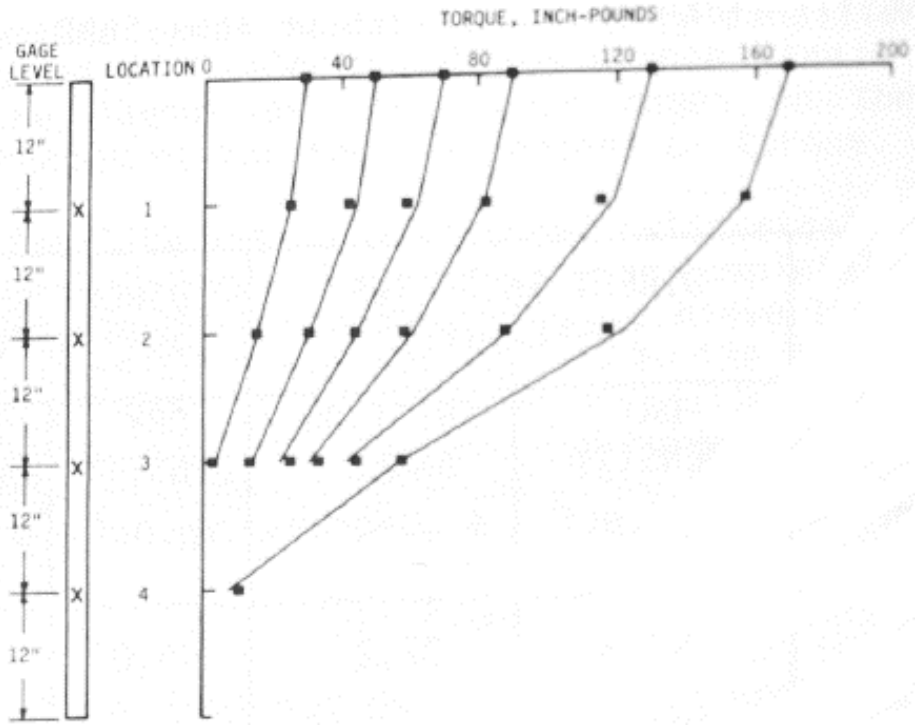

Figure 2.6: Torque distribution for circular pile embedded in dense sands *(Dutt and O'Neill 1983)*

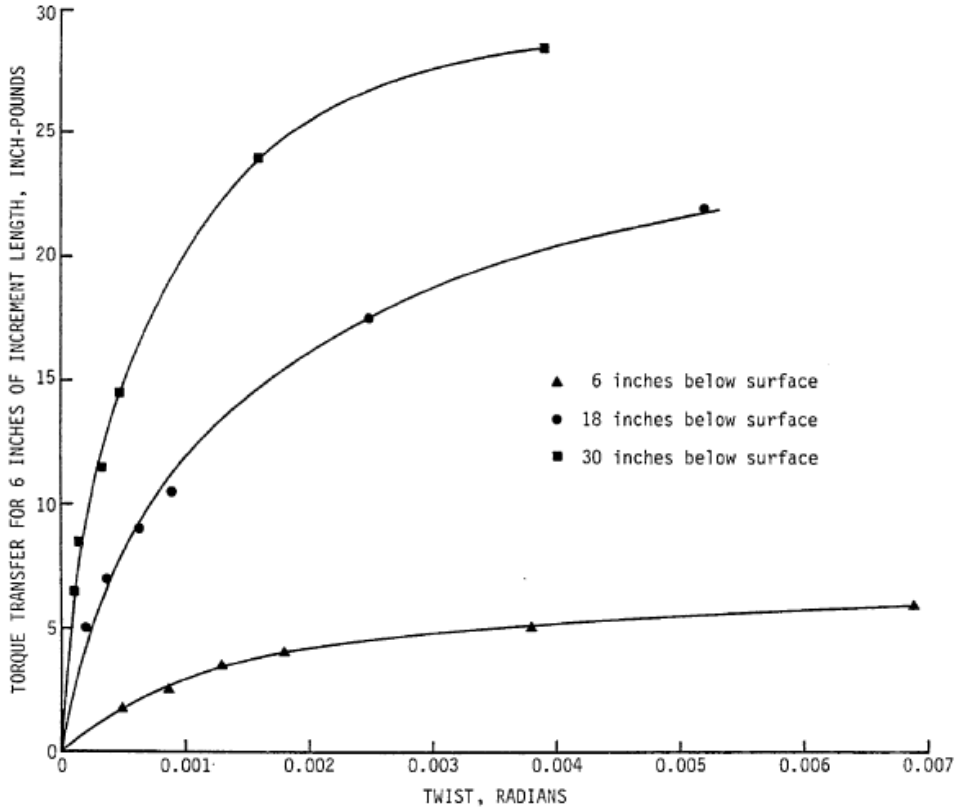

Figure 2.7: Shear stress-strain curves at different depth for circular pile embedded in dense sands *(Dutt and O'Neill 1983)*

Randolph *(Randolph 1983)* described torsional loading tests on a steel pile of 10.6 mm (0.42 in) diameter and a polypropylene pile of 11.2 mm (0.44 in) diameter jacked 300 mm (11.8 in) into normally consolidated Kaolin clay to study the effect of the flexibility of a pile on its performance under monotonic and cyclic loading. The shear modulus of the polypropylene pile was between 0.30 and 0.44 GPa (44 to 64 ksi), whereas the shear modulus of the steel pile was about 77 GPa (11×103 ksi). To achieve a consistent surface texture for the different piles, both piles were coated with thin layer of araldite (an adhesive) and fine sand. Monotonic loading was applied on the piles followed by cyclic loading. Cyclic loading tests were performed between 2 and 50% (point A in Figure 2.8a) and between 2 and 63% (point B in Figure 2.8a) of the peak capacity for the steel pile. For the polypropylene pile, the cyclic loading tests were conducted between 3 and 53 (point A in Figure 2.8b), 3 and 73% (point B in Figure 2.8b), and 3 and 93% (point C in Figure 2.8b) of the peak capacity.

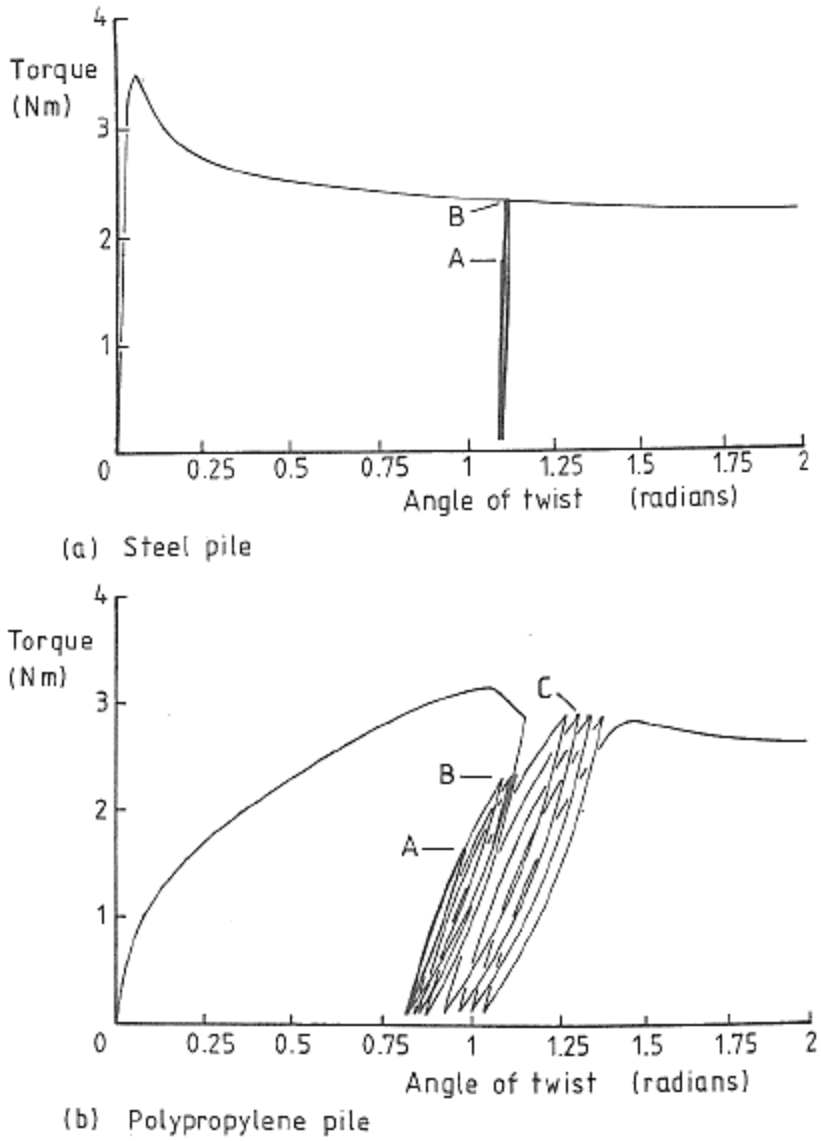

Figure 2.8: Torque-twist relationship for (a) steel pile and (b) polypropylene pile *(Randolph 1983)*

The torque-twist relationships for both test piles are shown in Figure 2.8. The steel pile, which had higher stiffness, reached its peak at the rotation of about 0.05 radians (3°). However, the torsional response was softer for the polypropylene pile, which achieved its peak value at the rotation of about 1.05 radians (60°). A reduction in torsional resistance was observed beyond the peak capacity. During the cyclic loading, no obvious degradation of torsional resistance was observed for the steel pile. For the polypropylene pile, the initial stiffness seemed constant during the cyclic loading; and permanent rotation was developed during every loading cycle.

Tawfiq *(Tawfiq 2000)* used a 1.2 m (4 ft) diameter and 1.5 m (5 ft) deep steel chamber, as shown in Figure 2.9, to perform torsion tests for a small-scale shaft model in sand. The shaft, which was made of plain concrete, was 508 mm (20 in) long with a diameter of 102 mm (4 in). The torque was applied using a loading wheel and two 20 gallon buckets that were filled with water at a

constant flow rate to achieve a constant rate of loading. Two sets of loading tests were conducted: the first consisted of a set of tests that allowed the development of both toe and shaft resistance, whereas the second set of tests was conducted to evaluate base and shaft resistance separately. The toe resistance was eliminated by placing two greased metal plates at the shaft bottom; and the side friction was eliminated by enlarging the borehole so that the shaft surface was separated from the surrounding soil. As shown in Figure 2.10, the tests by Tawfiq *(Tawfiq 2000)* indicated that the shaft resistance comprised about 91 percent of the total available torsional resistance (~27 ft-lbs or 0.04 kN-m) at approximately two radians (approximately 115 degrees). On the other hand, the base resistance was not observed to be larger than 5 ft-lbs (0.007 kN-m) when evaluated alone, and about 2.5 to 3 ft-lbs (0.0034 to 0.004 kN-m) when evaluated with shaft resistance.

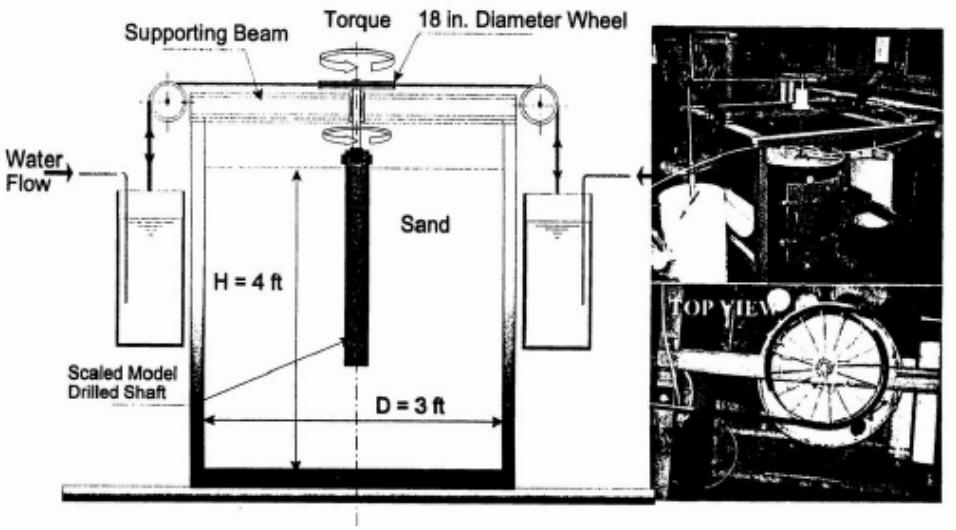

Figure 2.9: Scaled model torsional testing apparatus *(Tawfiq 2000)*

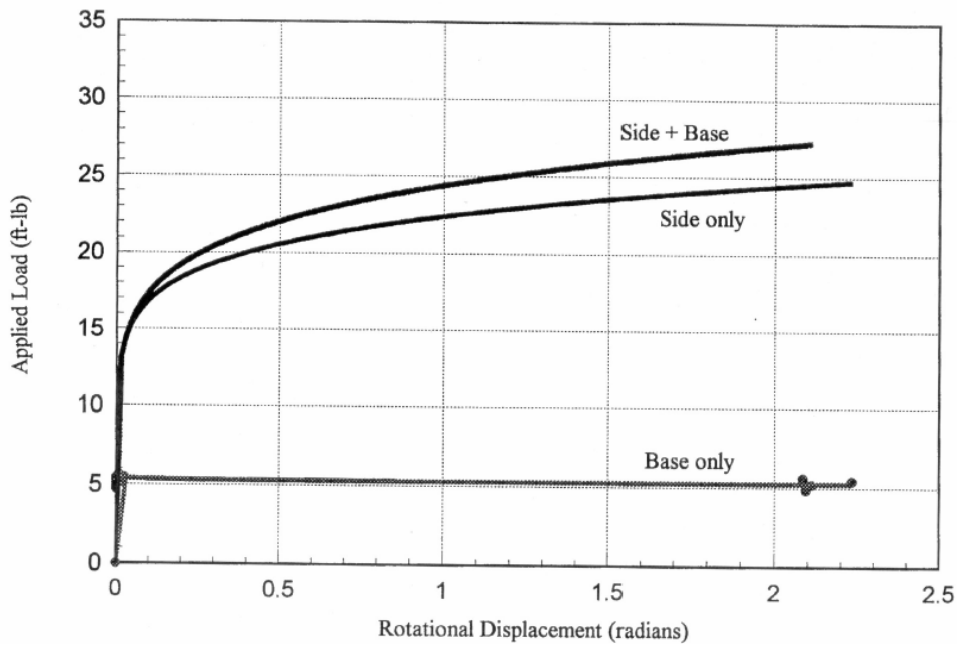

Figure 2.10: Relationship between torque and rotation *(Tawfiq 2000)*

2.2.2 Torsional Loading Tests on Centrifuge Model Piles and Shafts

Bizaliele *(Bizaliele 1992)* conducted static and cyclic torsion tests on aluminum model piles of 21 mm (0.83 in) diameter, 1 mm (0.04 in) wall thickness, and 340 mm (13.4 in) embedded length in sands. The total length of the model pile was 380 mm (15 in). With the chosen acceleration level of 50g, the model piles simulated prototype piles of 1.05 m (41 in) diameter and 17.0 m (56 ft) embedded length. Strain gages were mounted at 45° to the axis of the pile at five levels. The applied load and resulting rotation was measured using a load cell and a linear variable displacement transducer, respectively. The sand used in this test was uniformly-graded with an effective grain size D10 of 0.12 mm and angle of internal friction of 38°. The maximum and minimum dry density was 1.69 and 1.42 g/cm3, respectively. Figure 2.11 shows the centrifuge model setup. The static pile head torque-twist behavior is depicted in Figure 2.12. A linear response was observed for applied torque up to 8 N-m (6 lb-ft); the response transitioned to nonlinear for greater torsion. The maximum torque was approximately 28 N-m (24 lb-ft) at approximately 0.07 radians of pile head twist, followed by softening. The shaft resistance at each level was calculated using the measured shear strain. Figure 2.13 shows the magnitude of torsional shaft resistance at different depths (n.b., L = depth and r = shaft radius) as a function of the number of cycles. Results indicated that a small change in shaft resistance was observed for the first 10 cycles. After that, little variation of the shaft resistance with additional cycling was observed.

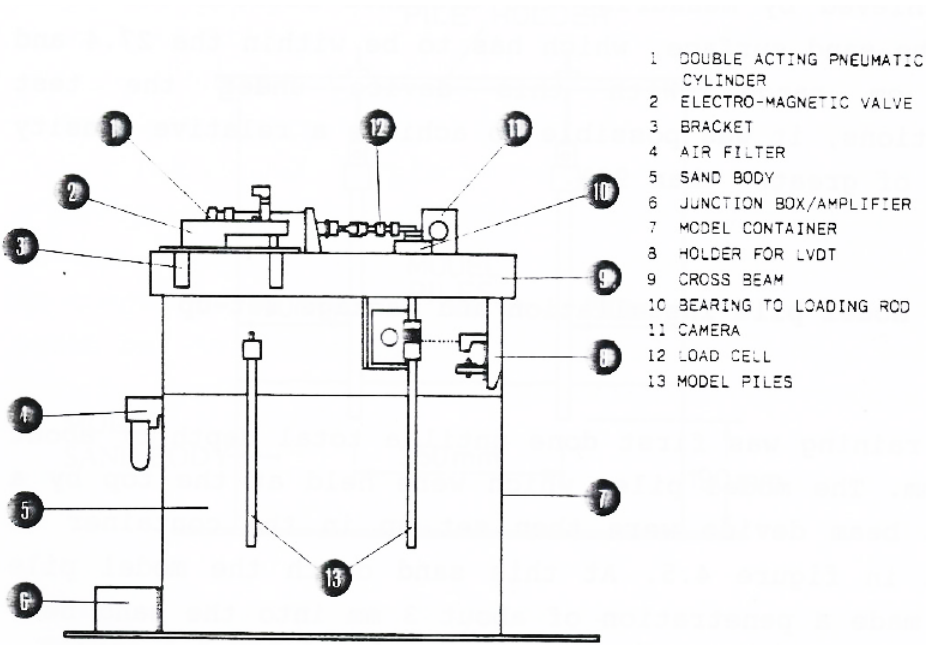

Figure 2.11: Centrifuge model setup (Bizaliele 1992)

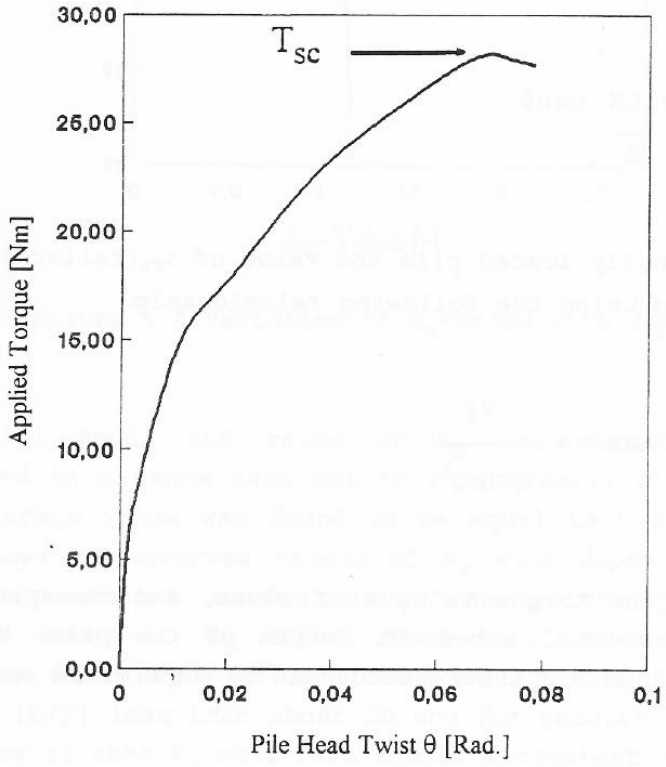

Figure 2.12: Static pile head torque-twist behavior in model scale *(Bizaliele 1992)*

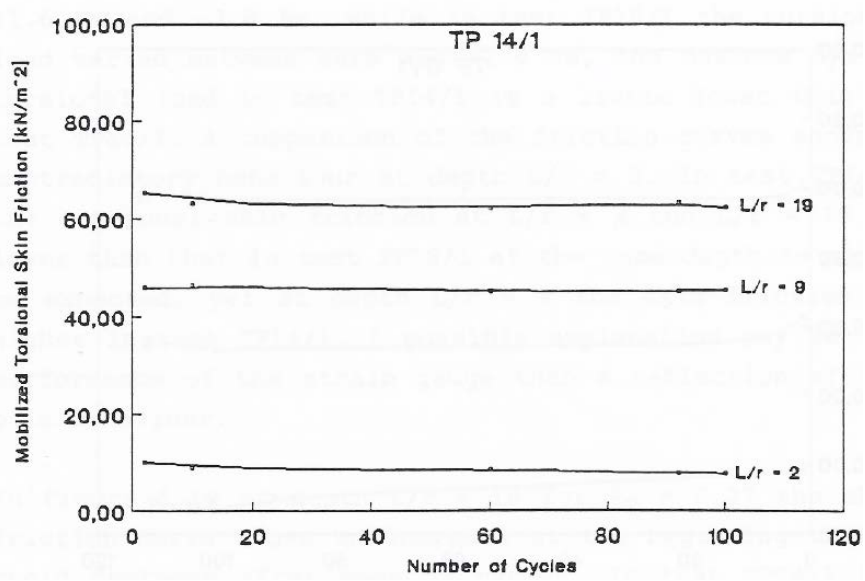

Figure 2.13: A typical distribution of torsional skin friction at different depth as a function of the number of cycles *(Bizaliele 1992)*

Laue and Sonntag *(Laue and Sonntag 1998)* performed torsion tests on hollow aluminum model piles with a diameter of 15 mm (0.6 in) and a length of 170 mm (6.7 in) in sand. The acceleration level was 100g, and the model piles represent prototype piles of 1.5 m (5 ft) diameter and 17.0 m (56 ft) length. Two types of sand in a dense state were used: Normsand (angle of internal friction = 38°) and fine Fontainebleau sand (angle of internal friction = 37°). The gradation of the test sands is shown in Figure 2.14.

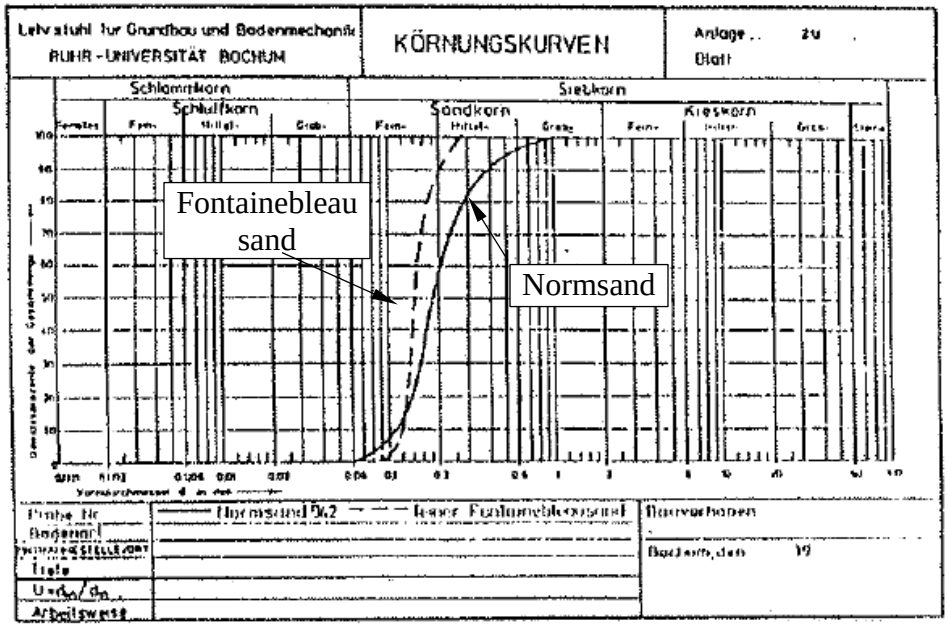

Figure 2.14: Gradation of the Normsand and fine Fontainebleau sand *(Laue and Sonntag 1998)*

Figure 2.15 shows the torque-rotation response under different soil-shaft interface and soil conditions as summarized in Table 2.2. The torque-rotation response of smooth-shaft TP 2.1 was consistent with a hyperbolic relationship, whereas the rough-shaft TP 3.2 exhibited a near-linear perfectly-plastic response; neither pile exhibited post-peak softening. The torque-rotation response of the smooth-shaft pile TP 6.1 was also consistent with a hyperbolic curve, requiring significant rotation to achieve the peak resistance. However, the rough-shaft TP 6.2 achieved a peak torsional load at approximately 1° of rotation, as a result of the rough interface being modeled. The results show that the relative value of roughness and gradation influenced the torsional resistance of pile. Tests with combined axial and torsional loads were performed and the results depicted in Figure 2.16. It shows that the applied torque increased without any rotation of piles at the beginning of the test. Due to the limitation of the loading system, the maximum torsional resistance was not obtained for the rough pile in Normsand under 500 N axial loading. The existing axial loads increased the torsional capacity for the smooth pile in Normsand from about 1.8 N-m (1.3 lb-ft) to 2.8 N-m (2.1 lb-ft). A cyclic loading test was also performed. Figure 2.17 shows the results of the first four cycles; the initial stiffness and post-yield slope for each loading cycle were quite similar.

Table 2.2: Summary of test conditions evaluated by Laue and Sonntag *(Laue and Sonntag 1998)*

Test Designation	Shaft Interface Condition	Soil Evaluated
TP 2.1	Smooth	Normsand
TP 3.2	Rough	Normsand
TP 6.1	Smooth	Fine Fontainebleau sand
TP 6.2	Rough	Fine Fontainebleau sand

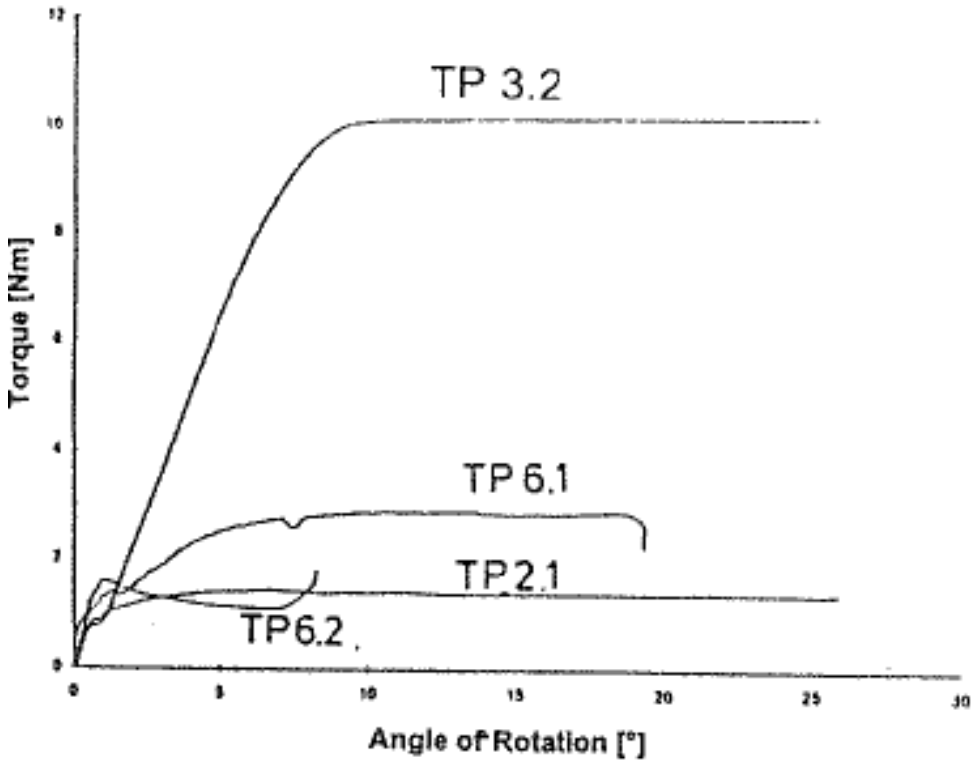

Figure 2.15: Comparison on the torque-rotation response *(Laue and Sonntag 1998)*

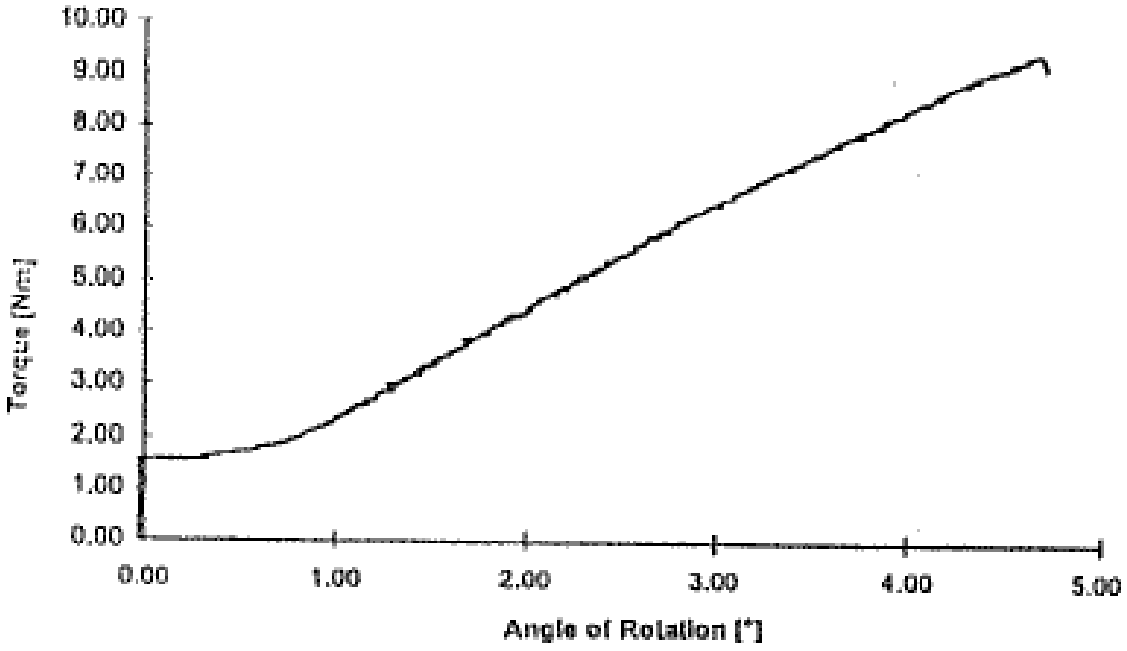

(a)

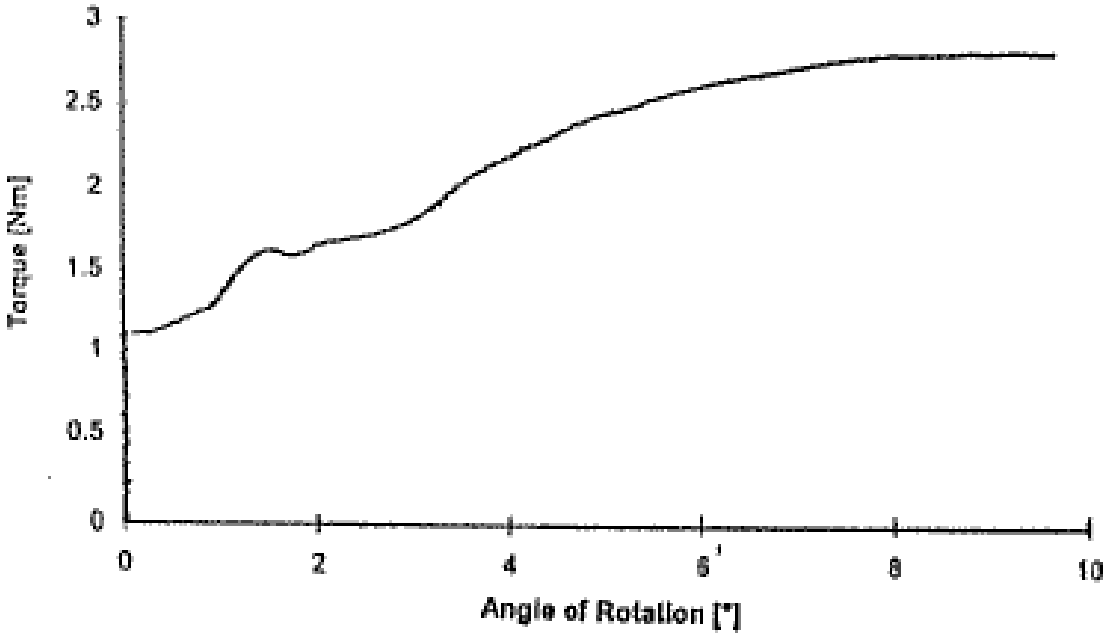

(b)

Figure 2.16: Torque vs. rotation response of (a) rough pile in Normsand with an axial load of 500 N and (b) smooth pile in Normsand with an axial load of 100 N *(Laue and Sonntag 1998)*

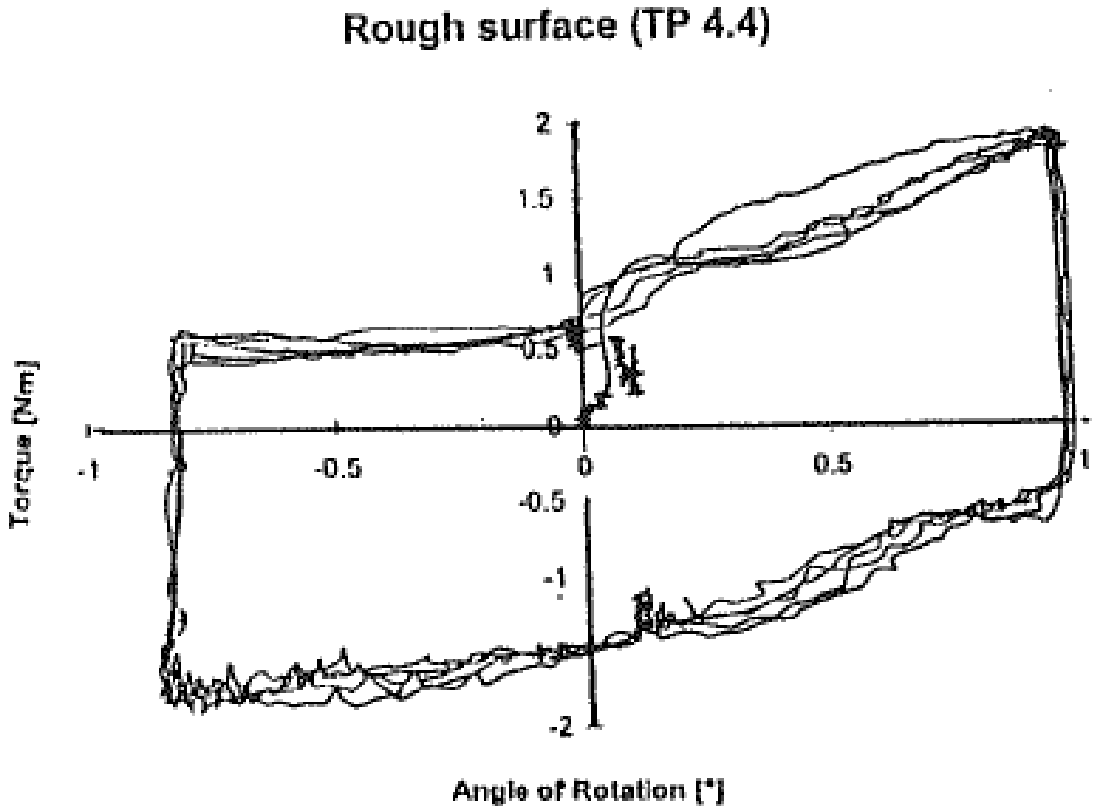

Figure 2.17:Pile under cyclic torsional loading *(Laue and Sonntag 1998)*

A number of centrifuge tests on high mast sign/signal structures (mast arm, pole, and drilled shaft) were conducted in University of Florida to determine the optimum depth of drilled shafts subjected to combined torsion and lateral loads *(McVay et al. 2003, McVay and Hu 2003, and Hu 2003)*. The prototype shaft diameter was 1.5 m (5 ft), and the prototype embedment length ranged from 4.6 m (15 ft) to 10.7 m (35 ft). The shafts were constructed in dry and saturated silica-quartz sand from Edgar, FL, compacted to loose, medium dense, and dense conditions. To investigate the effect of various construction methods, steel casings and wet methods, using bentonite slurry and KB polymer slurry produced by KB Technologies Ltd. (http://www.kbtech.com), were evaluated. Table 2.3 summarizes the centrifuge tests, whereas Figure 2.18 shows the centrifuge test setup.

Table 2.3: Summary of the centrifuge tests conducted in University of Florida

	McVay et al. ***(McVay et al. 2003)***	**McVay and Hu** ***(McVay and Hu 2003)***	**Hu** ***(Hu 2003)***
Construction Method	Steel casings and wet methods using bentonite slurry	Wet methods using polymer slurry	Wet methods using bentonite and polymer slurry
Soil state with relative density	Loose (29%), medium dense (51%) and dense (64%)	Loose (34%) and dense (69%)	Loose (34%) and dense (69%)
Prototype embedment length m (ft)	4.6, 7.6, and 10.7 (15, 25, and 35)	7.6 and 10.7 (25 and 35)	7.6 and 10.7 (25 and 35)

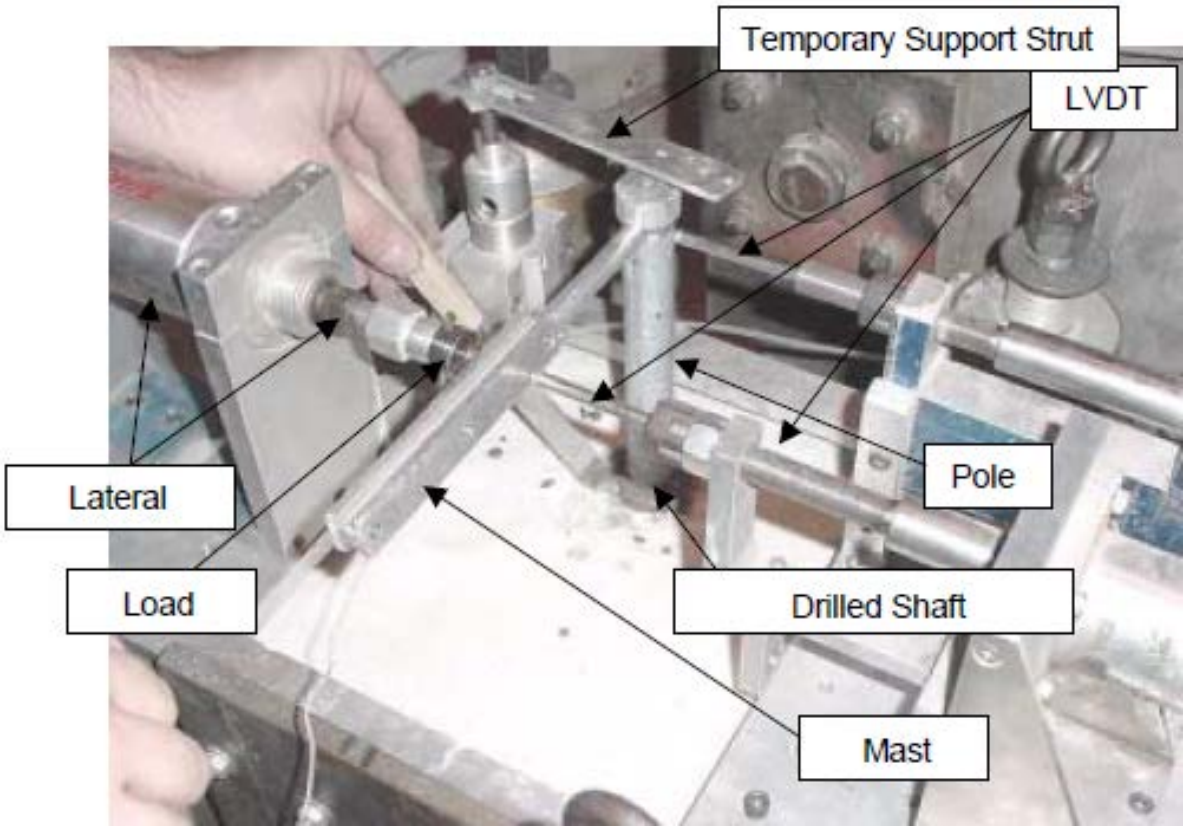

Figure 2.18: Centrifuge test setup *(McVay et al. 2003)*

Torque was applied using a lateral load applied on the middle and tip of the mast arm. Some typical test results of the relationship between torque and shaft rotation from Hu *(Hu 2003)* are shown in Figure 2.19. No definitive peak was observed for the shafts constructed using both types of slurries. Summaries of the torsional capacity of the shafts constructed using bentonite and KB polymer slurry are listed in Table 2.4 and Table 2.5, respectively. For both cases, the loading point did not have significant effects on the torsional capacity. For the shafts constructed using bentonite slurry, the results from the shaft constructed in loose sand are not significantly different than the shaft constructed in dense sand. The torsional capacities increased with the increasing embedment length. The average torsional capacity of drilled shafts constructed with bentonite slurry and 7.6 m (25 ft) and 10.7 m (35 ft) embedment length were 1216 and 1979 kN-m (corresponding to 897 and 1460 kip-ft), respectively.

For the drilled shafts constructed using KB polymer slurry, a significant increase of torsional capacity was observed for the shafts in dense sand comparing to the shafts in loose sand. The average torsional capacities in dense and loose sand of drilled shafts with 7.6 m (25 ft) were 1510 and 2222 kN m (corresponding to 1114 and 1639 kip-ft); and the average torsional capacities in dense and loose sand of drilled shafts with 7.6 m (35 ft) were 2080 and 3043 kN-m (corresponding to 1534 and 2244 kip-ft). This may be due to the efficiency of the polymer strands in a dense pore network, with smaller void spaces to span, than in a loose pore network. Other test results from University of Florida can be found in McVay et al. *(McVay et al. 2003)*, McVay and Hu *(Hu 2003)*, Hu *(Hu 2003)*.

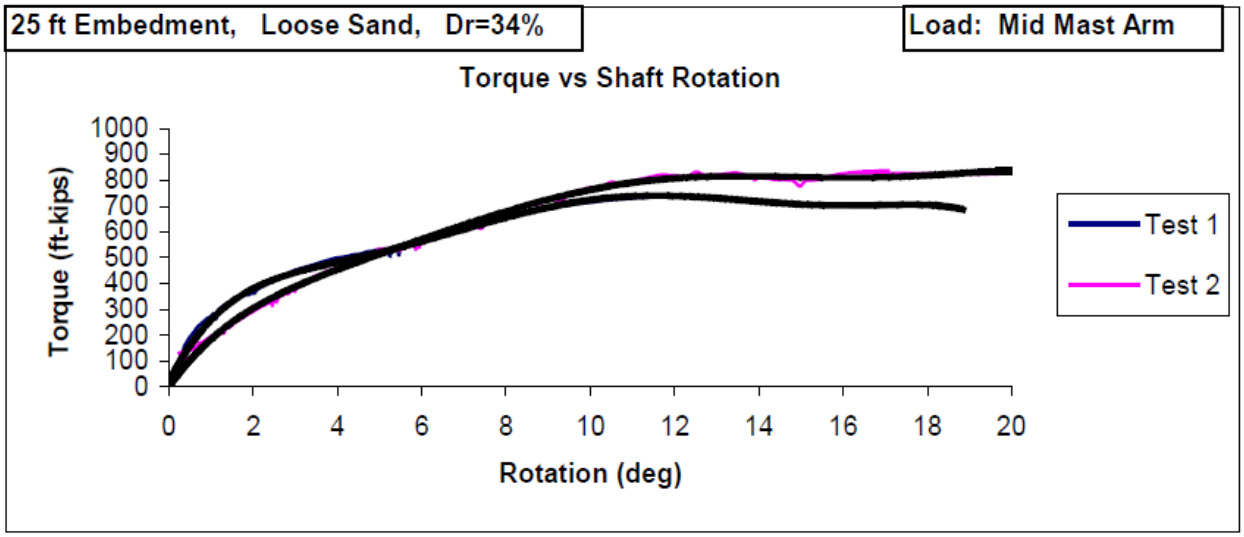

(a)

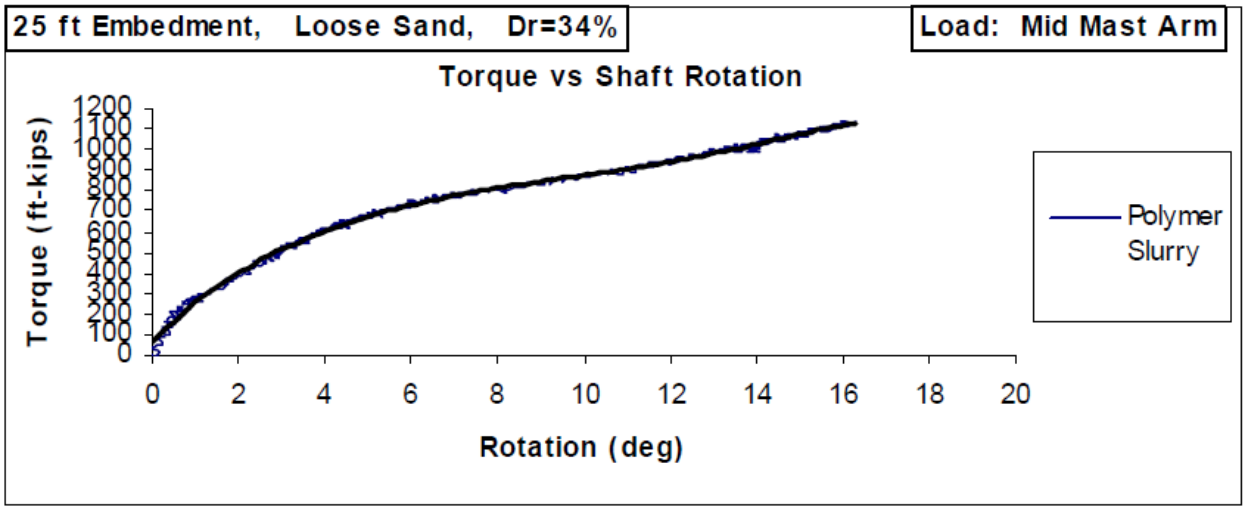

(b)

Figure 2.19: Torque-shaft head rotation response for shafts constructed using (a) bentonite and (b) polymer slurry with 25 ft embedment length in loose sand *(Hu 2003)*

Table 2.4: Summary of the torsional capacity of the shafts constructed using bentonite slurry (based on the data provided by Hu *(Hu 2003)*)

Point of load application	Soil State	Shaft Embedment Length, m (ft)	Applied Torque kN-m (kip-ft)
Mid mast arm	Dense	7.6 (25)	1207 (890)
	Dense		1464 (1080)
	Loose		1003 (740)
	Loose		1112 (820)
Arm tip	Dense	7.6 (25)	1288 (950)
	Dense		1003 (740)
	Loose		1308 (965)
	Loose		1342 (990)
Mid mast arm	Dense	10.7 (35)	1952 (1440)
	Dense		2291 (1690)
	Loose		1993 (1470)
	Loose		2156 (1590)
Arm tip	Dense	10.7 (35)	1817 (1340)
	Dense		1817 (1340)
	Loose		1898 (1400)
	Loose		1912 (1410)

Table 2.5: Summary of the torsional capacity of the shafts constructed using KB polymer slurry (based on the data provided by Hu *(Hu 2003)*)

Point of load application	Soil State	Shaft Embedment Length, m (ft)	Applied Torque kN-m (kip-ft)
Mid mast arm	Dense	7.6 (25)	2420 (1785)
	Loose		1467 (1082)
Arm tip	Dense	7.6 (25)	2024 (1493)
	Loose		1552 (1145)
Mid mast arm	Dense	10.7 (35)	3277 (2417)
	Dense		3097 (2284)
	Loose		2122 (1565)
Arm tip	Dense	10.7 (35)	2755 (2032)
	Loose		2050 (1512)
	Loose		2069 (1526)

Zhang and Kong *(Zhang and Kong 2006)* studied torsional load transfer using aluminum tubes of 300 mm (1 ft) in length, 15.7 mm (0.6 in) in outside diameter, and 0.9 mm (0.035 in) in wall thickness under 40g acceleration. The prototype length, outside diameter, and wall thickness for this level of acceleration was equal to 12 m (39 ft), 628 mm (24 in), and 36 mm (1.4 in), respectively. A quartz-based uniform sand with D_{50} = 0.14 mm and grain size distribution shown in Figure 2.20 was used. The relative densities evaluated were 32% and 75% to represent the loos and dense condition, respectively. Figure 2.21a shows the layout of the typical centrifuge test. The test piles were instrumented with strain gages along the length of model piles as shown in Figure 2.21b. The test piles were pushed into the sand bed after the centrifuge was spun to 40 g and the ground settlement ceased to develop. The embedded length of the prototype pile was 10.8 m (35 ft). Six tests were performed with various loading rates (i.e., 1, 3, and 8 degree/s) for each of the two relative densities, for a total of 12 tests. The torque-twist curves are shown in Figure 2.22, and indicate an approximately hyperbolic relationship. With a rotation of 1°, the applied torque was about 75% and 57% of the torsional capacity in the loose and dense sand, respectively. The torsional resistance was almost fully mobilized at approximately 4° for all of the cases. As expected, the relative density of the sand had a significant influence on the torsional resistance. Figure 2.23 displays the torque distribution along pile shaft at the loading rate of 1.0 degree/second. For this case, the toe resistance contributed 23% and 40% of the total torsional resistance in the loose and dense sands, respectively. However, this finding is not consistent with the results from Tawfiq *(Tawfiq 2000)* and Dutt and O'Neill *(Dutt and O'Neill 1983)*, in which the contribution of toe resistance was less than 10%. The manifestation of the toe resistance in the centrifuge test could be a result of the downward acceleration of the sand deposit, which possibly imparted a drag load due to downward movement relative to the shaft.

To study the effect of loading rate, a semi-log plot, as shown in Figure 2.24, was used to fit a trend line to the test data, given by:

$$T_u(\dot{\theta}) = T_u(\dot{\theta}_{ref})\left[1+\alpha \log\left(\frac{\dot{\theta}}{\dot{\theta}_{ref}}\right)\right] \quad \textbf{(2.1)}$$

where $T_u(\dot{\theta})$ and $T_u(\dot{\theta}_{ref})$ = torsional capacities at loading rates $\dot{\theta}$ and $\dot{\theta}_{ref}$, respectively, α = a coefficient, which is 0.04 for the loose sand and close to zero for the dense sand.

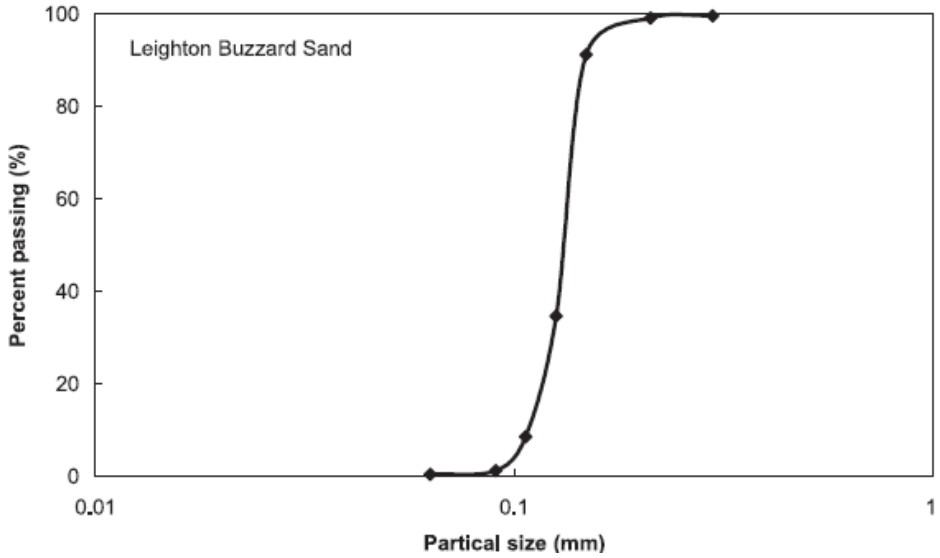

Figure 2.20: Grain size distribution of the test sand *(Zhang and Kong 2006)*

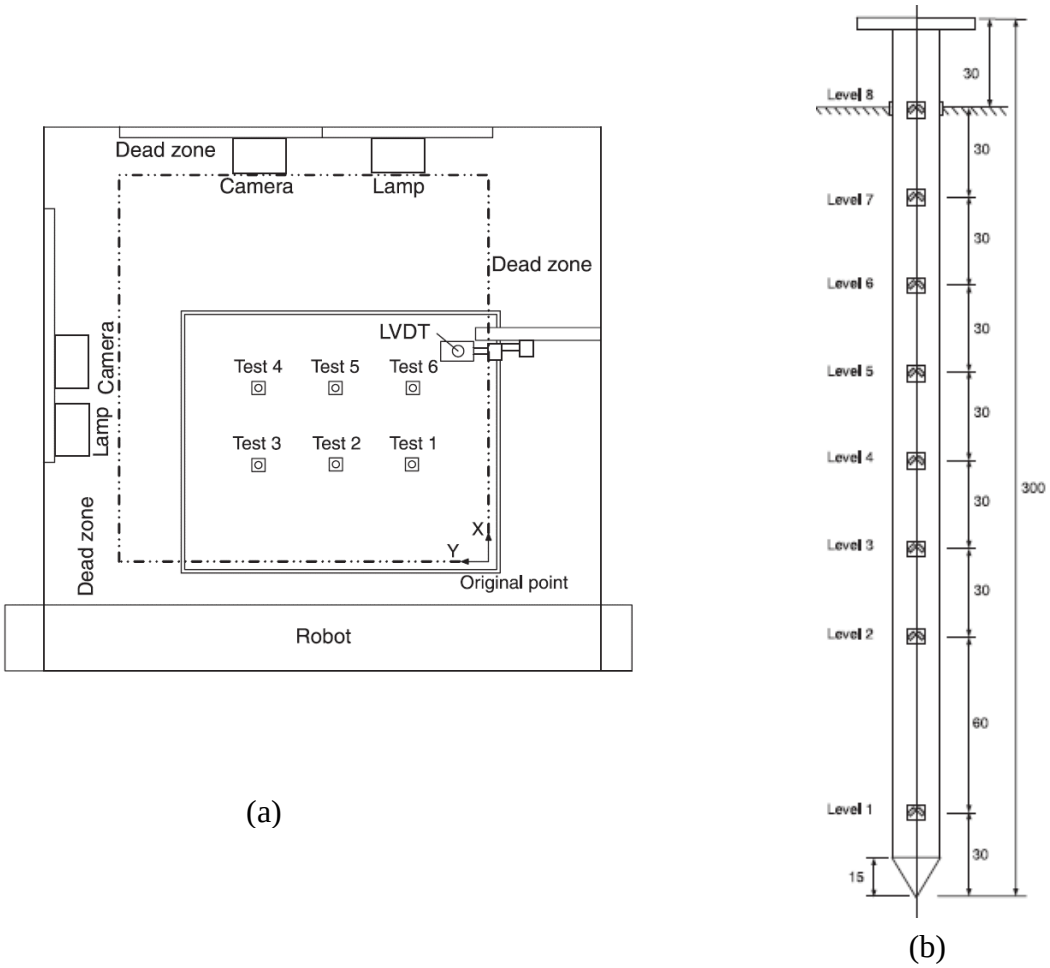

Figure 2.21: (a) Test layout, and (b) instrumentation showing dimensions in mm *(Zhang and Kong 2006)*

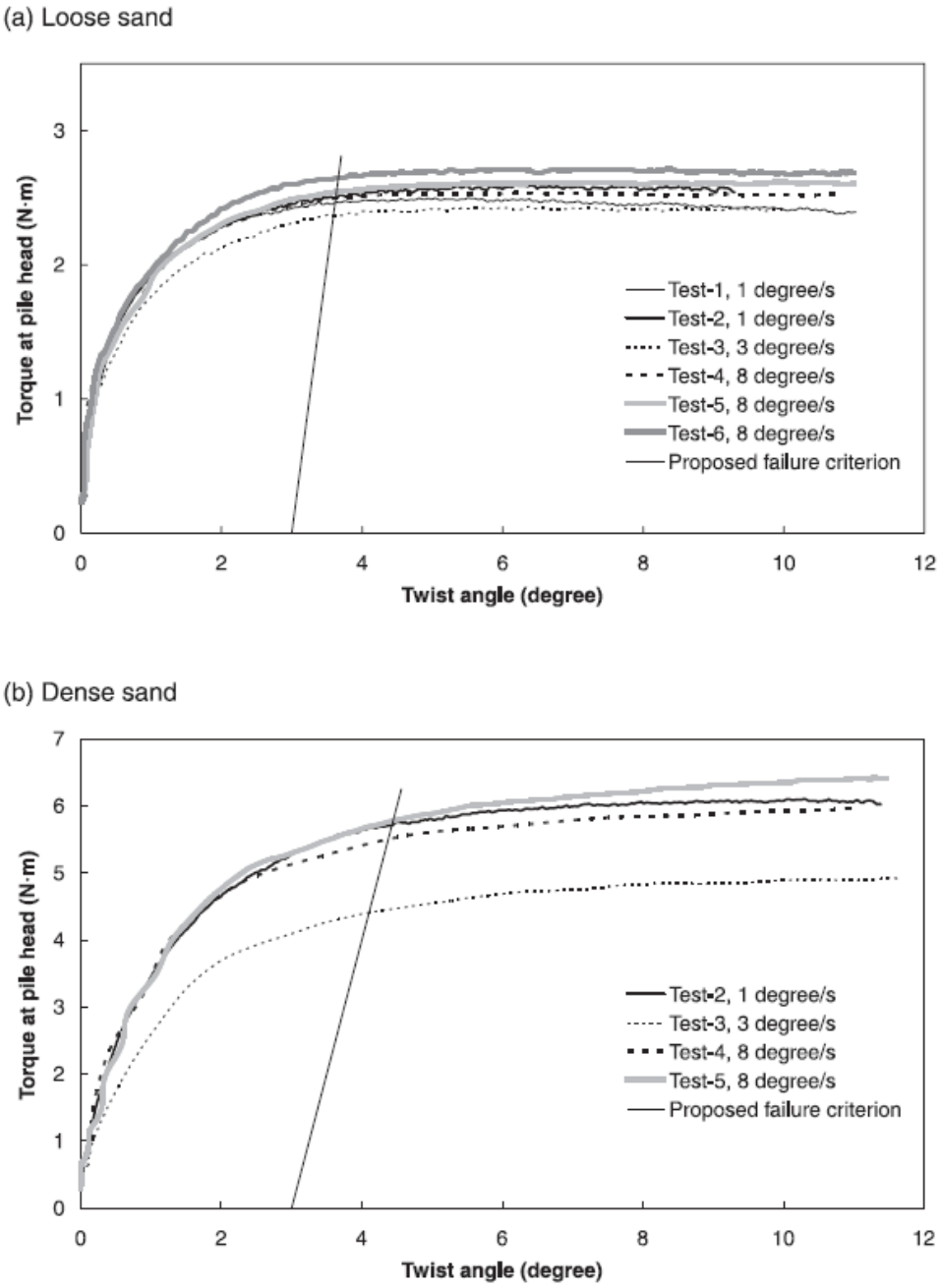

Figure 2.22: Torque-twist curves *(Zhang and Kong 2006)*

(a) Loose sand

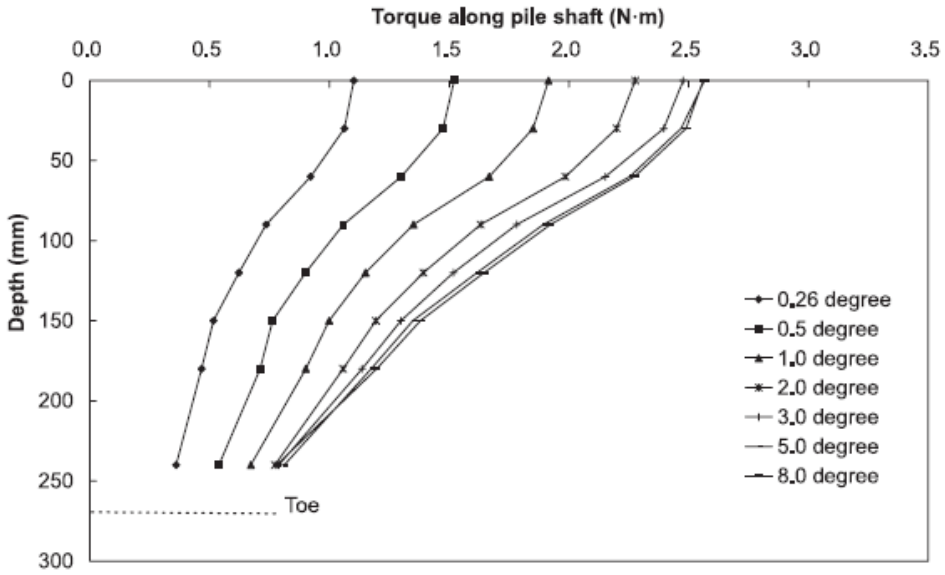

(b) Dense sand

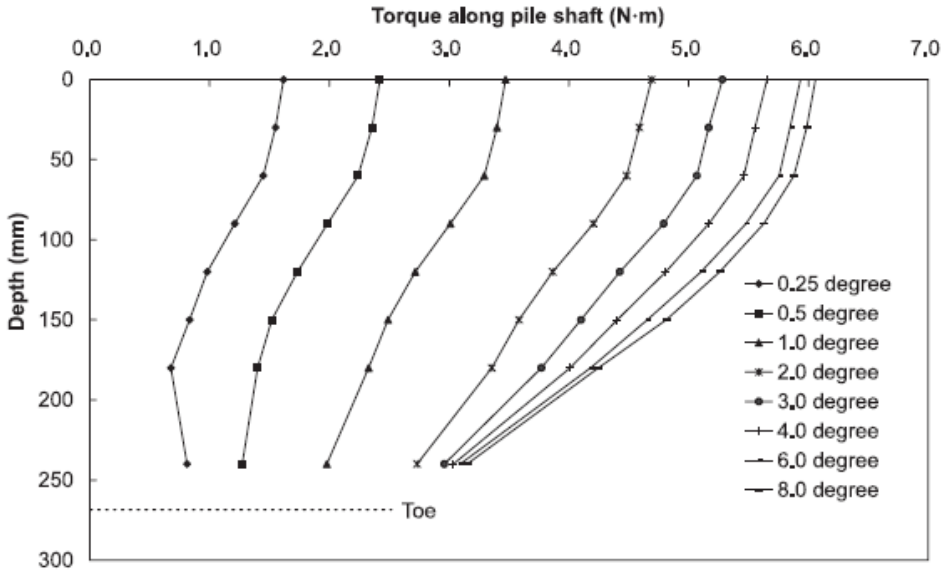

Figure 2.23: Torque distribution along pile shaft at a loading rate of 1.0°/s *(Zhang and Kong 2006)*

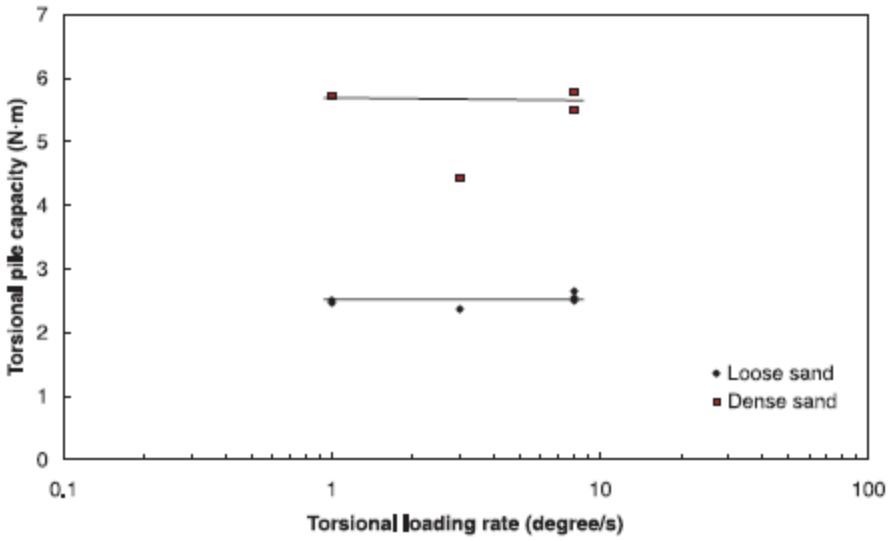

Figure 2.24: Effect of loading rate on torsional pile capacity *(Zhang and Kong 2006)*

2.2.3 Torsion Tests on Full-scale Driven Piles and Drilled Shafts

In what may be the first reported test of torsional capacity, Stoll *(Stoll 1972)* applied torque to two driven steel pipe piles filled with concrete, designated Pile A-3 and Pile V-4. The steel piles are of 0.27 m (10.75 in) external diameter and 6.3 mm (0.25 in) wall thickness. Figure 2.25 shows the setup of the loading test. The soil profiles and driving logs for each test pile are shown in Figure 2.26, and indicates the piles were driven in heterogeneous soil conditions. The test piles were driven to a final penetration resistance of 50 to 60 blows/foot. The resulting embedded length of Pile A-3 and Pile V-4 were 17.4 m (57 ft) and 20.7 m (68 ft), respectively. Based on Figure 2.26, the length of pile above ground surface for Pile A-3 and Pile V-4 were 1.0 m (3 ft) and 0.7 m (2 ft), respectively. The rotation at the top of each test pile and applied torque were monitored and are shown in Figure 2.27. The torsional resistance of both piles increased with the increase of pile rotation until failure at approximately 0.055 radians (3.2°). No definitive peak was observed for either of the test piles.

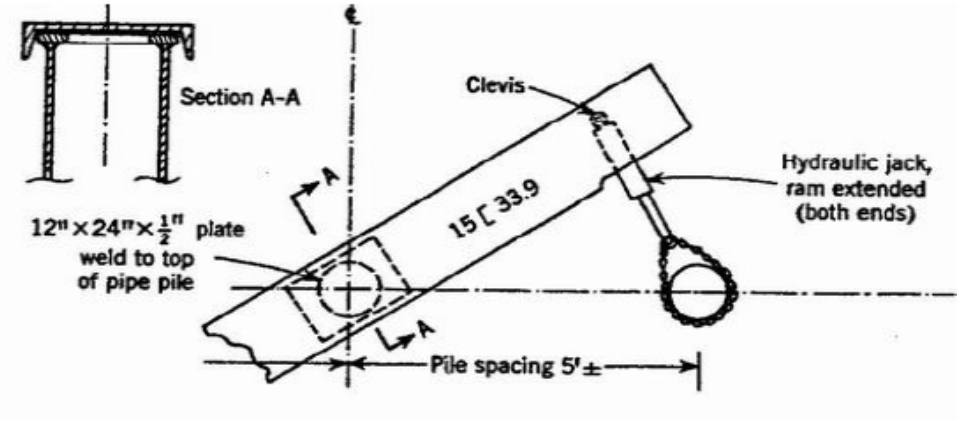

Figure 2.25: Pile torque shear test setup *(Stoll 1972)*

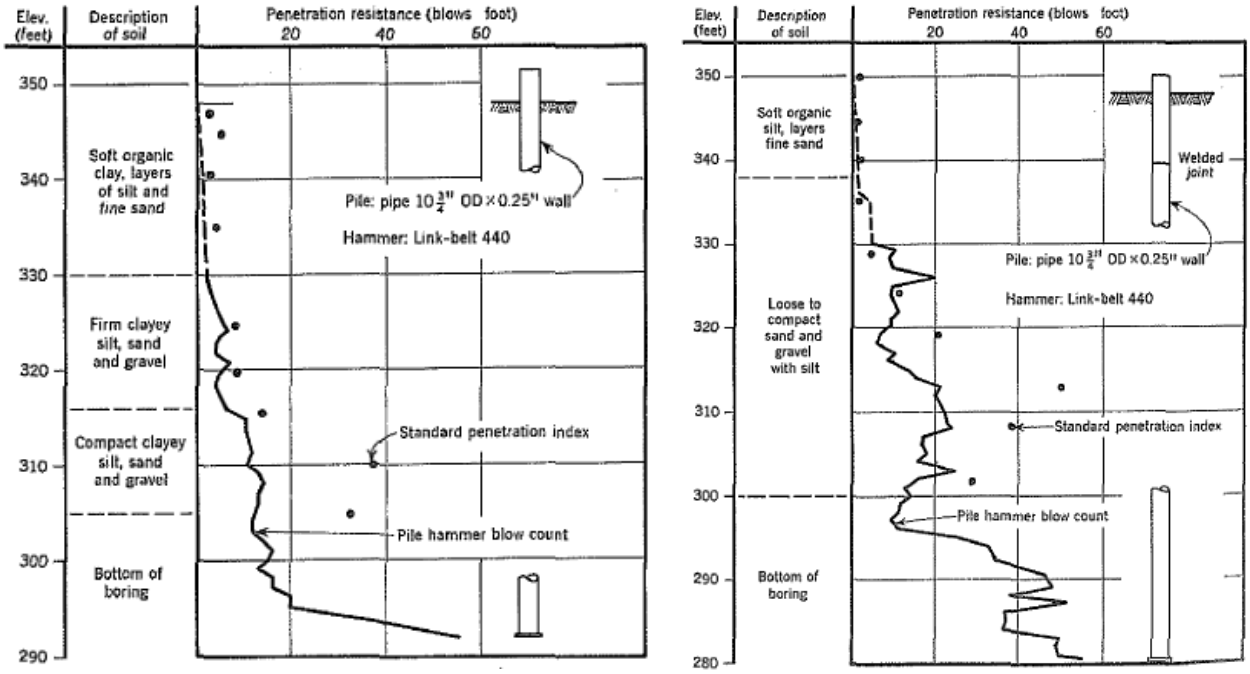

(a) (b)

Figure 2.26: Soil profile and driving log for (a) Pile A-3 (b) Pile V-4 *(Stoll 1972)*

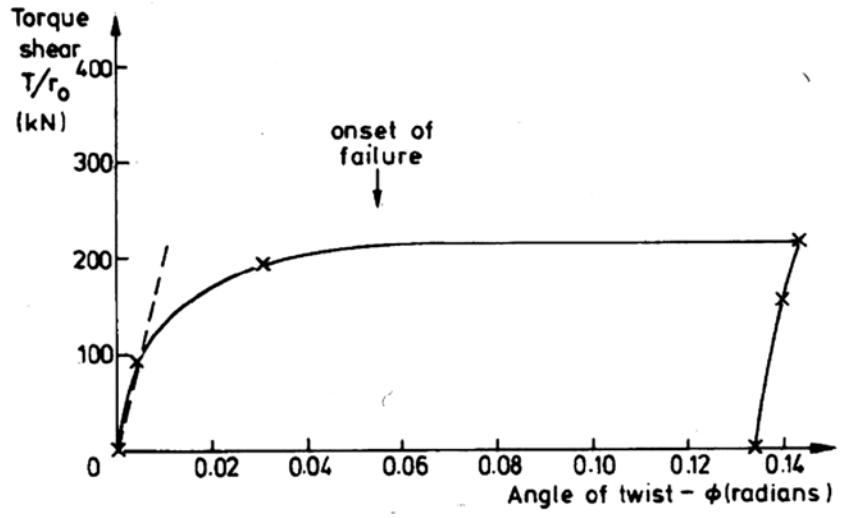

(a)

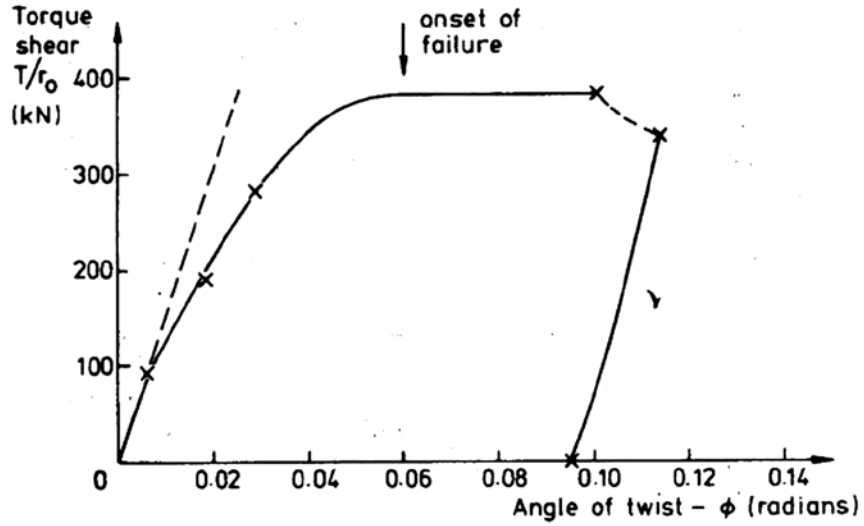

(b)

Figure 2.27: Results from torsional load tests: (a) Pile A-3 (b) Pile V-4 *(Randolph 1981, originally from Stoll 1972).* Note: 0.1 radians = 5.7 degrees.

In addition to the model tests, Tawfiq *(Tawfiq 2000)* performed full-scale field tests on three 1.2 m (4 ft) diameter by 6.1 m (20 ft) depth drilled shafts constructed in Tallahassee FL. As shown in Figure 2.28, load was applied using a 3.1 m (10 ft) steel cantilever beam. One shaft was constructed with dry method (no slurry). The other two shafts were constructed using the wet method, with one supporting the drill cavity with a bentonite slurry and the other with a polymer slurry. Soil borings, as shown in Figure 2.29, were drilled at the proposed locations of the drilled shaft to investigate the soil conditions. The soil profiles are shown in Figure 2.30. Generally, a layer of silty sandy was encountered from ground surface to a depth of 0.3 m (1 ft), underlain by a layer of clayey sand or sandy clay to a depth arranging from 2.7 to 5.0 m (9 to 16 ft). Below this layer is a stratum of clayey, silty, fine sand underlain by a layer of sand with silt for the dry

shaft (TH1) or sandy clay for the shaft using polymer slurry (TH2). The groundwater table was below the depth of the base of the foundation (over 20 ft).

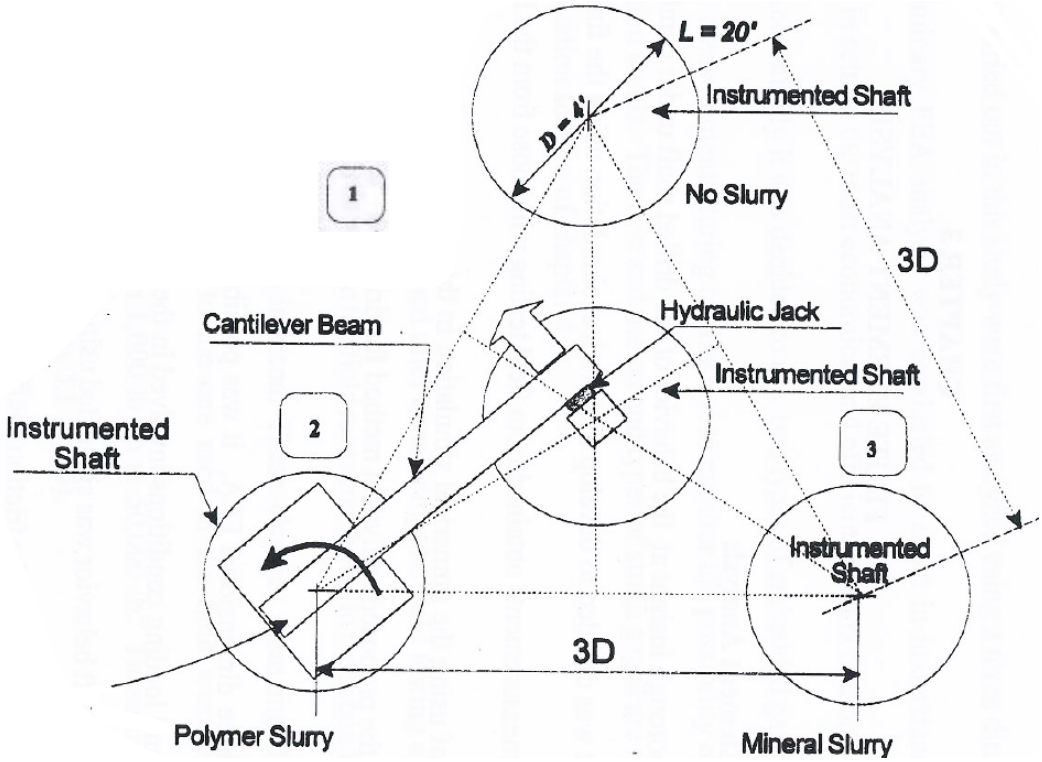

Figure 2.28: Full-scale test setup *(Tawfiq 2000)*

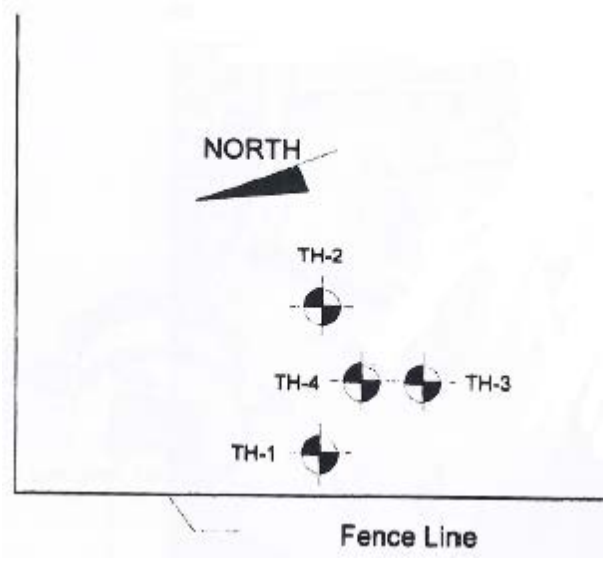

Figure 2.29: Location of test shafts and borings *(Tawfiq 2000)*

The test results for the shafts constructed using (a) dry method and (b) bentonite slurry are shown in Figure 2.31. The load-rotation response for the shaft constructed using polymer slurry was not provided by the author. It is noted that the applied torque can be calculated by multiplying the applied load with the length of loading arm, which was 3.1 m (10 ft). The induced rotation of the dry shaft was limited to 0.45°, with corresponding maximum torque of 664 kN-m (490 kip-ft), as the shaft experienced structural failure.

The maximum applied torque for the shaft constructed using bentonite slurry was 380 kN-m (280 kip-ft), which was 43% less than the maximum applied torque of the dry shaft, as shown in Figure 2.31b. For the torsional loading test on the shaft constructed using polymer slurry, Tawfiq (2000) reported that the performance of the shaft was similar to the dry shaft at the torque of 380 kN-m (280 kip-ft). Owing to the experience with dry shaft, the upper 1.5 m (5 ft) of soil around the polymer slurry-constructed shaft was removed during loading to avoid structural failure. The maximum applied torque for the shaft constructed using polymer slurry was 569 kN-m (420 kip-ft). Considering that the final embedded length for the shaft constructed using polymer slurry was 4.6 m (15 ft), the torsional capacity for this shaft with same embedded length may be larger than the dry shaft. Note that there is a concern regarding the setup of the test: the center-to-center distance from the reaction shaft to each test shaft was only about 2.1 m (7 ft) and the clear span between shafts was only 0.9 m (3 ft). Therefore, the effect of shaft-to-shaft interaction should have been investigated. Since the torsional load transfer was not studied in this test, the effect of interaction between the shafts could not be explored.

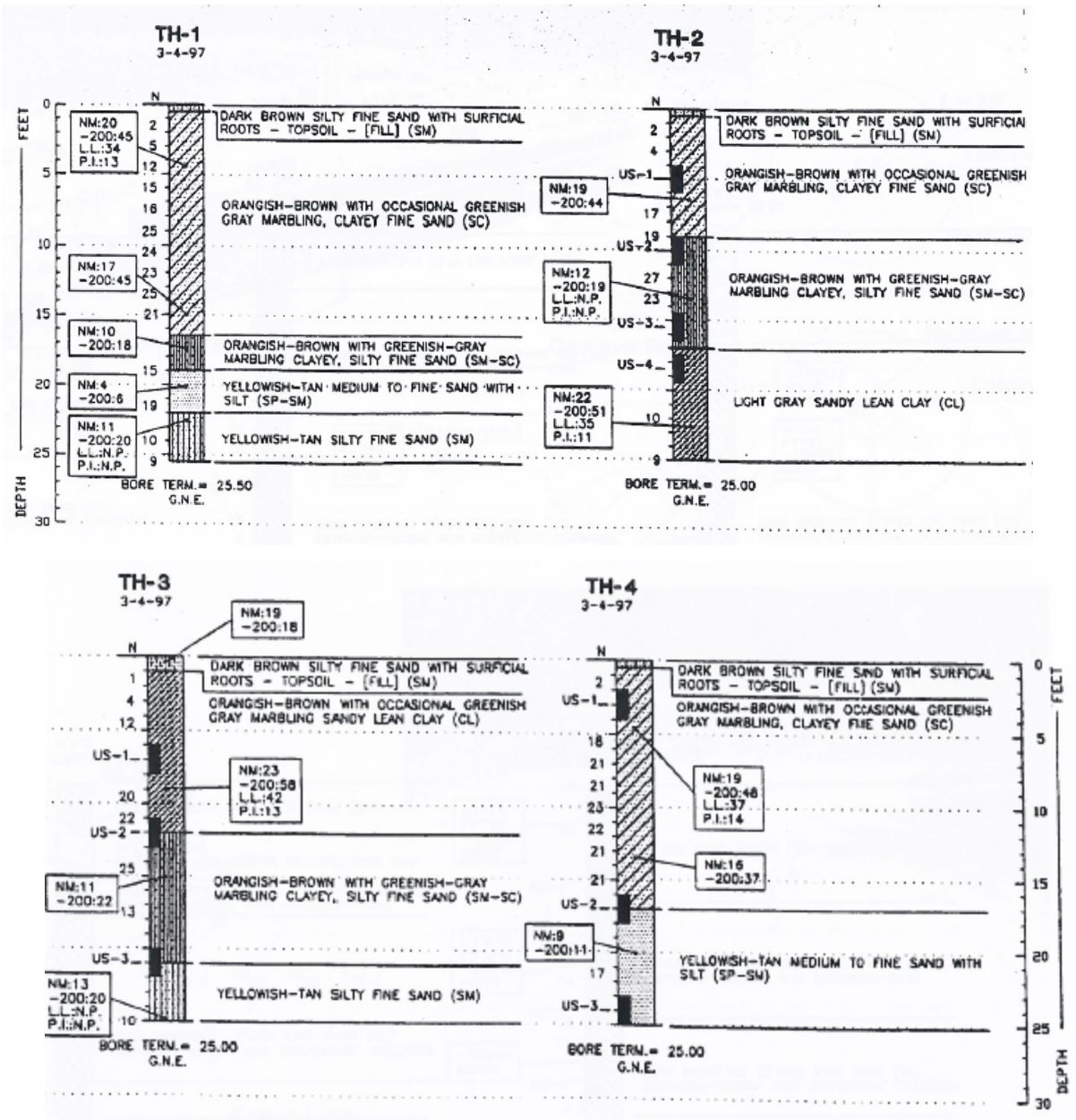

Figure 2.30: Soil profile at test site *(Tawfiq 2000)*

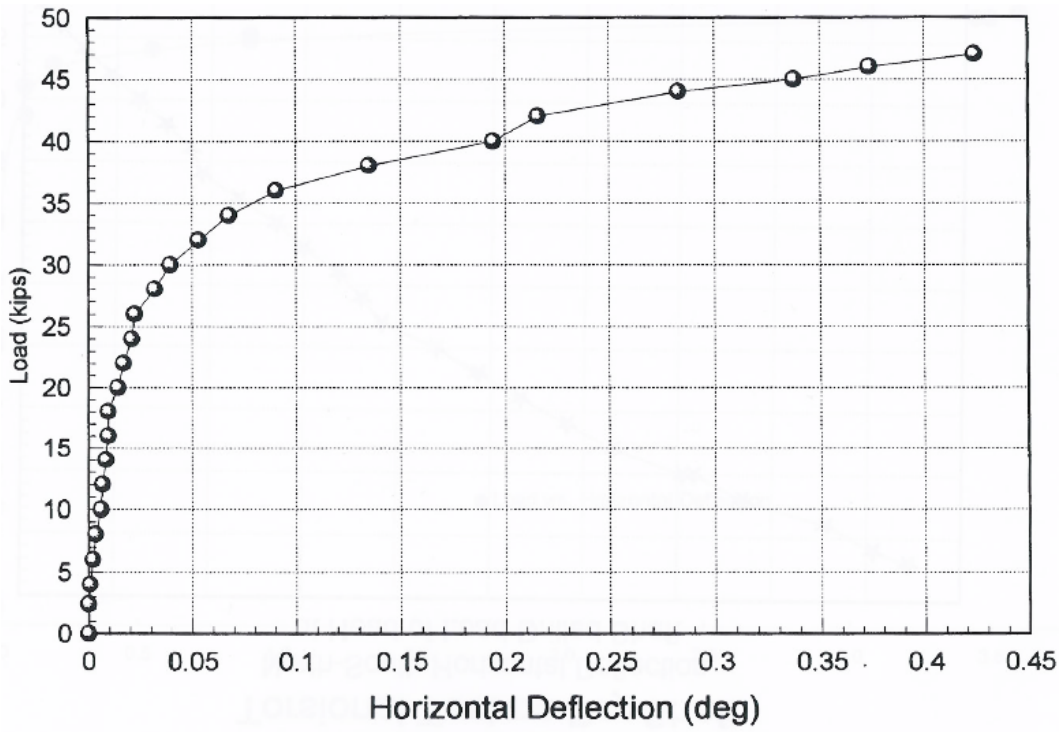

(a)

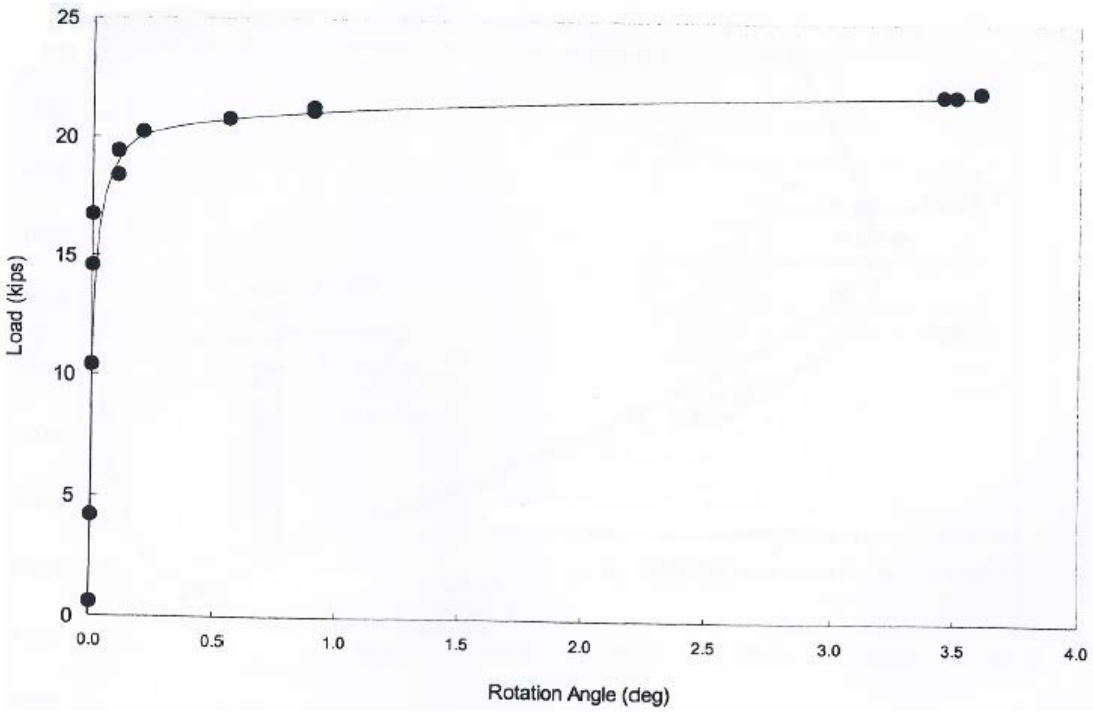

(b)

Figure 2.31: Test results of shafts constructed using (a) dry method and (b) bentonite slurry *(Tawfiq 2000)*

McVay et al. *(McVay et al. 2014)* performed a series of full-scale torsional loading tests on three drilled shafts in Keystone Heights, FL. The drilled shafts included one with a 1.2 m (4 ft) diameter and 3.7 m (12 ft) embedded length (designated TS1), and the other two shafts were constructed with a 1.2 m (4 ft) diameter and 5.5 m (18 ft) embedded length (designated TS2 and TS3). All of the shaft heads were 0.46 m (1.5 ft) above ground surface. The soil profile for each test shaft is shown in Figure 2.32. No temporary casing was used during excavation of the test shafts. The shaft cavities were drilled using the dry method to a depth of about 1.8 m (6 ft), and then bentonite slurry was used to support the cavity for the remainder of the shaft excavation. After installation of the test shafts, Mast arm-pole assemblies were attached to the test shafts. The lengths of pole and arm were 6.7 and 12.2 m (22 and 40 ft), respectively. Lateral loading was applied with increments of 0.5 kips on the mast arm at an offset distance of 10.7 m (35 ft), as shown in Figure 2.33, to supply the torque to the test shaft. A load cell was installed between the mast arm and a crane-mounted winch cable to measure the load associated with the applied load. Upon the observation of failure for shafts TS2 and TS3, the shafts were unloaded. Three types of instrumentation were used to measure the rotation of the test shafts, including two total stations and survey monitoring, two sets of string potentiometers (four potentiometers in each set), and a set of four dial gauges. The water table was about 3 m (10 ft) below ground surface.

Figure 2.34 displays the relationship between applied torque and rotation for each test shaft. The torsional resistances were fully-mobilized at 95, 285, and 232 kN-m (corresponding to 70, 210, and 171 kip-ft) for TS1, TS2, and TS3, respectively. The difference of torsional capacity between TS2 and TS3 can be attributed to the difference in soil profile. TS2 was constructed with a greater length in the sand layer, which provided more torsional resistance.

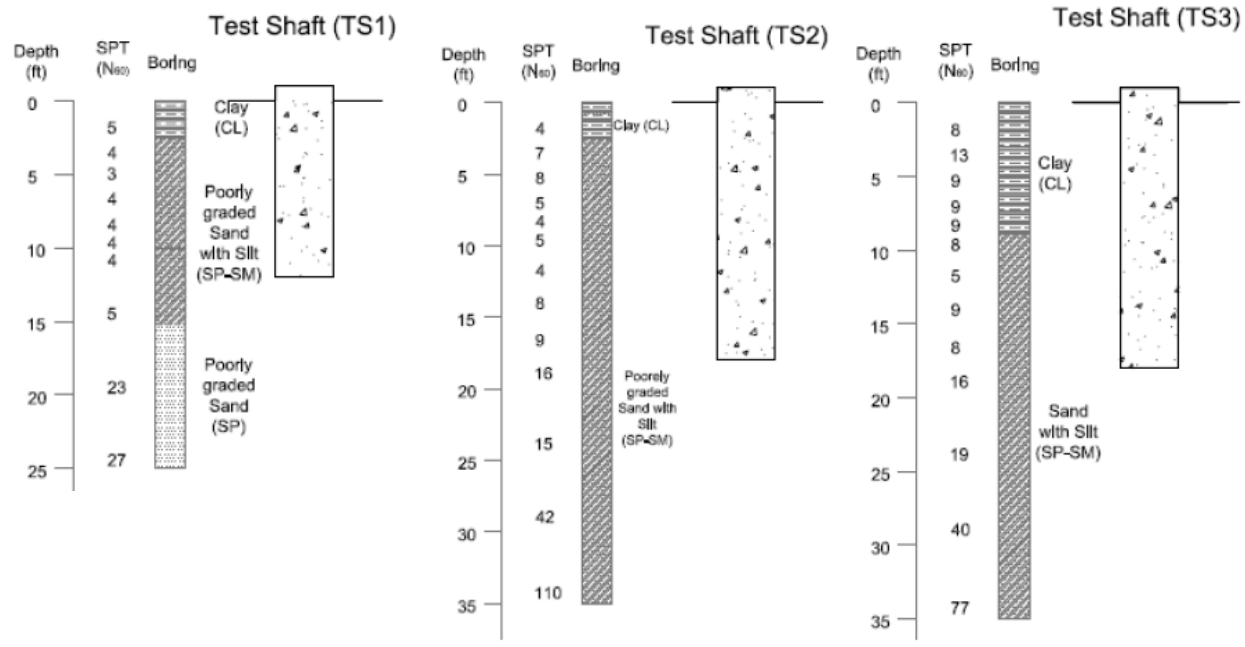

(a) (b) (c)

Figure 2.32: Soil profile at the location test drilled shafts *(McVay et al. 2014)*

Figure 2.33: Combined torsion and lateral loading *(McVay et al. 2014)*

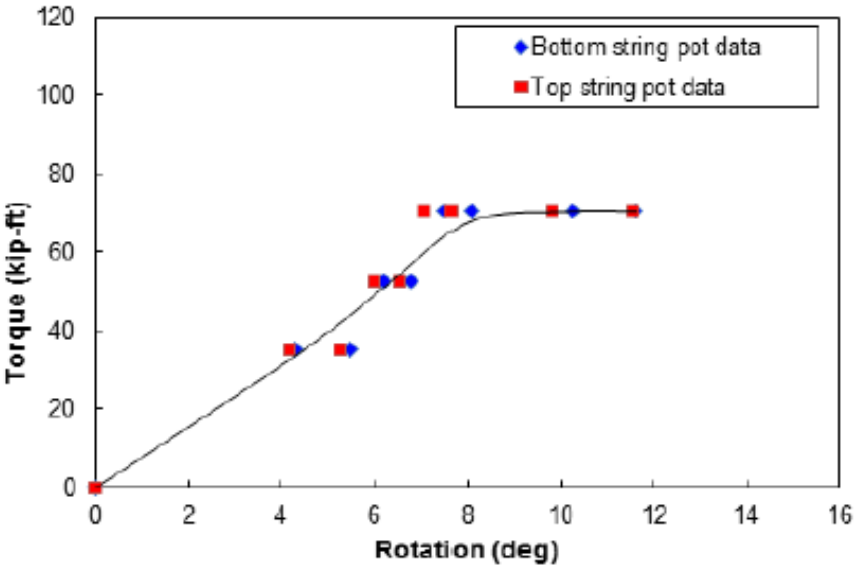

(a)

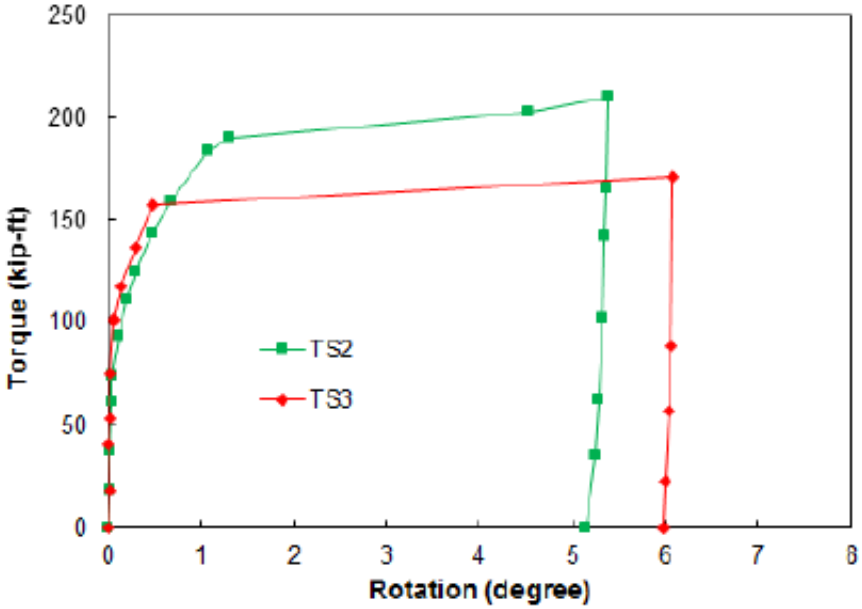

(b)

Figure 2.34: Torque vs. rotation response of (a) TS1 and (b) TS2 and TS3 *(McVay et al. 2014)*

2.3 ANALYTICAL METHODS FOR TORSIONAL CAPACITY

The torsional loading tests in the previous section provide information on the effect of some of the shaft design variables on the torsional resistance possible of drilled shafts. However, the capacity of shafts must be predicted before a loading event in order to proceed with their implementation of the support of traffic signal and sign installations. Thus, some discussion of the available design methodologies is warranted. In general, the torsional capacity of drilled shafts consists of shaft and toe torsional resistance, the functional form given by:

$$T = T_s + T_t \quad \textbf{(2.2)}$$

where T_s = shaft torsional resistance, and T_t = toe torsional resistance.

Simple design methods are available to estimate the torsional shaft and toe resistance of drilled shafts, including three FDOT methods as summarized by Hu *(Hu 2003)*: Florida Structures Design Office Method, the District 5 Method, and District 7 Method, and the Colorado Department of Transportation (CDOT) design method developed by CDOT *(Nusairat et al. 2004)*. The Florida District 7 and CDOT design methods can be used for the drilled shafts embedded in both cohesive and cohesionless soils. The Florida Structures Design Office Method and District 5 Method are suitable for the drilled shafts embedded in cohesionless soils. These methods are described further below.

2.3.1 Florida Structures Design Office Method

The Florida Structures Design Office Method (Hu 2003) assumes that the soil behaves as a rigid, perfectly-plastic material and the shaft behaves as a rigid body under simple torsional load at the ultimate or fully-mobilized soil resistance. The unit shaft resistance, r_s, in cohesionless soil is given by:

$$r_s = K_0 \sigma'_{vz} \tan\delta \quad \textbf{(2.3)}$$

where K_0 = at rest lateral earth pressure coefficient, σ'_{vz} = effective vertical stress at the mid-point of the layer of interest, and δ = effective soil-shaft interface friction angle, which can be assumed equal to the effective friction angle of soil, ϕ', for a drilled shaft. Then, the total shaft resistance can be obtained by:

$$T_s = \frac{\pi D^2}{2} L \cdot r_s \quad \textbf{(2.4)}$$

where D = shaft diameter, L = shaft length.

The toe resistance may be estimated using:

$$T_t = \frac{D}{3} W \tan\delta \quad \textbf{(2.5)}$$

where W = shaft weight. Note that the axial load applied on drilled shafts is neglected for evaluating the toe resistance using this method.

2.3.2 Florida District 5 Method

The Florida District 5 Method (Hu 2003) allows the designer to use one or both of two approaches to calculate the torsional capacity of drilled shafts in cohesionless soils. The first approach calls for the use of a program called SHAFTUF developed by University of Florida to obtain the ultimate shaft resistance, Q_s. Then, the torsional shaft resistance, T_s, and toe resistance, T_t, are given by:

$$T_s = \frac{D}{2} Q_s \quad \textbf{(2.6)}$$

$$T_t = \frac{D}{3}(W + Q_a)\tan\left(\frac{2}{3}\delta\right) \quad \textbf{(2.7)}$$

where Q_a = axial load applied on drilled shafts, and all the other variables have been defined previously. The second approach employs the β-Method *(e.g., O'Neill and Hassan, 1994)* for shafts under axial loading. In this approach, the unit shaft resistance in cohesionless soil is given by:

$$r_s = \beta \sigma_{vz}^{'} \quad \textbf{(2.8)}$$

where β = load transfer ratio for effective-stress normalized unit shaft resistance and has been correlated to depth and the STP blow count, N:

$$\beta_{nominal} = 1.5 - 0.135\sqrt{z},\ 1.2 \geq \beta_{nominal} \geq 0.25 \quad \text{for} \quad N \geq 15 \quad \textbf{(2.9)}$$

$$\beta = \frac{N}{15}\beta_{\text{nominal}} \quad \text{for} \quad N < 15 \quad \textbf{(2.10)}$$

where z = depth from ground surface to the mid-layer of interest. Then, the total shaft resistance can be obtained using Equation (2.5). The toe resistance is estimated using:

$$T_t = \frac{D}{3}(W + Q_a)\tan\delta \quad \textbf{(2.11)}$$

2.3.3 Florida District 7 Method

In the Florida District 7 Method *(Hu 2003)*, the unit shaft resistance is given by:

$$r_s = \alpha \cdot s_u + K\sigma_{vz}^{'}\tan\delta \quad \textbf{(2.12)}$$

where s_u = average undrained shear strength over the depth of interest, K = coefficient of lateral earth pressure ranging from K_0 to 1.75, and α = an adhesion factor, which is a function of the average undrained shear strength for the stratum of interest, as proposed by O'Neill and Reese *(O'Neill and Reese 1999)* for shafts under axial loading:

$$\alpha = 0.55 \text{ for } \frac{s_u}{P_a} \leq 1.5 \quad \textbf{(2.13)}$$

$$\alpha = 0.55 - 0.1\left(\frac{s_u}{P_a} - 1.5\right) \text{ for } 1.5 \leq \frac{s_u}{P_a} \leq 2.5 \quad \textbf{(2.14)}$$

$$\alpha = 0.45 \text{ for } \frac{s_u}{P_a} > 2.5 \quad \textbf{(2.15)}$$

where P_a = atmospheric pressure in the same units as s_u. O'Neill and Reese *(O'Neill and Reese 1999)* suggested that when s_u / P_a is larger than 2.5, the shaft resistance under axial loading should be calculated by considering the cohesive soil as intermediate geomaterial. The unit soil

resistance from ground surface to a depth of 1.5 m (5 ft) or to the depth of seasonal moisture change is neglected due to the potential loss of shaft resistance as soil expands and contracts induced by wetting and drying or freezing and thawing near the ground surface *(Brown et al. 2010).*

The torsional shaft resistance, T_s, is given by:

$$T_s = \frac{\pi D^2}{2}(L - 1.5)r_s \quad \textbf{(2.16)}$$

where D and L are in meters, and toe resistance, T_t, is estimated by

$$T_t = \frac{4D}{9}(W + Q_a)\tan\delta \quad \textbf{(2.17)}$$

2.3.4 CDOT Design Method

In the CDOT Design Method *(Nusairat et al. 2004)*, the unit shaft resistance in cohesive soils is equal to the undrained shear strength over the depth of interest, and the side resistance in cohesive soils for the top 1.5D of the shaft is neglected. The shaft resistance, T_s, for cohesive soils is given by:

$$T_s = \frac{\pi D^2}{2} \cdot (L - 1.5D) \cdot s_u \quad \textbf{(2.18)}$$

whereas the toe resistance, T_t, is given by:

$$T_t = \frac{\pi D^3}{12} s_u \quad \textbf{(2.19)}$$

For shafts in cohesionless soils, the unit shaft resistance is given by:

$$r_s = K\sigma'_{vz}\tan\delta \quad \textbf{(2.20)}$$

where K = the coefficient of lateral earth pressure is given by:

$$K = \frac{2L}{3D}(1 - \sin\phi') \quad \textbf{(2.21)}$$

Then, the shaft and toe resistance in cohesionless soils can be computed using Equations (2.4) and (2.5).

2.4 SUMMARY

This chapter presented the torsional loading test data and design methods for torsional response available in the literature. The torsional loading tests were categorized into three types: small-scale model driven piles and drilled shafts loading tests, centrifuge loading tests, and full-scale load tests. The torsional load transfer was investigated in some scale model and centrifuge loading tests by measuring the shear strains along the test shafts. However, only three full-scale torsional loading tests were found in literature. Unfortunately, no load transfer observations were

reported for any of the full-scale tests, limiting our understanding of the contributions of shaft and toe resistance in torsion. Therefore, full-scale tests on drilled shafts instrumented to measure load transfer in torsion would address a major need for engineers concerned with the design of traffic sign and signal structures.

3.0 SITE CHARACTERIZATION

3.1 OVERVIEW

The Geotechnical Engineering Field Research Site (GEFRS) at Oregon State University (OSU) is located near the western edge of the main portion of the OSU campus, adjacent to the Hinsdale Wave Research Lab (Figure 3.1). This test site has been used for over twenty years to conduct geotechnical experiments at full-scale. Figure 3.2 shows an aerial photograph of the test site with the location of the test shafts. The test shafts were installed between an existing, deep drilled shaft (EDS) and SW Jefferson Way. The geotechnical explorations and stratigraphy for the subsurface corresponding to the test shafts are presented in this chapter.

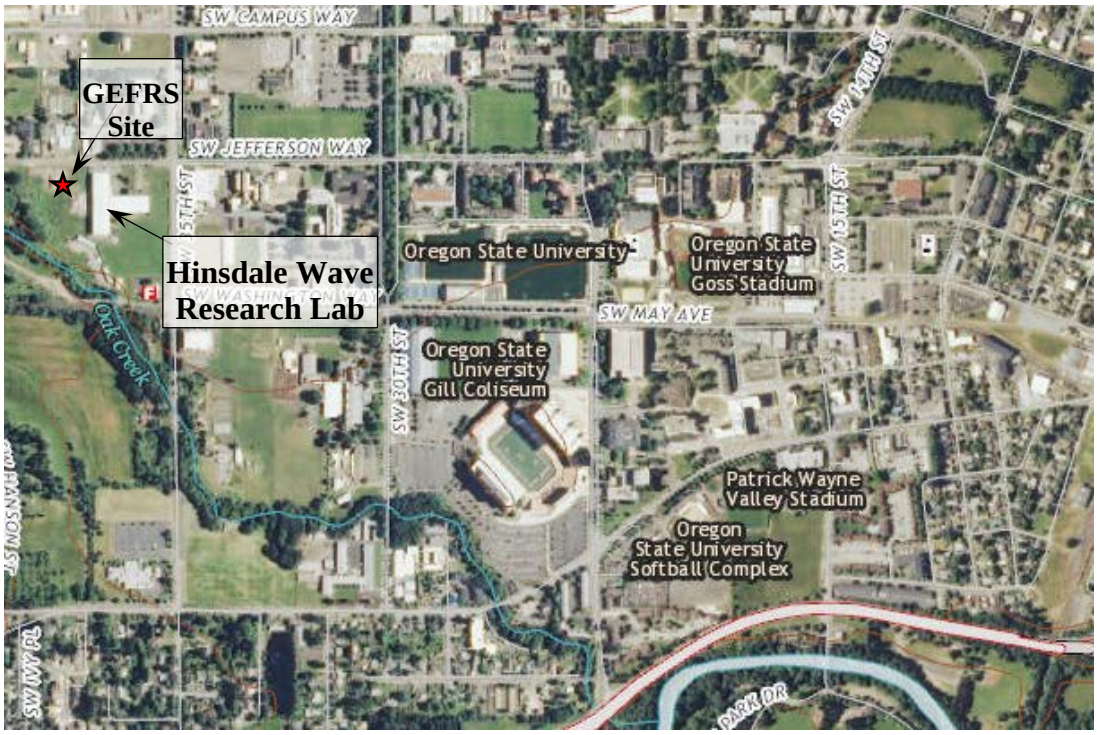

Figure 3.1: Project site *(Adapted from USGS National Map Viewer 2015)*

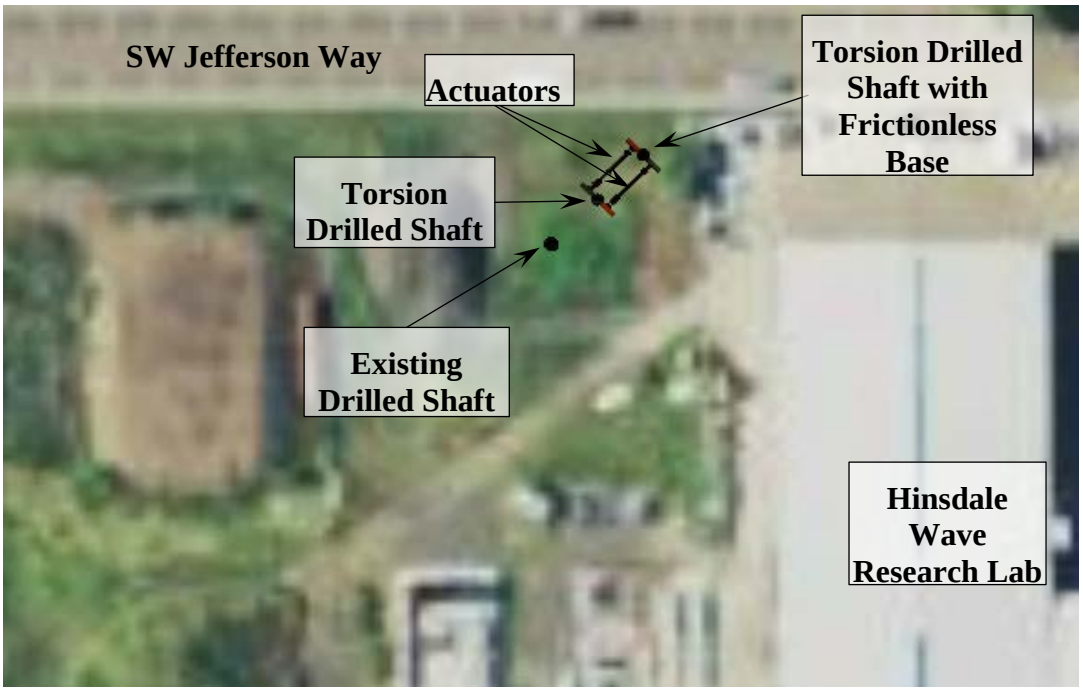

Figure 3.2: Aerial view of the test site

3.2 SITE SPECIFIC GEOTECHNICAL EXPLORATION

The site plan indicating the geotechnical explorations in relation to the test setup is shown in Figure 3.3. Three cone penetration tests (CPTs) were conducted, two at the centers of the proposed test shafts and one close to an existing drilled shaft. The full CPT logs are shown in Appendix A. CPT-2 was conducted at the center of the proposed test shaft designated TDS, whereas CPT-1 was located at the center of test shaft TDSFB (*n.b.*, these test shafts are described in detail below). One boring performed with SPTs, and one boring advanced for undisturbed sampling, was conducted in close proximity of the test shafts.

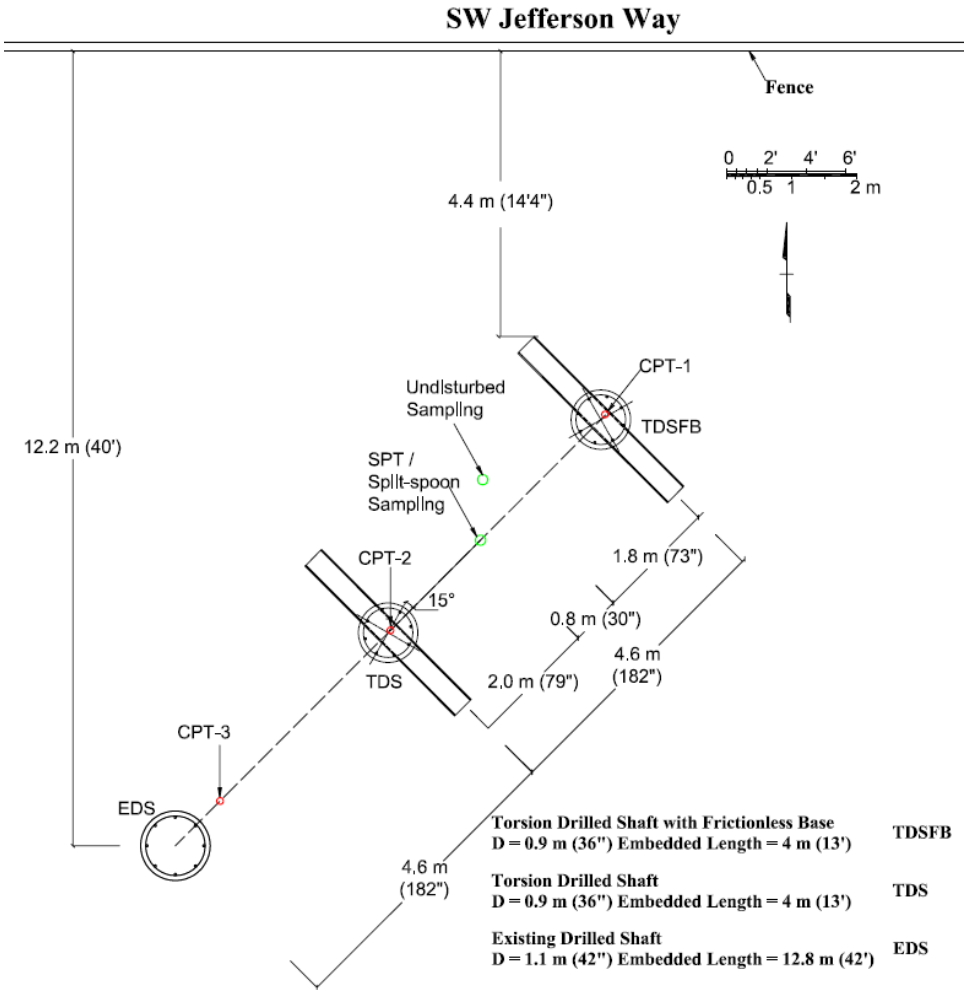

Figure 3.3: Test site layout and exploration plan

Figure 3.4 shows the location of the test shafts and subsurface profile based on the geotechnical in-situ and laboratory investigations. The groundwater table was measured 1.9 m (6.2 ft) below the ground surface on the day of the test, although wet conditions were noted above this depth due to the capillarity associated with the fine-grained soils present. Corrected cone tip resistance (q_t) profiles and SPT *N*-value profiles, respectively, are also illustrated in Figure 3.4. The subsurface consists of overconsolidated silty clay to clayey silt, to approximately 5.2 m (17 ft), and underlain by a layer of sand to silty sand. Other explorations conducted nearby indicated that this granular layer is generally on the order of 1.5 m (5 ft) thick. The near-surface soils, to a depth of 0.9 m (3 ft), desiccated and form a very stiff to hard crust (when dry), as indicated by high q_t and SPT *N* (conducted on 10/09/2014 and 10/14/2014, respectively) and is typical for the test site in general at the end of summer. From a depth of 0.9 m (3 ft) to approximately 5.2 m (17 ft), the silty clay to clayey silt is of medium stiff to very stiff consistency, and is associated with overconsolidation ratios on the order of 5 to 10 *(Dickenson 2006)*. A 1.1 m (3.6 ft) thick layer of medium dense, sand to silty sand was encountered in CPT-2 and in the excavated spoils of the test shaft installed at this location.

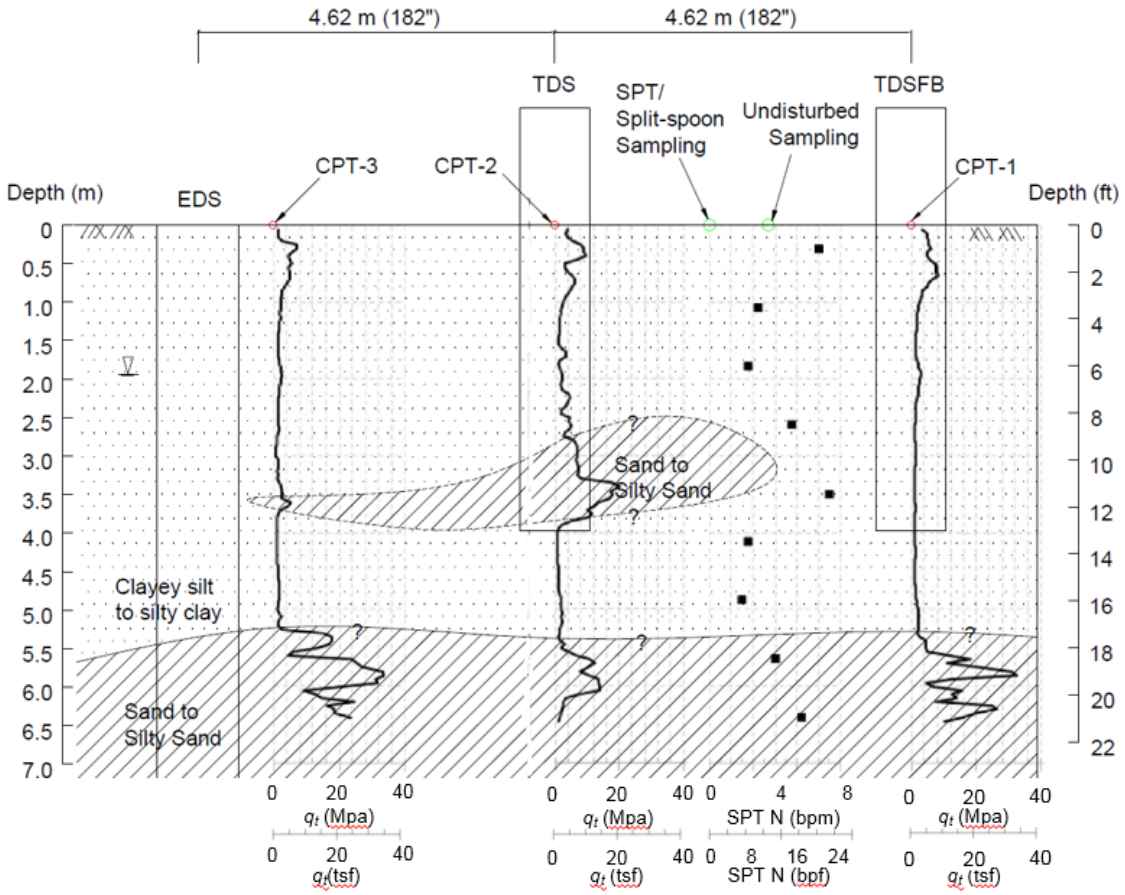

Figure 3.4: Subsurface profile at test site with the locations of test shafts and in-situ tests

4.0 DESIGN AND CONSTRUCTION OF THE TEST SHAFTS

4.1 OVERVIEW

This chapter presents the design details of test shafts, the fabrication and instrumentation of the reinforcing cages, and the test setup. The two test shafts studied herein were constructed to help evaluate the magnitude and distribution of load transfer along the shaft and toe in torsion. The test shafts are designated herein as the torsion test drilled shaft with production base (TDS; constructed using normal methods), and the torsion test drilled shaft with frictionless base (TDSFB); these locations are indicated on Figure 3.3 and Figure 3.4. The spacing between TDS and TDSFB was 4.6 m (15.2 ft) and larger than five diameters, avoiding shaft-to-shaft interaction. Section 4.2 describes the structural design of test shafts. The fabrication and instrumentation of the reinforcing cages and the construction of the test shafts are described in Section 4.3 and 4.4, respectively.

4.2 STRUCTURAL DESIGN OF TEST SHAFTS

The test shafts were designed to support Oregon Department of Transportation (ODOT) signal pole type SM3, as shown on Standard Drawing TM651 *(ODOT 2014)* and provided in Appendix B. For this type of signal pole, the standard maximum base reaction under standard signal arm loads, as shown in TM650 *(ODOT 2014)* is listed in Table 4.1. The diameter selected for both test shafts was 0.9 m (36 in) according to ODOT Standard Drawing TM653. Per ODOT Traffic Structures Design Manual *(ODOT 2015a)* procedures for lateral load requirements, the Broms *(Broms 1964)* method was used to determine the embedded length of the shaft, equal to 4.0 m (13 ft); however, per current ODOT design procedures, torsion was not explicitly considered in sizing the length or diameter. Based on ODOT Standard Drawing TM653, the required steel reinforcement consisted of 8 – #8 longitudinal bars and #4 hoops at 152 mm (6 in) spacing with 457 mm (18 in) hoop lap length. Figure 4.1 illustrates the design of the test shafts.

Table 4.1: Standard maximum base reaction for SM3 (ODOT 2014)

Standard Maximum Base Reaction	Value
Axial, kN (kips)	15.5 (3.49)
Shear, kN (kips)	34.56 (7.77)
Moment, kN-m (kip-ft)	187.69 (138.43)
Torque, kN-m (kip-ft)	112.36 (82.87)

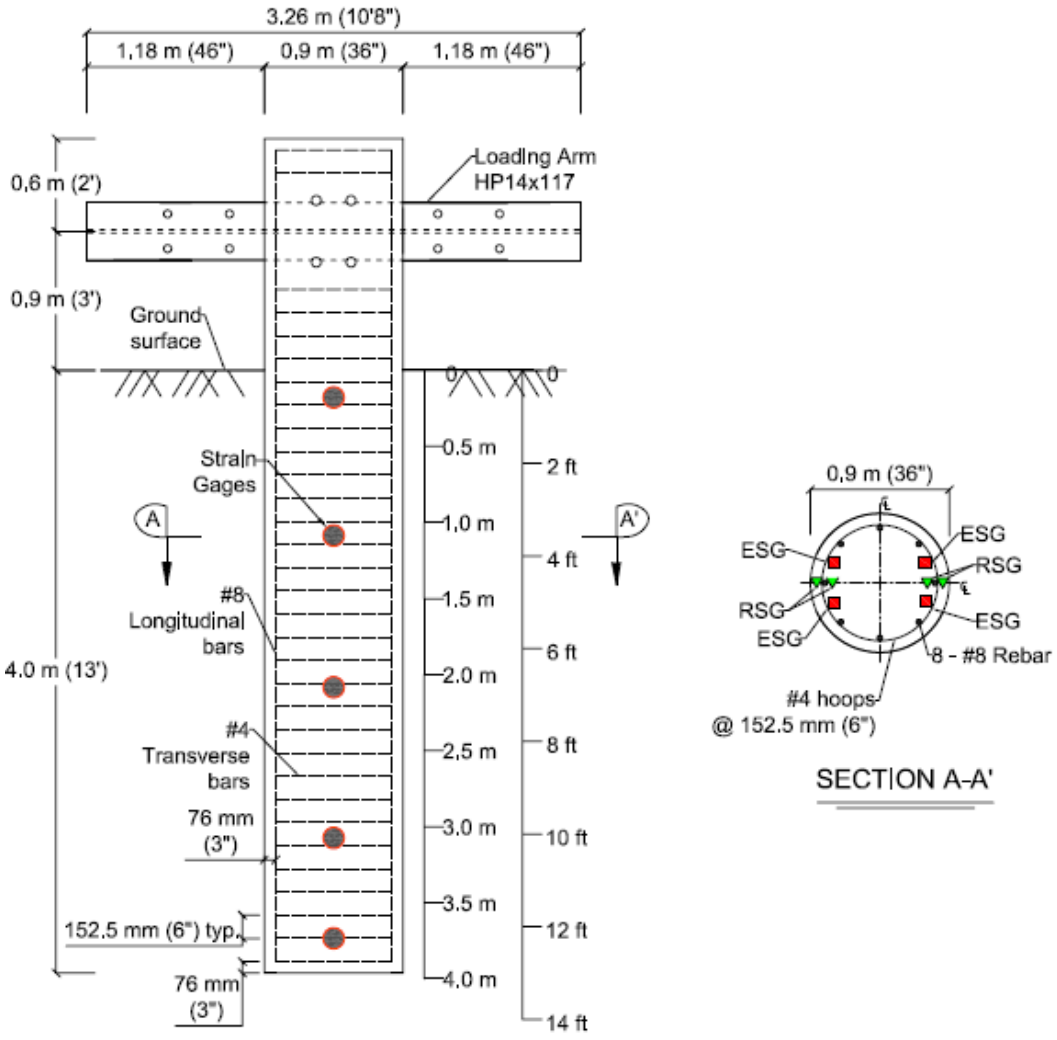

Figure 4.1: Schematic of drilled shaft elevation and cross-section of A-A'

To facilitate the application of torque to the test shafts, the shafts were designed with a total length of 5.5 m (18 ft), corresponding to a portion of the shaft with 1.52 m (5 ft) above the ground surface. Rotation was applied to the shafts using a displacement-couple applied to a 3.26 m (10 ft-8 in)-long steel HP 14x117 loading arm that was cast in the shaft, as shown in Figure 4.1. Hydraulic actuators, shown in Figure 4.2, were used to apply equal, but opposite, displacements to the loading arms. Based on the design, the total axial loads transferred to the test shafts embedded in the ground consisted of the summation of the self-weight of the shafts above ground surface, loading arms, and actuators. For each shaft, the axial load was approximately 50 kN (11 kips).

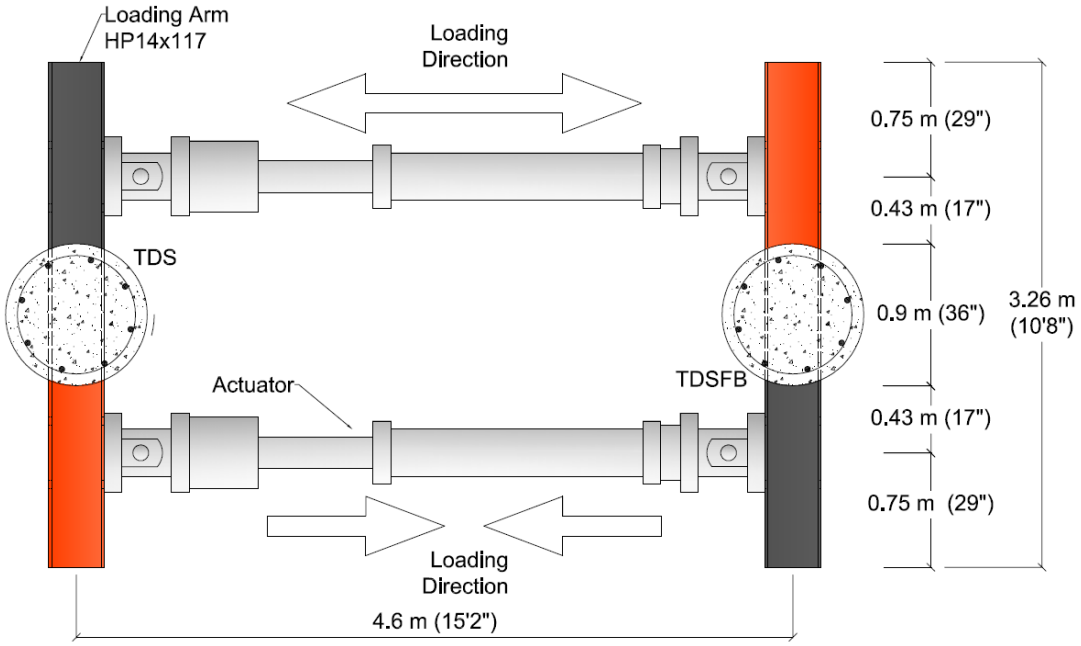

Figure 4.2: Plan view of torsion test

4.3 FABRICATION AND INSTRUMENTATION OF THE TEST SHAFTS

The reinforcement cages of the test shafts were constructed in the Hinsdale Wave Research Lab in accordance with the design requirements described previously. Then, concrete embedment strain gages (ESG) and resistance strain gages (RSG) were installed on the steel cages at five elevations, as shown in Figure 4.1. Each instrumented elevation consisted of two pairs of ESGs and two pairs of RSGs, for redundancy.

4.3.1 Fabrication of the Test Shafts

Plywood falsework was used to facilitate the construction of the rebar cages as shown in Figure 4.3. Eight longitudinal reinforcing bars were mounted onto the plywood boards for each steel cage. Then, hoops were tied to the longitudinal reinforcing bars at 152 mm (6 in) spacing. To achieve the required 76 mm (3 in) concrete cover, the outside to outside diameter of the steel cages was 762 mm (30 in) and were fitted with spacers in the field prior to installation.

Figure 4.3: Fabrication of a steel cage used in the test shafts

Sonotube concrete forms were used to form the shafts above ground surface. For each shaft, a 1.98 m (78 in) long sonotube was cut into two pieces at the location of loading arm (Figure 4.4a). Slots were cut to accommodate the loading arm on upper piece of sonotube, as shown in Figure 4.4b.

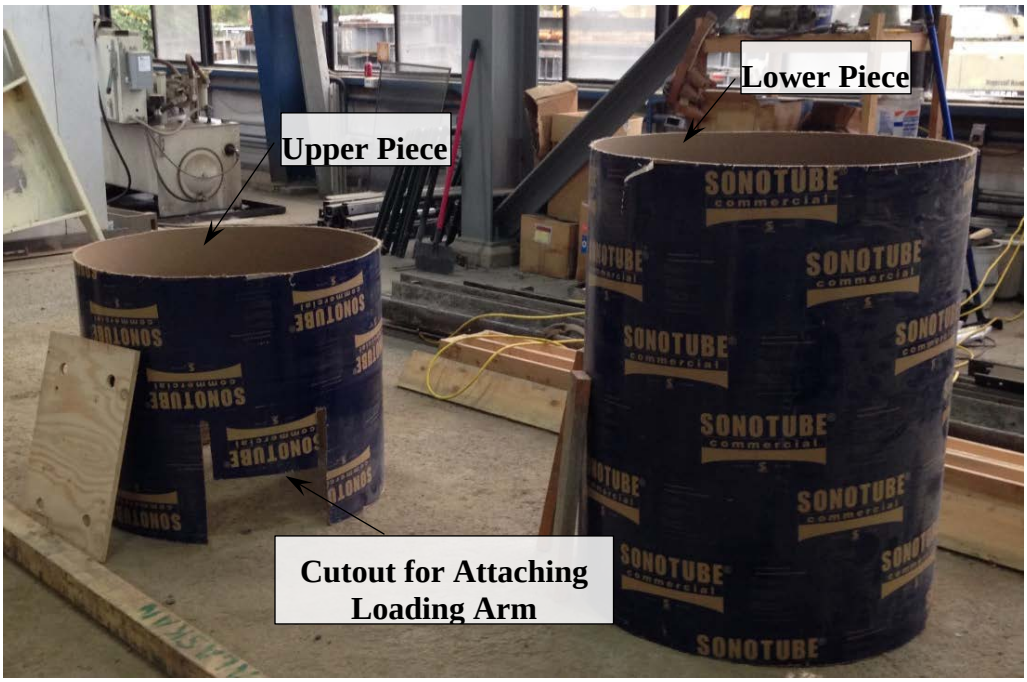

(a)

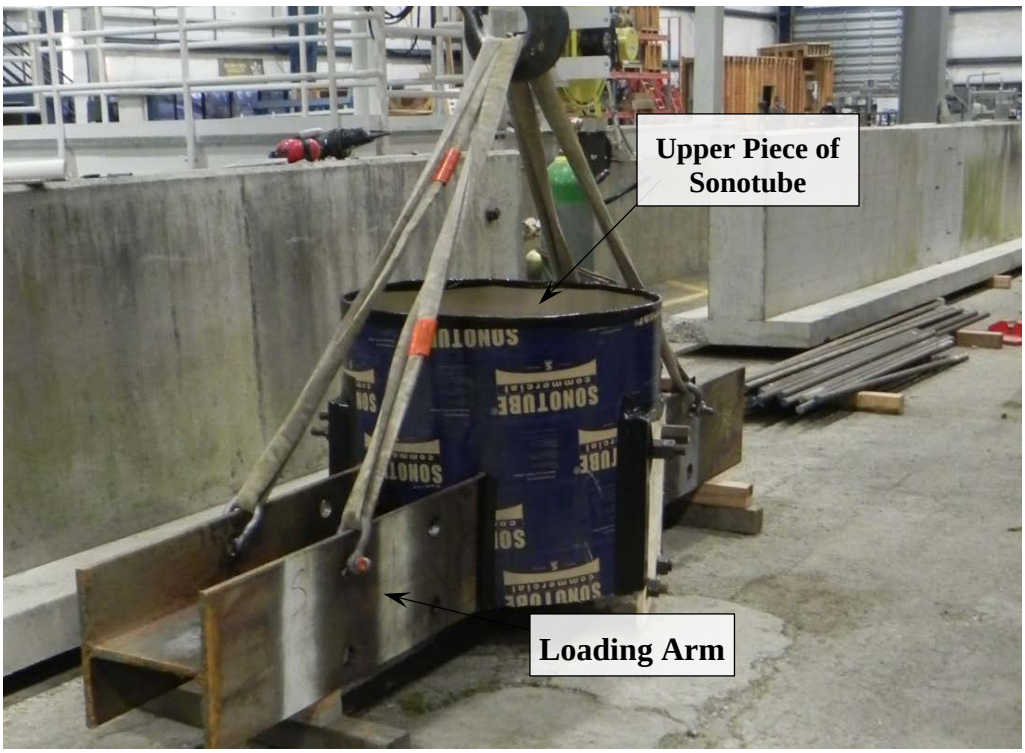

(b)

Figure 4.4: Round Sonotube concrete forms

The near-zero base shear condition for TDSFB was achieved by placing a layer of bentonite chips at the bottom of the shaft, and separating the chips from the shaft using a plywood board. The plywood separator was used to prevent mixing of the structural concrete with the bentonite, so that the hydrating concrete would not pull water from the swelled bentonite during curing. The plywood, as shown in Figure 4.5, was cut with a diameter of 6.35 mm (0.25 in) smaller than the shaft diameter so that the plywood could be easily lowered into the drill hole. To allow free water to pass through the plywood, 16 holes with the diameter of 25.4 mm (1.0 in) were drilled through the board.

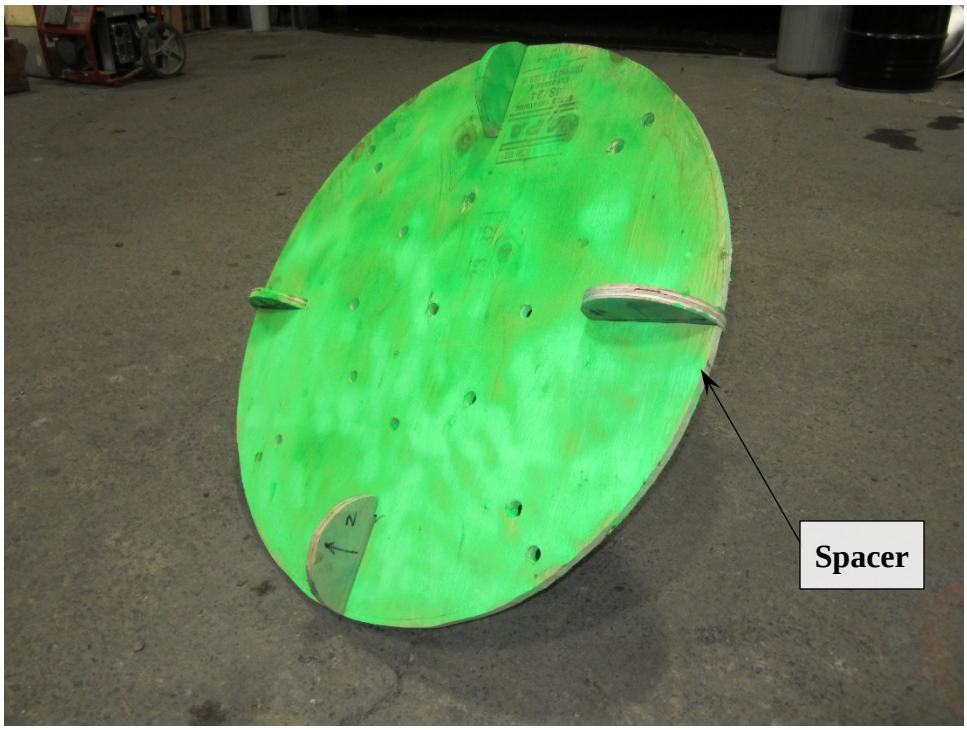

Figure 4.5: Plywood board used to separate bentonite toe and concrete for TDSFB

4.3.2 Instrumentation of the Test Shafts

Each shaft was instrumented with 20 RSGs, placed on the longitudinal bar to measure flexural strains. The RSGs were installed using the following procedure: (1) flatten and smooth the surface of the longitudinal bar at the proposed location for the RSG using a grinder; (2) produce cross-grain scratches on the area using wire meshes to improve the adhesion of the epoxy; (3) degrease the prepared surface using acetone; (4) install the RSG using Cyanoacrylate (Instant Adhesive); and (5) cover the RSG with a protective layer of M-Coat. Figure 4.6 and Figure 4.7 show the RSGs before being covered by M-Coat, and RSGs with the M-Coat protection. The model of the resistance strain gages used was FLA-5-11-5LT, which are manufactured by Tokyo Sokki Kenkyujo, Co. *(Tokyo Sokki Kenkyujo Co. Ltd. 2015)*. The strain limit is 50,000 με, and the gage factor is 2.13±1%.

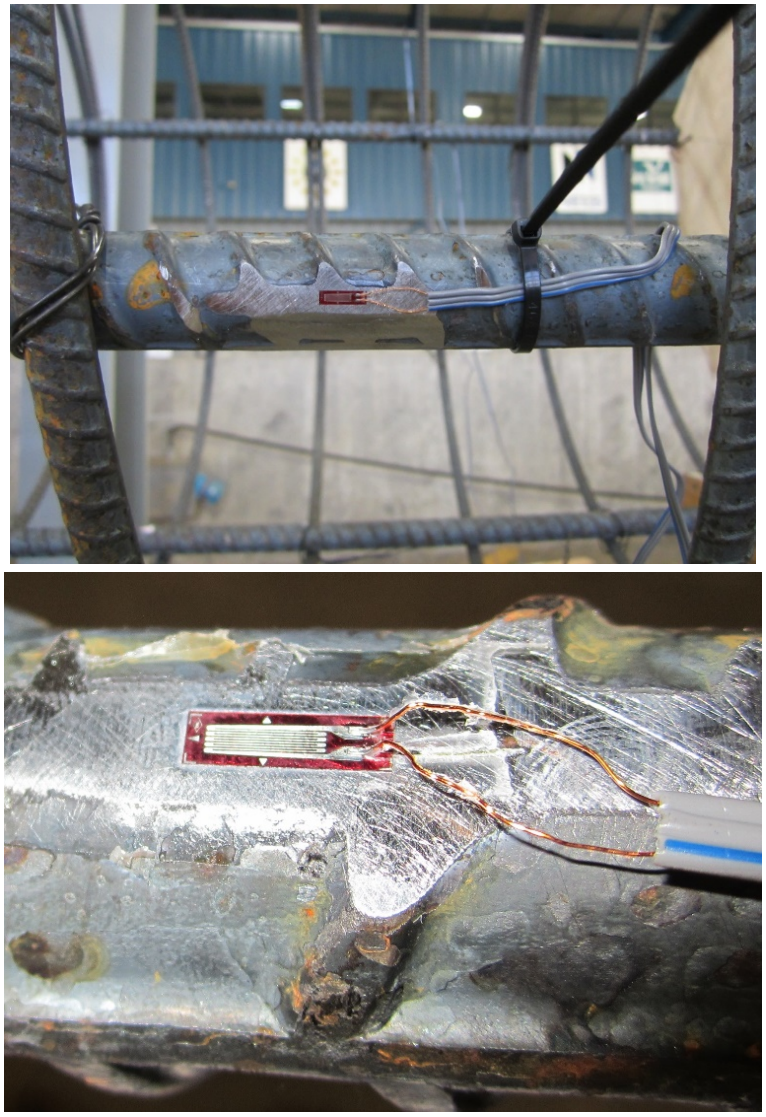

Figure 4.6: Photographs showing the RSG on a longitudinal bar

Each shaft was also instrumented with 20 concrete embedded strain gages (ESGs) at the same elevations as the RSGs. Geokon model 4200A-2 concrete embedded strain gages *(Geokon, Inc. 2015)* were chosen for this project. The range for each ESG is 3000 με with a resolution and accuracy of 1.0 με and ±3.0 με, respectively. The ESGs were installed with a 45° inclination to the longitudinal axis to measure the torsionally-induced shear strains, as shown in Figure 4.7.

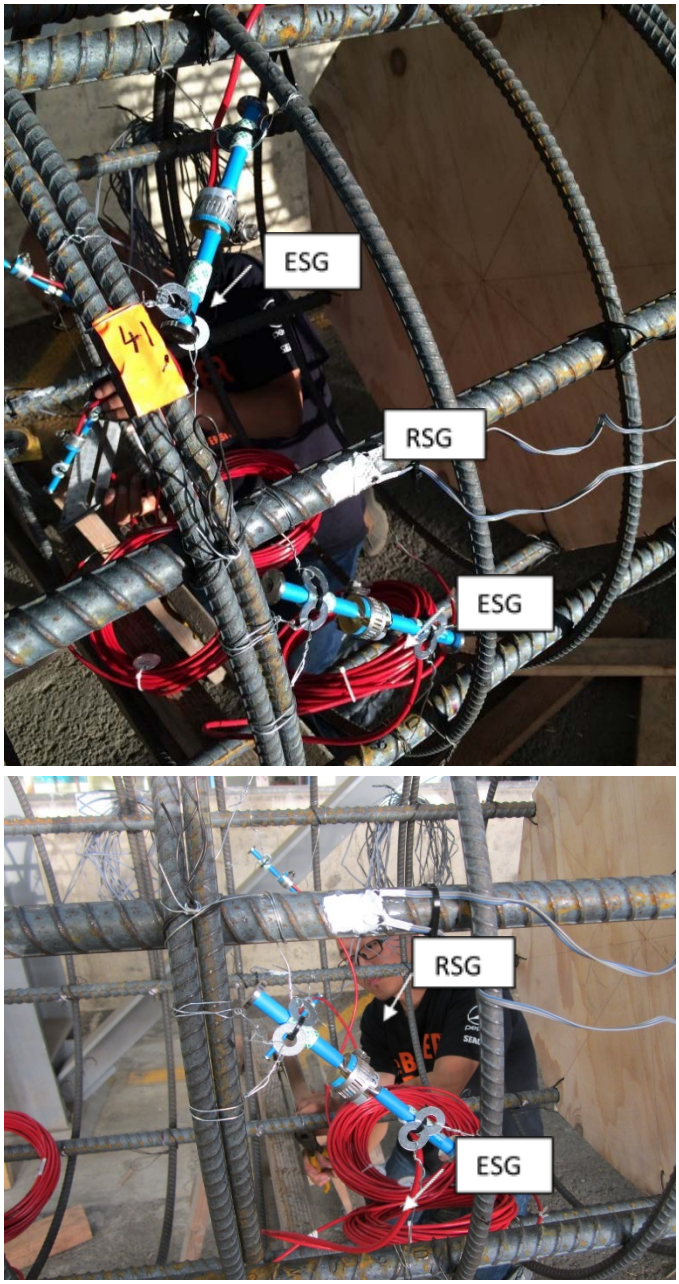

Figure 4.7: Photographs of the ESGs and a protected RSG

For each test shaft, two string-potentiometer installations were attached to each loading arm to monitor the displacement of the loading arms and determine the individual rotation of each shaft as shown in Figure 4.8. Two sets of load cells were used to measure the forces developed from the displacement imposed by the actuators. The torque exerted at the shaft head was calculated as the product of the moment arm and measured force.

Figure 4.8: Schematic of string-potentiometers arrangement

4.4 CONSTRUCTION OF TEST SHAFTS

Test shafts were installed on October 31, 2014 by PLI Systems, Inc. The dry method of construction was used for both test shafts. Figure 4.9 displays the excavation for one of the test shafts using excavator-mounted drilling rig. No caving was observed during the excavation of TDSFB; and some minor raveling of the saturated sand was observed for TDS. The drilled holes of TDSFB and TDS are shown in Figure 4.10 prior to cleaning the bottom of each shaft. Shaft TDSFB was over-drilled by 152 mm (6 in), and then the bentonite chips were placed evenly across the bottom of the cavity, as shown in Figure 4.11. During the excavation of TDS, the hole was accidently overdrilled by 152 mm (6 in). Figure 4.12 shows the placement of steel cages for TDS and TDSFB. Wheel spacers were used on both steel cages to help center the cage within the augered cavity. The plywood separator (in green color), as shown in Figure 4.12b, was attached at the bottom of steel cage of TDSFB. For TDS, the lower and upper pieces of sonotube were assembled together before being placed over the reinforcement cage the hole and pushed 0.46 m (18 in) below ground, as shown in Figure 4.13a. However, it was challenging to handle the ESG and RSG cables using this method. For TDSFB, the lower piece of sonotube was pushed into the hole first; and then the cables for the ESGs and RSGs were easily managed. Finally, the upper piece of sonotube with loading arm was mounted onto the lower piece sonotube, as shown in Figure 4.13b.

Figure 4.9: Excavating hole using excavator mounted drilling machines

(a) **(b)**

Figure 4.10: Drilled holes of (a) TDSFB and (b) TDS before the bottom was cleaned

Figure 4.11: Placing bentonite chips at the bottom of excavation of TDSFB following clean-out

(a) **(b)**

Figure 4.12: Placing the steel cages for shafts (a) TDS, and (b) TDSFB

(a) **(b)**

Figure 4.13: Placing sonotube concrete forms for (a) TDS and (b) TDSFB

The concrete mix design used for the fabrication of the test shafts was based on the Oregon Standard Specifications for Construction (*ODOT 2015b*) and was the best match developed by the concrete company supplying the mix. Unfortunately, the exact range in slump could not be matched with the concrete mix design. Table 4.2 summarizes the selected concrete mix design. The measured slump of the fresh concrete was within the design range, but smaller than the

Oregon Standard Specifications for Construction (8 ± 1.5 in or 203 ± 38 mm). However, the concrete showed good workability during construction, which did not influence the final consolidation and finishing as revealed following exhumation of the shaft. Concrete was placed within the augered cavity using a tremie pipe. Selected properties of the fresh concrete delivered to the site were measured on a truck-by-truck basis. The measured properties of the fresh concrete is summarized in Table 4.3. The slump of the concrete from each truck was within the required design range. However, the air content of concrete from Truck-2 is higher than the designed value.

Table 4.2: Concrete mix design

Mix Number	031-7HN3U2S0
Comp. Strength 28 days, MPa (psi)	28 (4,000)
Slump, mm (in)	213 ± 50 (7 ± 2)
Air Content (%)	5% ± 1.5%
Plastic Unit Weight, kg/m^3 (pcf)	2225 (138.9)
Maximum w/c Ratio	0.48
Fly Ash	10.6%
Maximum Aggregate	#89 aggregate

Table 4.3: Measured properties of fresh concrete

	Truck-1	**Truck-2**
Temperature of Concrete	20.6°C	18.9°C
Unit Weight, kg/m^3 (pcf)	2285 (142.6)	2163 (135.0)
Slump, mm (in)	140 (5.50)	159 (6.25)
Air Content (%)	3.5%	9%

Six concrete cylinders (4-in diameter by 8-in long) were collected from each truck to test the compressive strength at 14 and 28 days, as well as on the test day. Table 4.4 presents a summary of the compressive tests results. It is observed that the measured 28-day compressive strength, 42.5 MPa (6,158 psi) was much greater than the design 28th day compressive strength, 28 MPa (4,000 psi). The strength on the day of the test was slightly higher, and represents the strength on day 45. Figure 4.14 shows the test shafts, as well as the 16-channel multiplexers for observation of the ESGs, approximately one week following construction. The cables of the RSGs were spliced and connected with the data logger several weeks following construction.

Table 4.4: Concrete compressive strength

Time	Compressive strength, MPa (psi)
14th day	35.2 (5,106)
28th day	42.5 (6,158)
Test day, 45th day	45.1 (6,537)

Figure 4.14: Test shafts after construction

4.5 SUMMARY

The test shafts were designed to support signal pole type SM3 based on ODOT Standard Drawing TM653 (Appendix B). The reinforcing cages of the test shafts were constructed and instrumented in the Structural Engineering Research Lab. Each shaft was instrumented using 40 strain gages distributed over five depths to observe torsional and flexural strains, string-potentiometers to observe displacement and rotation, and load cells to observe the applied torque at shaft head. The dry method of construction was used for both test shafts. To create near-zero base shear condition for shaft TDSFB, bentonite chips and a plywood separator were placed evenly across the bottom of the cavity. The loading test protocol, results, and analyses are presented in the following chapter.

5.0 TEST RESULTS AND INTERPRETATION

5.1 OVERVIEW

The torsional loading test (Figure 5.1) was conducted on December 15, 2014, during a strong storm, ideal conditions for evaluating the performance of signal pole foundations in Oregon. The loading protocol is presented in Section 5.2. The technique and method used to process the string-potentiometer data and embedded strain gage data are given in Section 5.3 and 5.4, respectively. To determine the as-built condition and the variation of diameter along the test shafts, both of the shafts were exhumed, cleaned, and as-built dimensions measured, as presented in Section 5.5. The response of the test shafts under quasi-static loading is discussed in Section 5.6. Section 5.7 compares the ultimate torsional resistance observed from quasi-static loading test with the results using several design approaches. Some findings from the cyclic loading test for both test shafts are presented in Section 5.8.

Figure 5.1: Torsional loading test in progress

5.2 LOADING PROTOCOL

Rotation of the shafts was applied using two hydraulic actuators operated in displacement control, as shown in Figure 4.2. Displacements were held at 5 minute time intervals at each target shaft rotation to ensure stabilization of strains and sufficient time for the collection of strain gage data. The loading test commenced with a target of 0.1° of incremental rotation at the soil-shaft interface. However, the lens of medium dense sand located near the base of TDS prevented significant rotation of this shaft, and the rotation of TDSFB was used to guide the loading procedure. After the rotation of TDSFB reached about 1.75°, the specified incremental rotation was increased to 0.5° until 5° of total rotation. Then, the incremental rotation was increased to 1° until about 13° of total rotation was achieved. The duration of the test to this point was approximately three hours.

Thereafter, the shafts were unloaded to achieve a zero load condition, and the zero-load rotation was noted. Then, a series of cyclic loads were applied between 13° and the zero-load rotation. There were three 5-minute time intervals after the 1st, 6th, 10th, and 20th loading cycle, respectively, to ensure stabilization of strains and sufficient collection of strain gage data. During the loading test, the sampling rate of the RSGs, load cells and string-potentiometers was three samples per second. Because the ESGs were of the vibrating wire type, the sampling rate was considerably slower, with 2 minutes required to sample the forty ESGs (i.e., 3 seconds per gage in series).

5.3 DATA SMOOTHING OF STRING-POTENTIOMETER DATA

String-potentiometers were used to monitor the rotation of the loading arms by measuring the displacement of loading arm at two locations per shaft. To reduce the observed noise in the string-potentiometer data, the observed displacements were smoothed using a weighted smoothing function given by:

$$S_j = \frac{1}{16}\left(Y_{j-3} + 2Y_{j-2} + 3Y_{j-1} + 4Y_j + 3Y_{j+1} + 2Y_{j+2} + Y_{j+3}\right) \quad \textbf{(5.1)}$$

where S_j = the j^{th} point in the smoothed data, Y_j = the j^{th} point in the original data, j = 4 to n-3, and n is the total number of points in the recorded data. Figure 5.2 shows an example of the string-potentiometers data smoothing for the string-potentiometer east of TDSFB. Shaft rotations were then computed directly, and independently, using the smoothed loading arm displacement data.

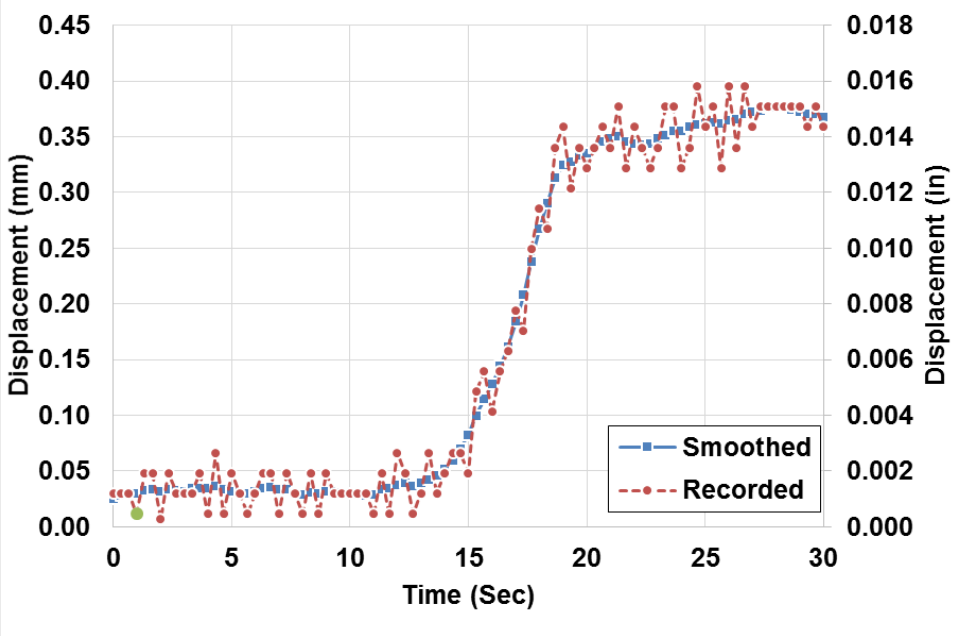

Figure 5.2: String-potentiometers data smoothing

5.4 INTERPRETATION OF MEASURED TORSIONAL SHEAR STRAINS

The methodology for processing the torsional strains was derived from mechanical shafts subjected to torsion, as shown in Figure 5.3a (*Gere and Timoshenko 1997).* For the shaft in Figure 5.3a, the stress element abcd is in a state of pure shear (Figure 5.3b) with magnitude τ. Since the strain gages installed in the shaft were inclined 45^{o} from the longitudinal axis, a wedge-shaped element with a 45° inclination taken by cutting stress element *abcd*, as shown in Figure 5.3c, was used to form the representative element for analysis. Due to force equilibrium on the wedge-shaped element, the stresses ($\tau_{45°}$ and $\sigma_{45°}$) on the inclined face are given by:

$$\tau_{45^o} = 0, \quad \sigma_{45^o} = \tau \tag{5.2}$$

Similarly, the stresses $\tau_{-45°}$ and $\sigma_{-45°}$ can also be obtained:

$$\tau_{-45^o} = 0, \quad \sigma_{-45^o} = \tau \tag{5.3}$$

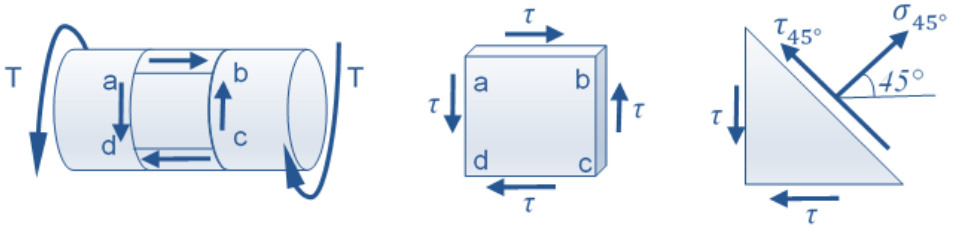

(a) **(b)** **(c)**

Figure 5.3: Analytical model for the assessment of shearing strains: (a) a shaft subjected to torsion, (b) a representative stress element, and (c) a wedge-shaped element *(modified from Gere and Timoshenko 1997)*

For an element inclined at 45° (Figure 5.4), the relationship between the strains ($\varepsilon_{45°}$ and $\varepsilon_{-45°}$) and shear stresses ($\sigma_{45°}$ and $\sigma_{-45°}$), is given by:

$$\varepsilon_{45^o} = \frac{\sigma_{45^o}}{E} - \frac{\nu\sigma_{-45^o}}{E} = \frac{\tau}{E} + \frac{\nu\tau}{E} = \frac{\tau}{E}(1+\nu) \quad \textbf{(5.4)}$$

$$\varepsilon_{-45^o} = -\varepsilon_{45^o} = -\frac{\tau}{E}(1+\nu) \quad \textbf{(5.5)}$$

where ν = Poisson's ratio and E = the Young's modulus, which was estimated based on the ACI 318-05 model *(ACI 318 2005)* using the concrete strength at the test day. In this element, the strain $\varepsilon_{45°}$ and $\varepsilon_{-45°}$ are equal to the strains measured using the ESGs. Therefore, the shear stresses at the location of ESGs can be obtained by:

$$\tau = \frac{E\varepsilon_{45^o}}{(1+\nu)} \quad \textbf{(5.6)}$$

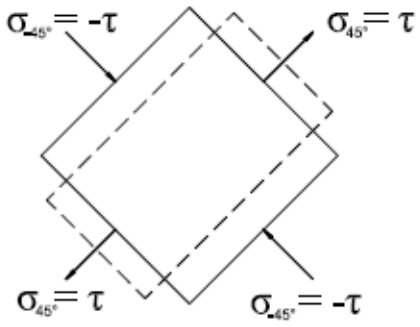

Figure 5.4: Model inclined element (modified from Gere and Timoshenko 1997)

Because the embedded strain gages were attached to the hoop reinforcements (Figure 4.1b, Figure 5.5), which were 76 mm (3 in) from the surface of the shaft, the strain directly at the soil-shaft interface was not measured. It was assumed that the shear stresses were distributed linearly with distance away from the center of the section, as shown Figure 5.5, as is commonly assumed

in structural mechanics applications *(Hibbeler, 2013)*. The maximum shear stress at the shaft surface is given by:

$$\tau_{max} = \frac{r}{\rho}\tau \tag{5.7}$$

where r = radius of shaft = 0.45 m (18 in), ρ = the distance from center to strain gages = 0.38 m (15 in), τ = the shear stresses at the location of ESGs estimated using Equation (3). The internal torque at the location of each ESG can then be computed by:

$$T = \frac{\tau_{max} J}{r} \tag{5.8}$$

where J = polar moment of inertia, which is given by

$$J = \pi r^4 / 2 \tag{5.9}$$

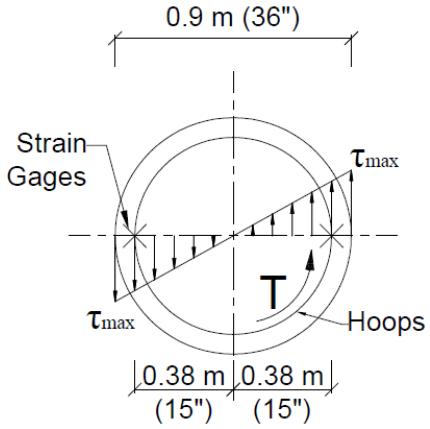

Figure 5.5: Shear stress distribution at the cross section of shaft

5.5 AS-BUILT CONDITION OF SHAFT

To accurately investigate the torsional load transfer, the as-built dimensions of the shafts were necessary, particularly with respect to the diameter of shaft given the large role of shaft resistance in the torsional capacity. After the torsion tests were completed, the test shafts were exhumed and pressure–washed, and the dimensions of the shafts were measured and recorded.

Figure 5.6 shows test shaft TDSFB being lifted from the excavation. Figure 5.7 and Figure 5.8 show the surface condition of the test shafts and the base condition of the test shafts, respectively. For TDS, about 0.3 m (1.0 ft) of the concrete appeared to have been contaminated with the clean to silty sand that was encountered during excavation of this shaft. The four ESGs that were located within 228 mm (9 in) of the toe appeared to have been affected by the poor quality material encapsulating them, as confirmed in the data described below. Indeed, the bottom 100 to 250 mm (4 to 10 in) of the longitudinal steel was exposed and bent following tipping by the excavator and removal by the crane. A portion of the base of TDSFB was also

exposed following exhumation. Based on the inspection of the shaft, it appeared that some amount of bentonite traveled between the small-diameter holes in the plywood base to mix with the concrete, as the concrete showed signs of bentonite contamination. The concrete was soft and was easily chipped with a screwdriver. One ESG was just barely exposed following removal; the effect of the softer base concrete was also apparent in the strain gage data as described subsequently.

Figure 5.6: Picking of test shaft TDSFB from the post-test excavation.

(a)

(b)

Figure 5.7: Exhumed test shaft (a) TDS and (b) TDSFB

(a) **(b)**

Figure 5.8: Shaft base of (a) TDS and (b) TDSFB

After the shafts were pressure washed, the perimeters were measured along the shafts for about every 0.3 m (1.0 ft). Figure 5.9 shows the diameter profile along the test shafts. The upper portion of the shafts, from shaft head to 1.98-m (78-in), had a uniform diameter due to the use of sonotubes. The concrete was pushed out of the bottom of the sonotubes during placing the concrete, which caused the increase of diameter close to the end of the sonotubes. The diameter at the bottom of both shafts increased slightly with depth.

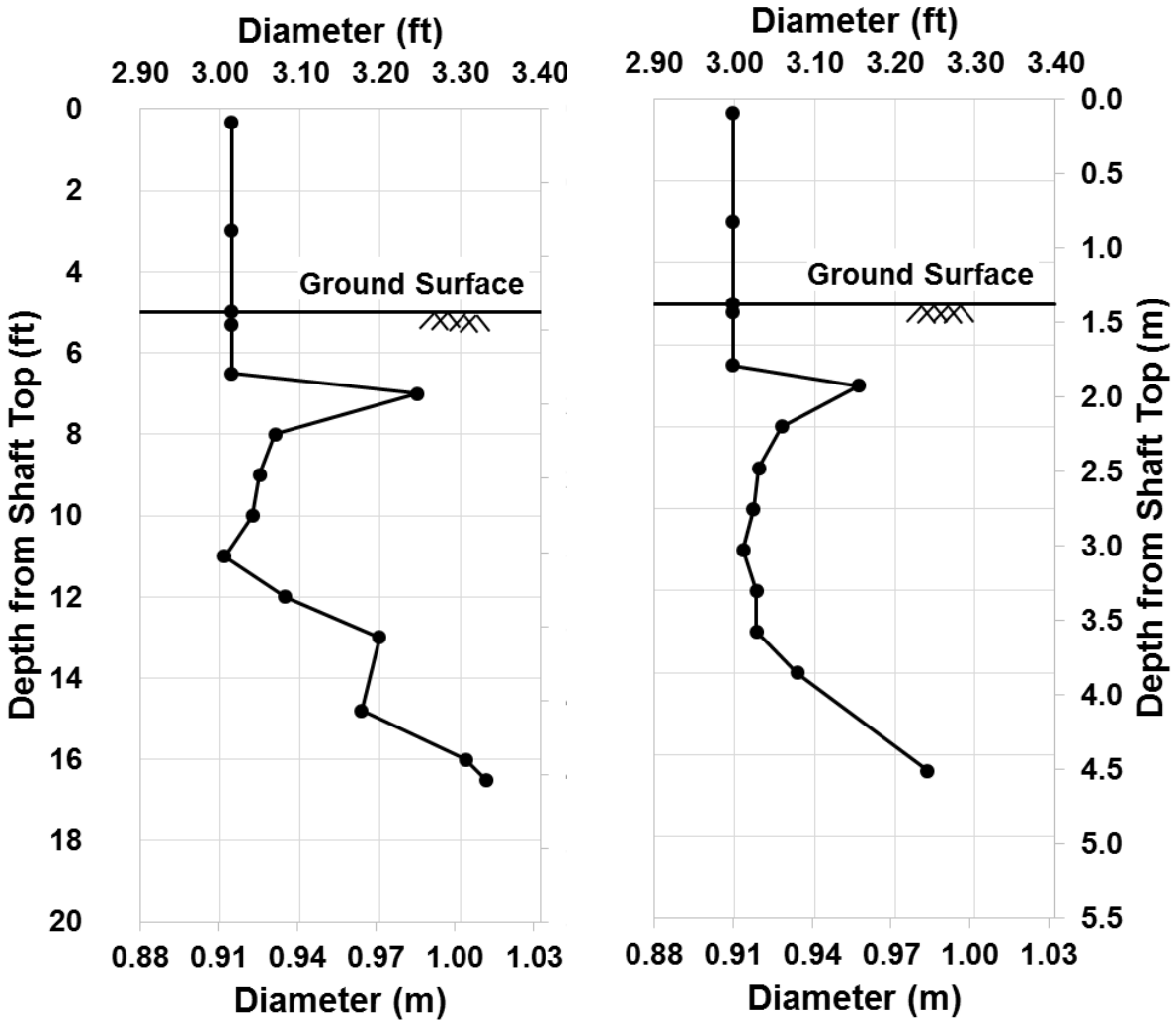

(a) **(b)**

Figure 5.9: Diameter along the test shaft (a) TDS and (b) TDSFB

5.6 QUASI-STATIC LOADING OF THE TEST SHAFTS

The quasi-static, monotonic loading test lasted approximately three hours. At the end of the test TDSFB shaft rotated approximately 13°, whereas TDS shaft only rotated about 0.11° as described previously. The following discussion presents the results of the quasi-static loading test.

5.6.1 Torque and Rotation Observed at Shaft Head

Figure 5.10 shows the measured torque-rotation response for TDSFB and TDS under quasi-static loading. In this figure, the applied load and rotation at the head of test shafts were measured directly using load cells and string-potentiometers, respectively. The torque at the shaft head was computed as the product of the moment arm and measured load. The torsional resistance for TDSFB transitioned from the initial stiff response to a softer response between rotations of approximately 0.2 to 0.5, and it became fully-mobilized (i.e., achieved the ultimate resistance) at a rotation of approximately 1.0°. The ultimate resistance was equal to 185 kN m (136 kip ft). The torsional resistance of TDSFB increased slightly due to change of loading rate at approximately rotation of 2° and 5° for shaft TDSFB, which is consistent with the strain rate effect on the undrained shear strength of plastic soils *(Sheahan et al. 1996)*. The data for the first 1.75° rotation of TDSFB as well as the data for the first 0.1° rotation of TDS are presented in Figure 5.11. However, the torsional resistance of TDS was not fully mobilized during the test, indicating that TDS had higher torsional capacity as compared to TDSFB due to the difference in soil profile.

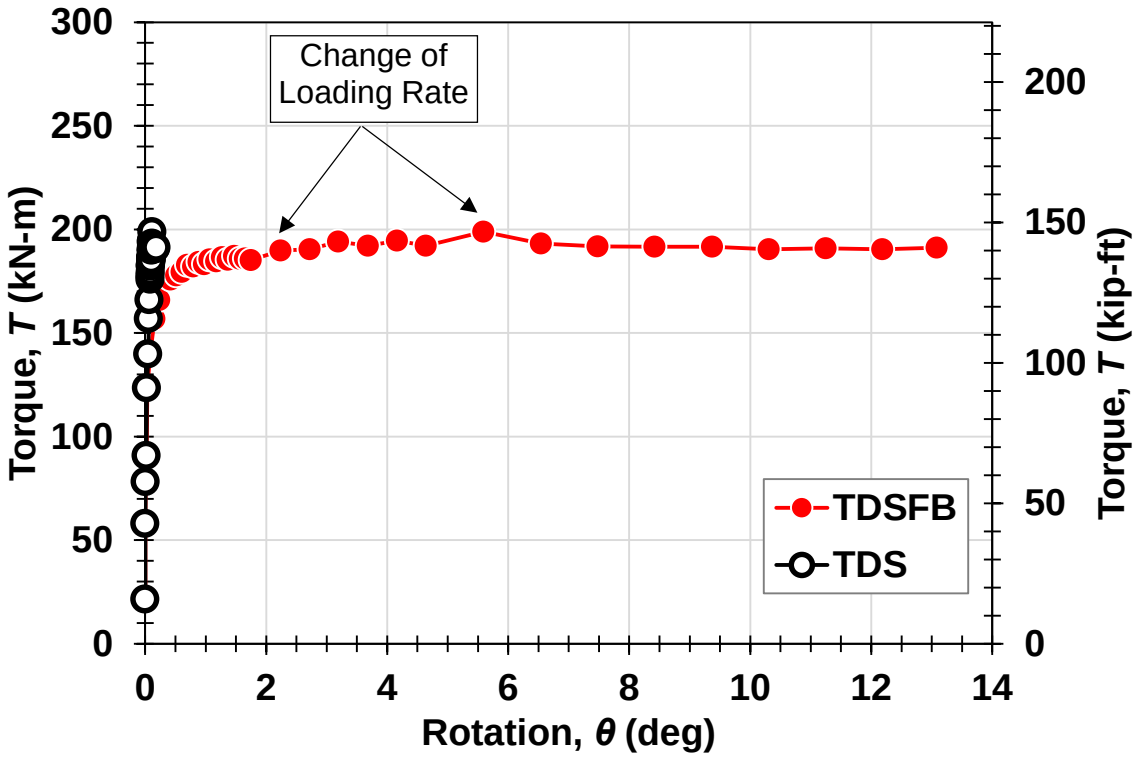

Figure 5.10: Measured relation between torque and rotation for Shaft TDS and TDSFB

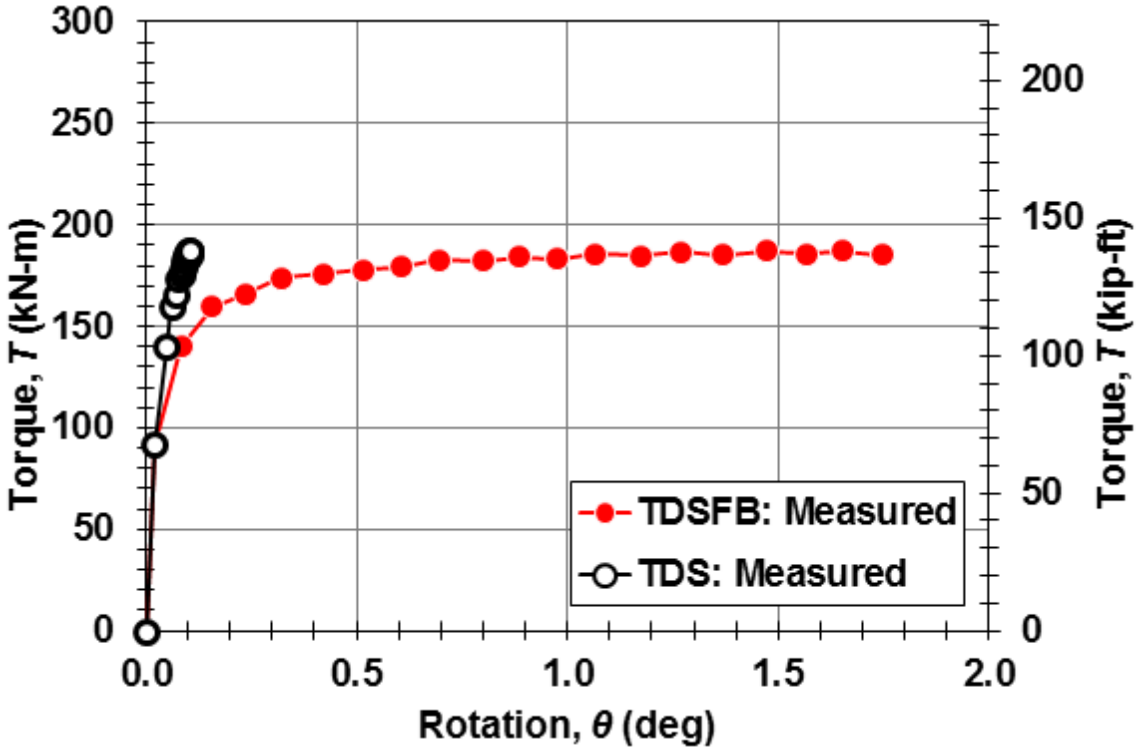

Figure 5.11: Torque–rotation response for both shafts and with rotation of TDSFB less than 1.75°. This corresponds to a rotation of TDS of less than 0.1° for the same magnitudes of torque.

The relationship between torque and rotation of TDSFB appeared well-modeled by a hyperbolic curve, as shown in Figure 5.12a, with R2 larger than 0.9999. Figure 5.12b shows the comparison between the measured and predicted response using the hyperbolic model. The average bias (i.e., the ratio of the measured and the predicted data) is 1.005; and the coefficient of variation of the bias is 0.009. Therefore, the hyperbolic model was used to explore the possible ultimate torsional resistance of TDS for comparison to an alternate ultimate torsional resistance estimate (described subsequently). Figure 5.13 compares the available torque-rotation data in hyperbolic space to a fitted line and shows the comparison between the measured and predicted response using the hyperbolic model. The average bias and the coefficient of variation are 0.9998 and 0.03, respectively. This indicates that the torsional response of TDS could be described by a hyperbola. The back-transformed hyperbolic curve is plotted against the observed torque-rotation response of TDS in Figure 5.14, and extrapolated to the expected value of its ultimate torsional resistance, equal to 250 kN-m (184 kip-ft). The validity of this estimate is explored in more detail below.

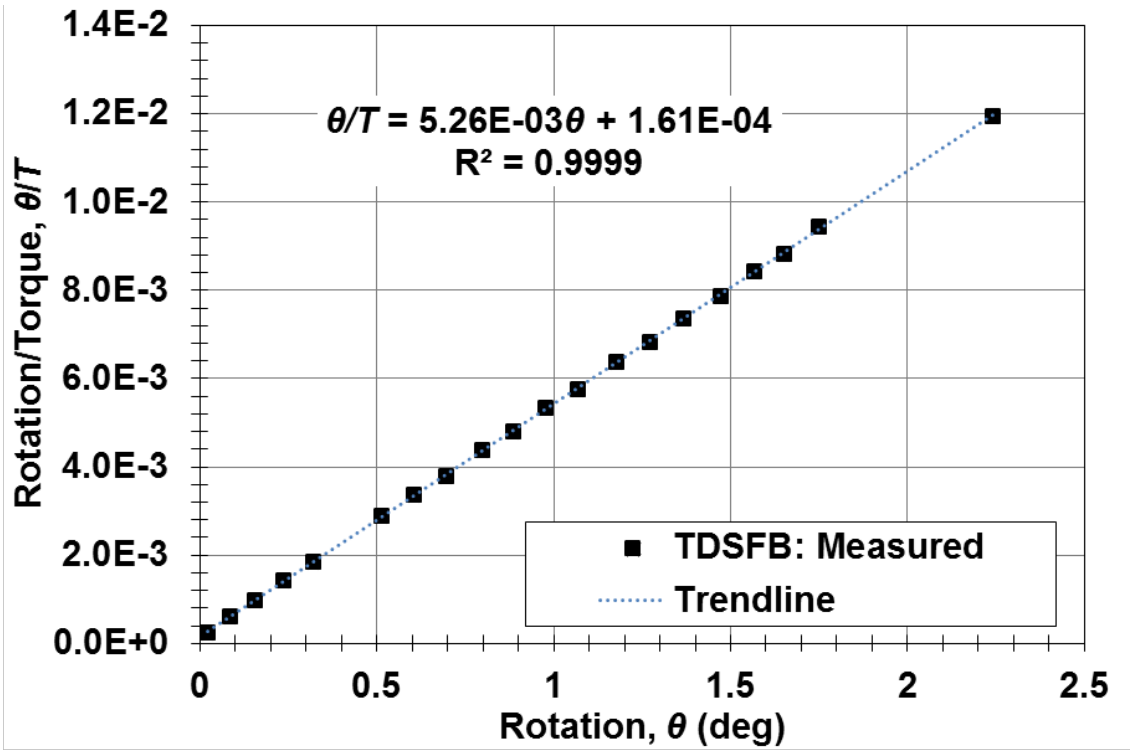

(a)

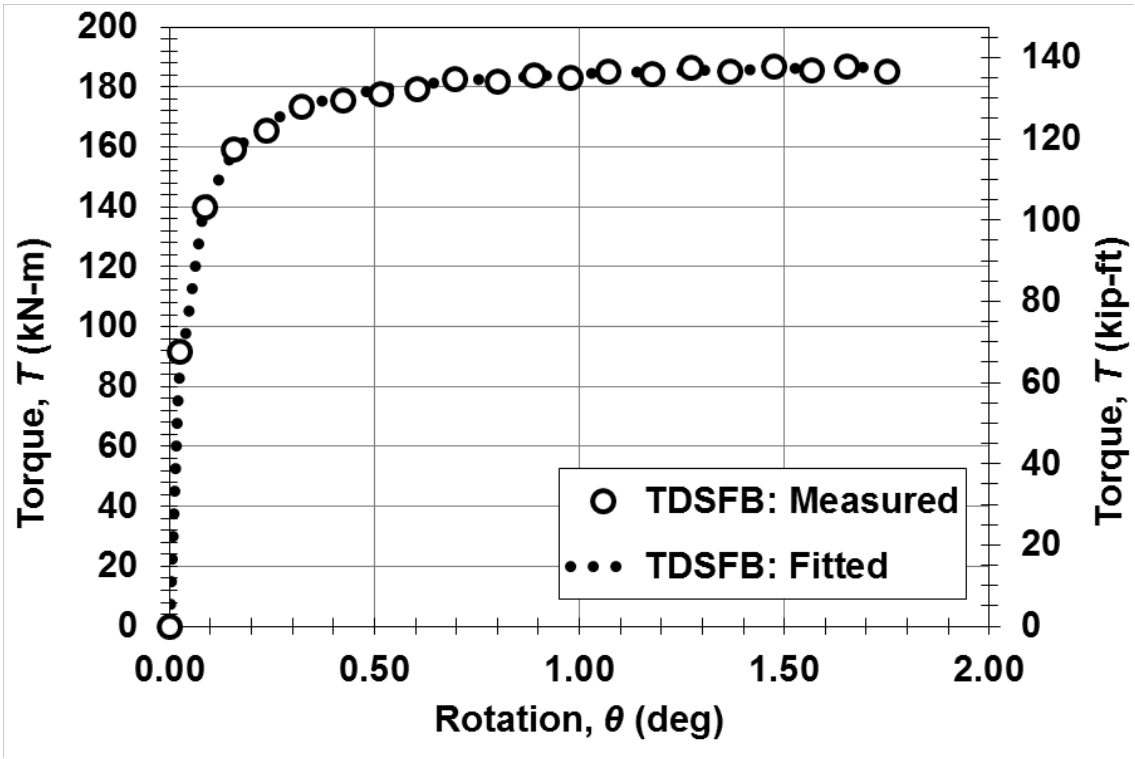

(b)

Figure 5.12: Hyperbolic model for TDSFB: (a) observed torque-rotation response in hyperbolic space and fitted hyperbolic model and (b) comparison between predicted and measured response

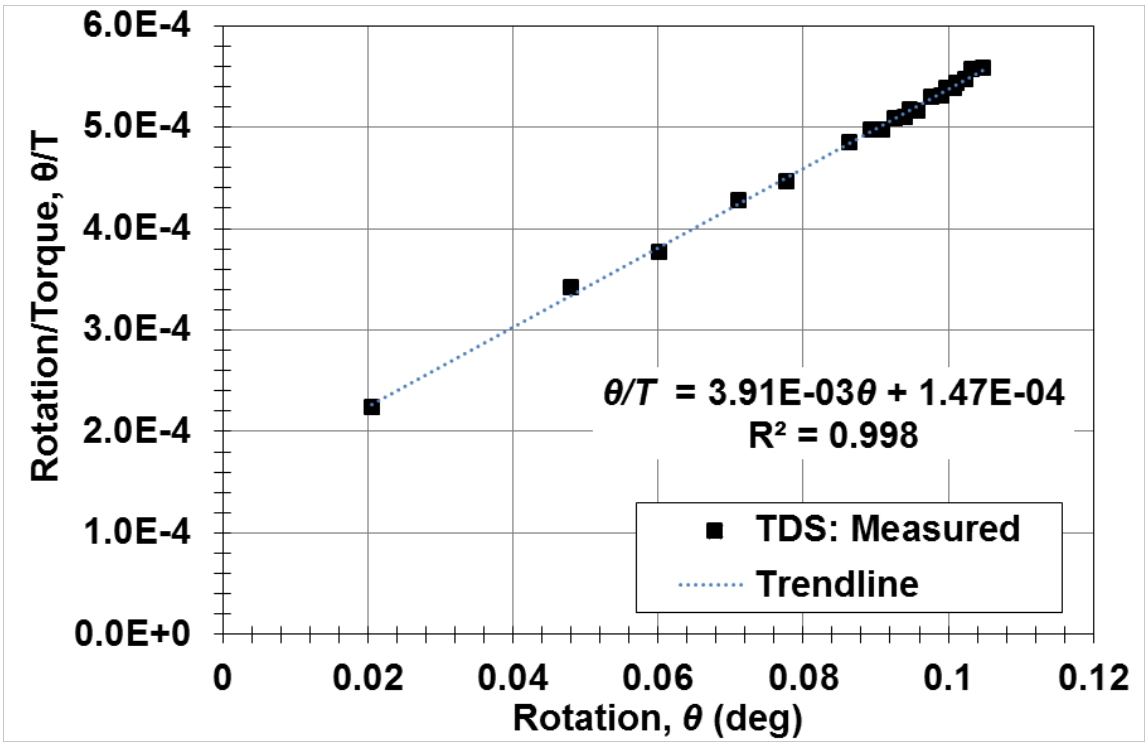

(a)

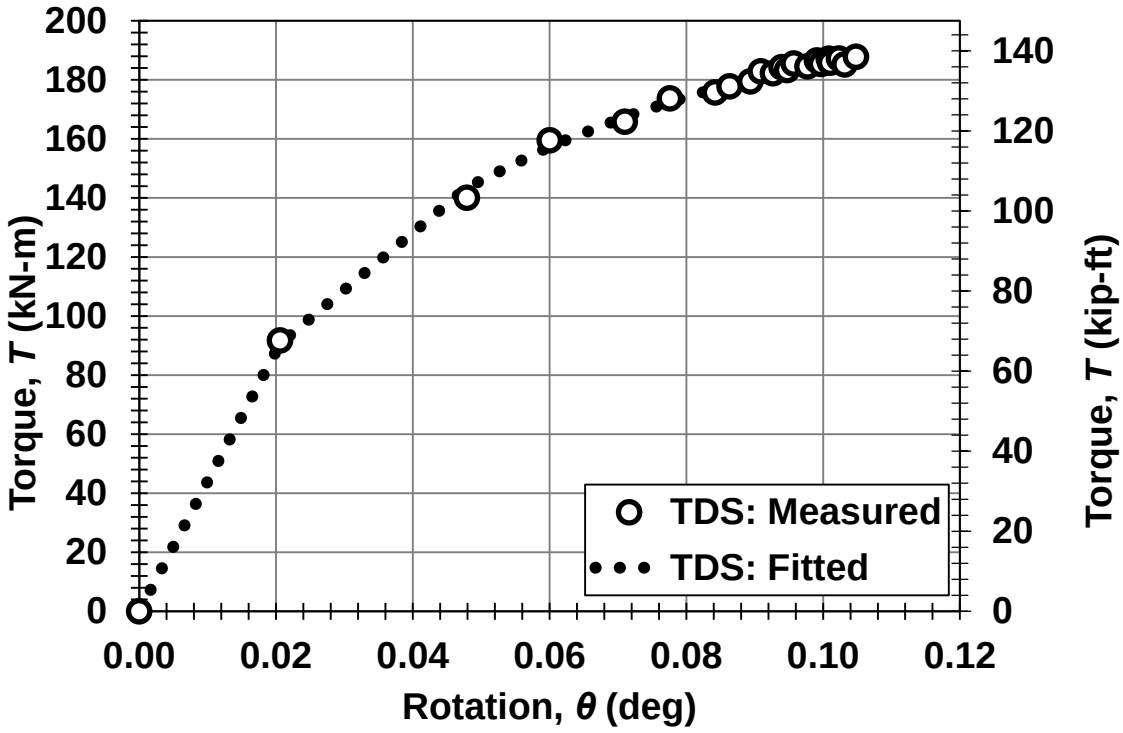

(b)

Figure 5.13: Hyperbolic model for TDS (a) observed torque-rotation response in hyperbolic space and fitted hyperbolic model and (b) comparison between predicted and measured response

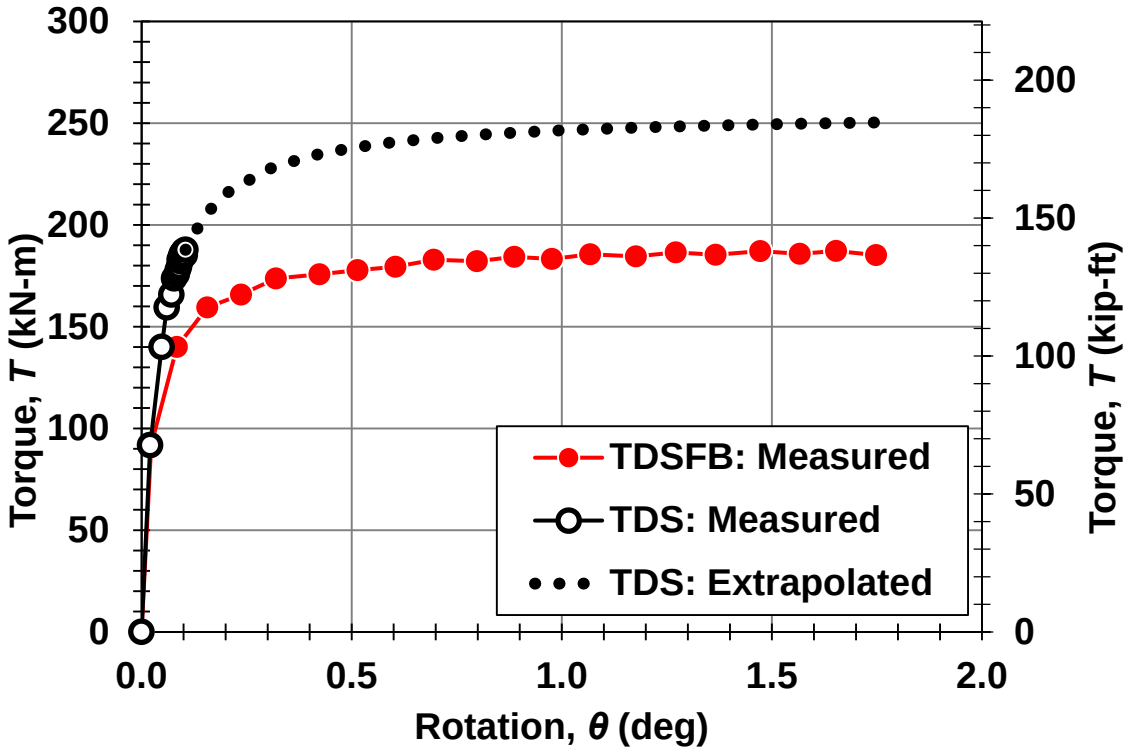

Figure 5.14: Relation between imposed torque and rotation

5.6.2 Torsional Load Transfer

The torsion along TDSFB at 1.75° of head rotation is shown in Figure 5.15b, including the torque at the shaft head, the internal torque estimated from the shear strain measured at instrumented depths, and the torque at shaft bottom. Figure 5.15a shows the measured torsion along TDS when the head rotations of TDS was 0.1°.

Based on the data observed from the bottom-most ESGs, as well as the condition of the gages upon exhumation of the drilled shafts, it was determined that the ESG data recorded from the bottom-most locations were unreliable; these are indicated as “unreliable gages” in Figure 5.15. Owing to the failure of the strain gages at the toe of shaft TDSFB, and construction with a bentonite base, the torsional resistance was assumed to be zero at the base of TDSFB. The toe resistance of TDS was estimated by:

$$T_5 = \left(\pi \cdot \frac{D^2}{4}\right) \cdot \alpha \cdot s_u \cdot \frac{D}{3} = \alpha \cdot s_u \cdot \left(\frac{\pi \cdot D^3}{12}\right) \qquad \textbf{(5.10)}$$

with s_u = 34 kPa. The cone tip resistance profile for each shaft is also included in this Figure 5.15 (with imperial units in Figure 5.16) to illustrate the correlation between the cone tip resistance and the torsional load transfer along the shaft.

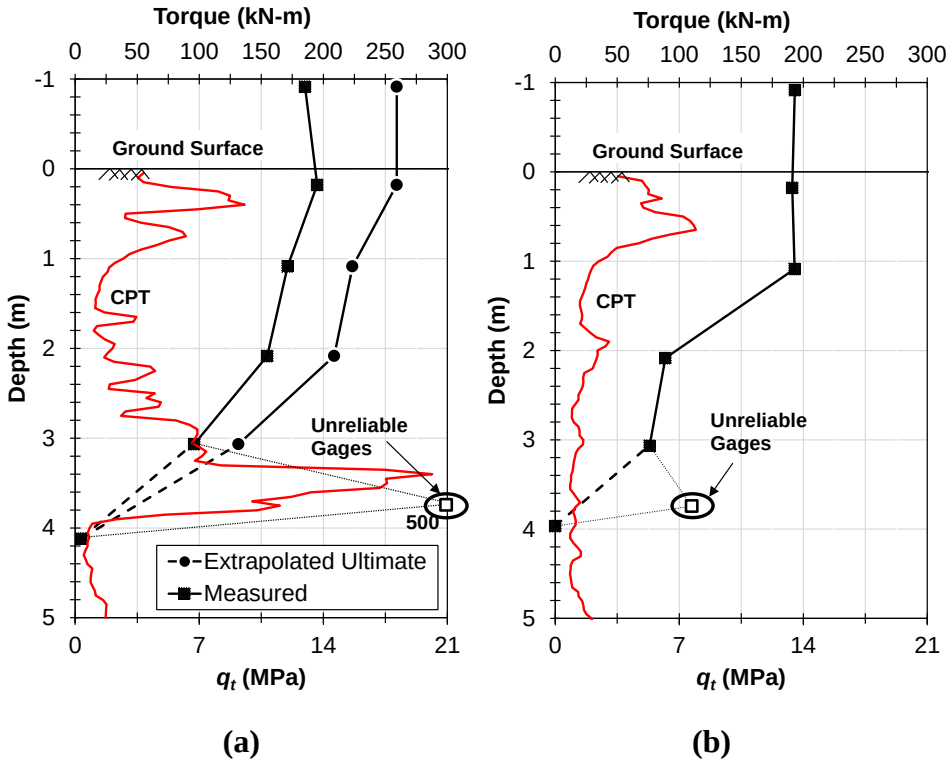

Figure 5.15: Torque profile for (a) TDS and (b) TDSFB with corrected cone tip resistance, q_t with metric units

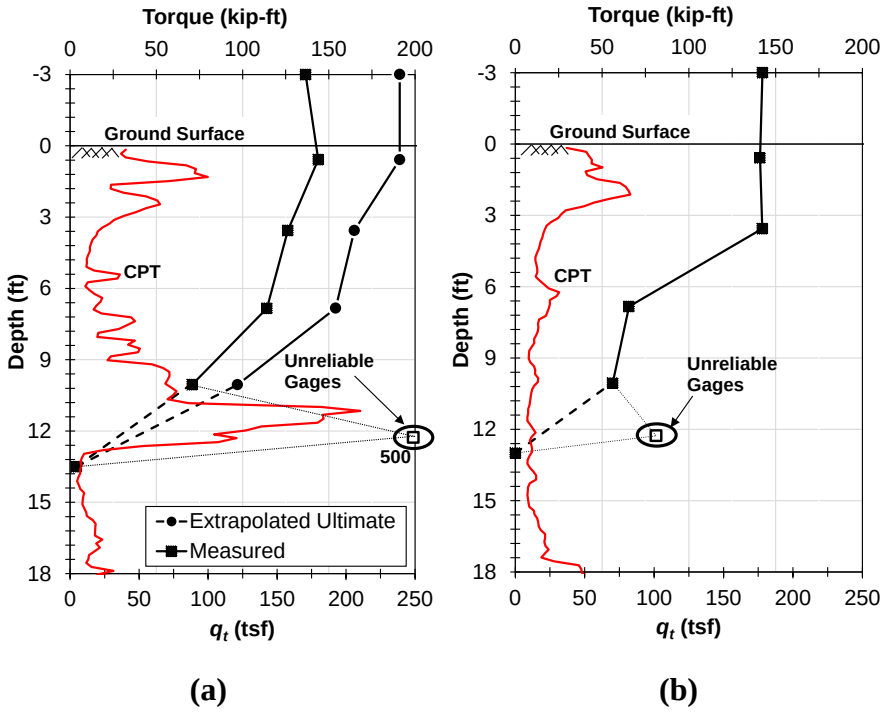

Figure 5.16: Torque profile for (a) TDS and (b) TDSFB with corrected cone tip resistance, q_t with imperial units

It is observed that the soil around TDSFB provided negligible torsional resistance from the ground surface until the depth of 1.1 m (3.6 ft), which is about one shaft diameter (D). Although a portion of this observation may be attributed to the use of the sonotube form, which extended 0.46 m (1.5 ft) below the ground surface, it cannot explain the total lack of unit shaft resistance for TDSFB. Thus, neglecting a small portion of unit shaft resistance of plastic soils near the ground surface, as described in some design methods, appears to have some merit. For example, the CDOT design method neglects the shaft resistance for the top 1.5D of shaft length *(Nusairat et al. 2004)*; and Florida District 7 Method neglects the shaft resistance for the top 1.5 m (5 ft). These design recommendations stem from the potential loss of soil resistance as the soil expands and contracts in response to wetting and drying, respectively, resulting in the formation of a gap between the soil and the shaft over time *(Brown et al., 2010)*. The internal torque of TDSFB reduced substantially from the depth of 1.1 m (3.6 ft) to 2.1 m (6.9 ft), indicating that significant torsional shaft resistance was mobilized along this portion of shaft. Thereafter, the internal torque decreased at a lower rate of torsion transfer from the depth of 2.1 m (6.9 ft) to 3.1 m (10.1 ft), indicative of relatively smaller shaft resistance along these depths. Based on the zero torsional resistance assumption at the base of TDSFB, the torsion transfer rate at the depths from 3.1 m (10.1 ft) to the bottom of the shaft is smaller than the torsion transfer rate at the depths from 1.1 m (3.6 ft) to 2.1 m (6.9 ft) but larger than the torsion transfer rate at the depths from 2.1 m (6.9 ft) to 3.1 m (10.1 ft). This observation is consistent with the reduction of cone tip resistance and overconsolidation with depth.

For shaft TDS, the torsional resistance from ground surface to a depth of 0.18 m (7 in) was observed to be negligible. The estimated internal torque at the depth of 0.18 m (7 in) was slightly larger than the torque developed at the shaft head, and this may be partially attributed to the use of a constant shear modulus for interpretation of the measured strains. However, as shown in Figure 5.17, shear cracks were observed on TDS and may indicate a decrease of the shear modulus following cracking. Considerable soil resistance was provided by the soils from the depth of 0.18 m (7 in) to the base of the shaft.

(a) **(b)**

Figure 5.17: Shear cracks observed on TDS following the test

5.6.3 Angle of Internal Twist and Implication for Load Transfer

In order to compute the true rotation at each instrumented elevation of the shaft and back-calculate accurate τ–θ curves, the variation of the angle of internal twist with depth must be computed. Based on the diameter profile and the torque recorded at each level for the shaft discussed in Section 5.5.2 and 5.6.2, respectively, the internal angle of twist can be estimated using:

$$\varphi = \frac{T \cdot \Delta L}{G \cdot J} \qquad \textbf{(5.11)}$$

where G = shear modulus of test shafts. Owing to the unreliable gages at the base of the shafts, and the possible uncertainty in the assumed toe resistance, the shaft head was chosen as the reference point for the computation of the angle of internal twist, and is therefore set equal to zero in Figure 5.18, which shows the angle of internal twist profiles corresponding to 1.75^{o} of rotation of TDSFB. The non-zero angle of internal twist at the shaft base does not imply true fixity at the base; rather the angle of internal twist is presented as a negative value to indicate that it is a subtractive quantity for computing the "true rotation" (see Section 5.6.4) for each section of shaft, which is the relative rotation between the specific section of the shaft and the

surrounding soils. The true rotation of each section along the shaft was computed by subtracting the rotation at the shaft head and the angle of internal twist at that section.

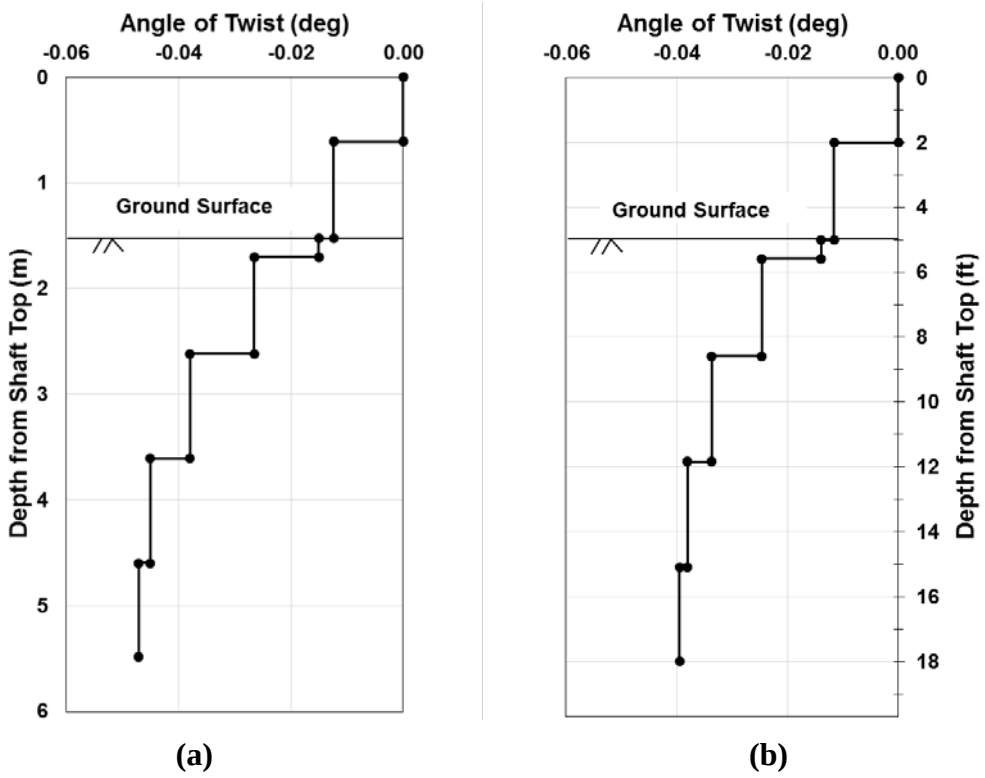

Figure 5.18: Angle of twist profile for (a) TDS and (b) TDSFB at 2° of TDSFB head rotation

5.6.4 Unit Torsional Soil Resistance

In order to apply the results of this study to other shafts, evaluate design models, and develop appropriate computational tools for assessing torsion load transfer, the experimental torsional load transfer must be reduced to the unit torsional soil resistance. The unit torsional soil resistance ($\tau = r_s$) was computed by considering the representative tributary area for each portion of the instrumented shaft, as shown in Figure 5.19. It is noted that the gages at the shaft toes were not taken into consideration, as described above. The torque at the instrumented depths was measured by the ESGs, whereas the torque at the ground surface was set equal to the torque, *T*, developed at the shaft head:

$$T_0 = T \tag{5.12}$$

The torque at the base of the shafts was equal to:

$$T_5 = 0, \quad \text{for TDS FB}$$

$$T_5 = \alpha \cdot s_u \left(\frac{\pi \cdot D^3}{12} \right), \quad \text{for TDS} \tag{5.13}$$

The unit soil resistance for each tributary area was calculated using:

$$\tau_t = r_{s,i} = \frac{2 \cdot \Delta T_i}{\pi \cdot D^2 \cdot \Delta L_i} \quad \textbf{(5.14)}$$

where ΔT_i = the difference in torque between the top and bottom of a tributary area, D = the shaft diameter, and ΔL_i = the height of tributary area, and i = represents the instrumented depth of interest.

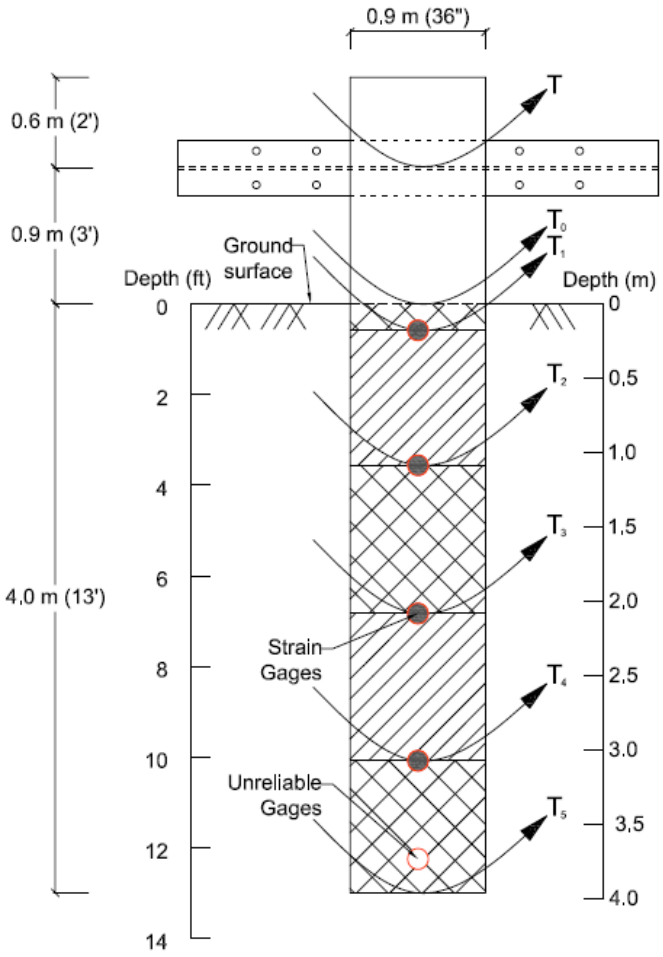

Figure 5.19: Tributary area used to compute the unit torsional soil resistance

The relationship between unit torsional soil resistance and rotation, known as a τ–θ curve, for each tributary area for TDS and TDSFB is shown in Figure 5.20 and Figure 5.21, respectively. It is noted that the rotation at the various depths in this figure correspond to the true rotation, as described above. It shows that the unit torsional soil resistance for TDS from the ground surface to the depth of 0.18 m (7 in) was mobilized at the beginning of the quasi-static test and then deceased gradually to zero as the test proceeded until the head rotation of 0.1°. The soil resistances for the tributary areas from the depths of 0.18 m (7 in) to 1.09 m (43 in) and from 1.09 m (43 in) to 2.08 m (82 in) appeared fully-mobilized at the rotation of approximately 0.1°. For the remainder of the shaft, the unit torsional soil resistance was not fully mobilized with the trend of increasing resistance at the rotation of 0.1°. However, for TDSFB the soil resistance

from ground surface until the depth of 1.1 m (3.6 ft) was negligible; and the soil resistance for the remainder of the shaft was fully mobilized at approximately 0.5°.

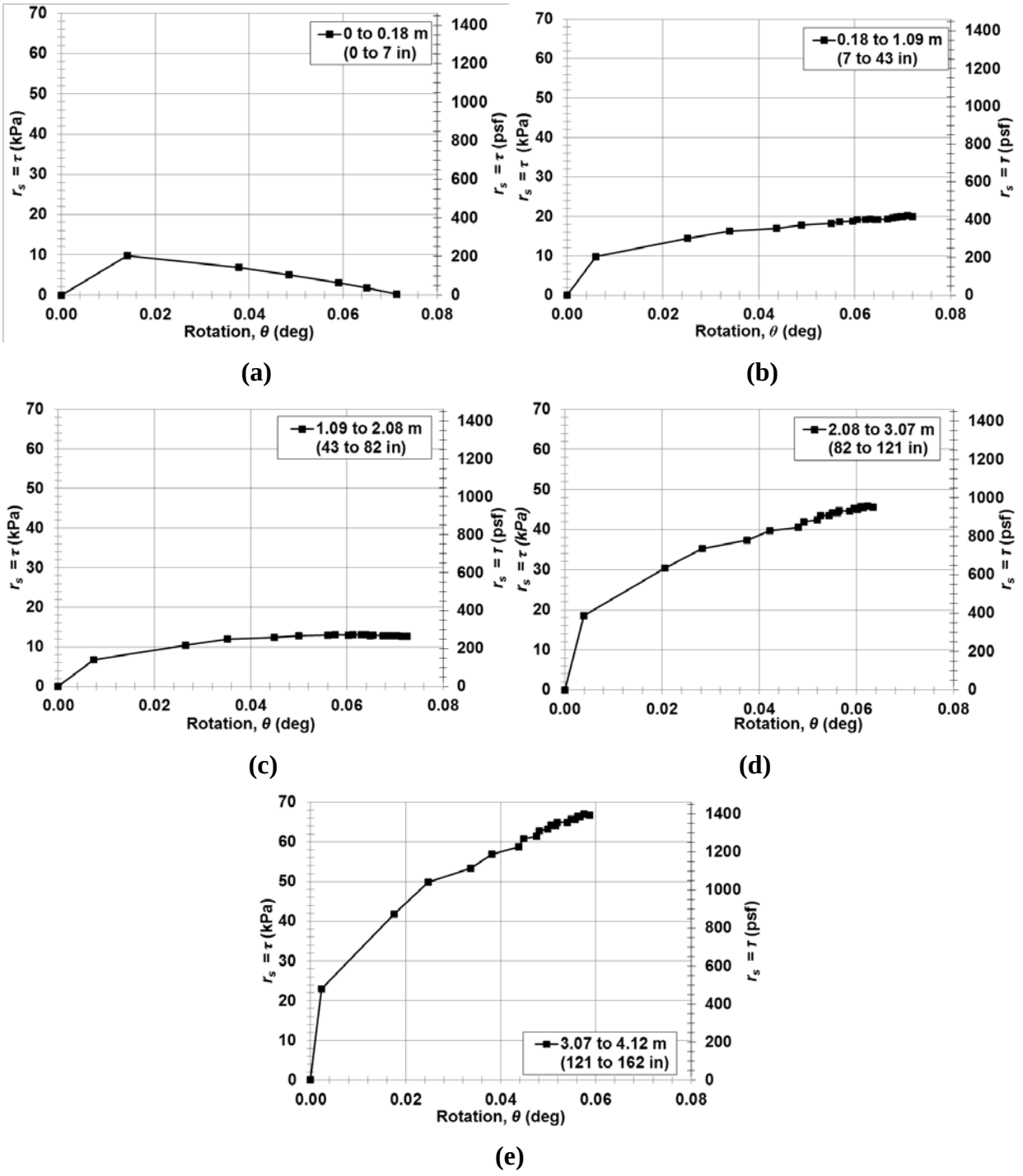

Figure 5.20: τ–θ curve for TDS at the depths of (a) 0 to 0.18 m (0 to 7 in) (b) 0.18 to 1.09 m (7 to 43 in) (c) 1.09 to 2.08 m (43 to 82 in), (d) 2.08 to 3.07 m (82 to 121 in), and (e) 3.07 to 4.12 m (121 to 162 in)

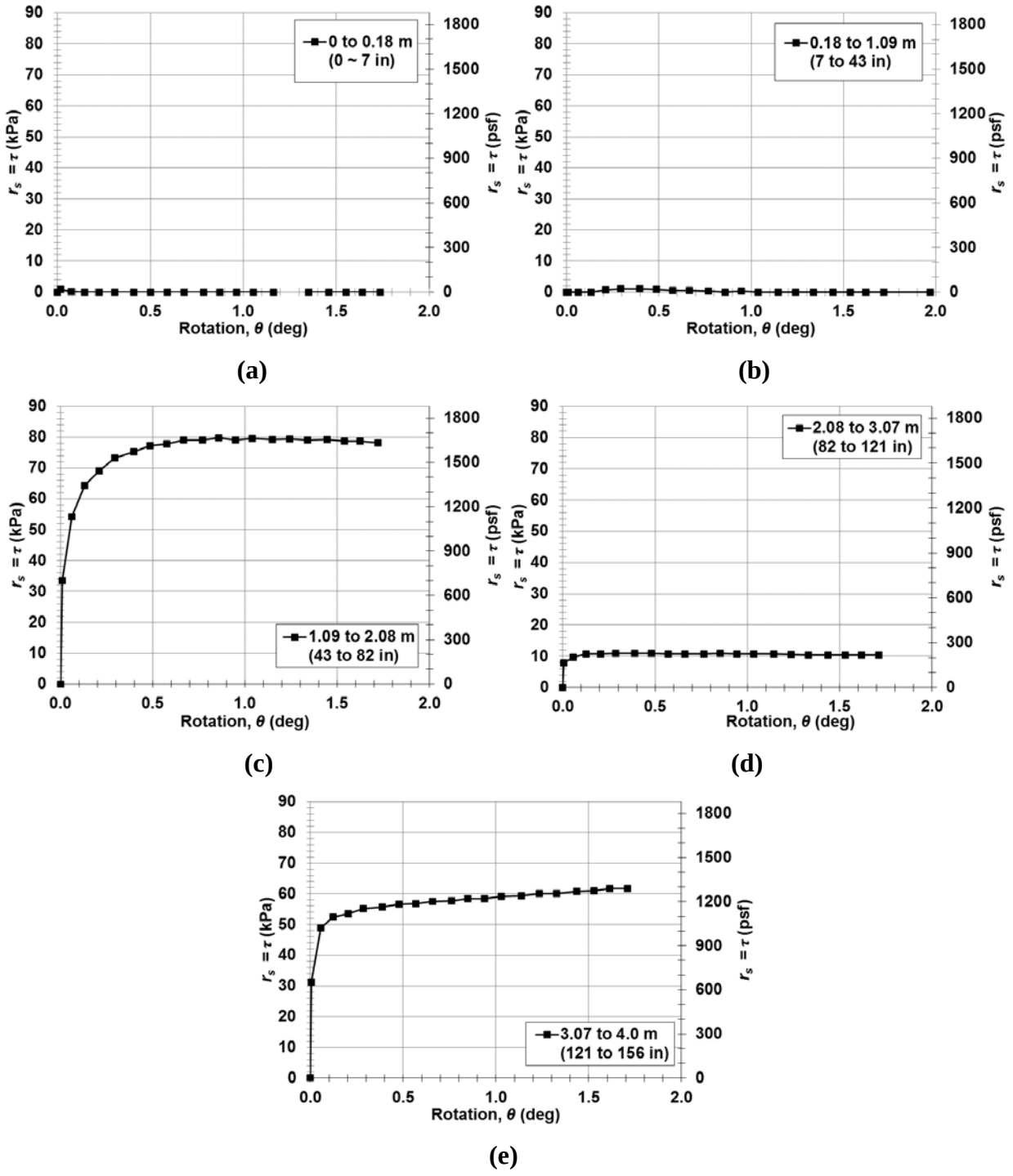

Figure 5.21: τ–θ curve for TDSFB at the depths of (a) 0 to 0.18 m (0 to 7 in) (b) 0.18 to 1.09 m (7 to 43 in) (c) 1.09 to 2.08 m (43 to 82 in), (d) 2.08 to 3.07 m (82 to 121 in), and (e) 3.07 to 4.0 m (121 to 156 in)

An investigation of the torsional load transfer indicated that the τ–θ curves for TDS could be well-modeled by a hyperbolic model except for the tributary area from ground surface to the depth of 0.18 m (7 in) as shown in Figure 5.22. Based on the observed response, the unit torsional soil resistance for the tributary area from ground surface to the depth of 0.18 m (7 in) was assumed to be zero beyond 0.1°. The hyperbolic τ–θ curves for each tributary area for TDS from 0.18 m to the bottom of the shaft are shown from Figure 5.23 to Figure 5.26. In some instances, one or more of the initial τ–θ data pairs were omitted from the hyperbolic curve fitting algorithm. The hyperbolic models were used to extrapolate to the ultimate unit torsional soil resistance for TDS at each of the instrumented depths and for rotations up to 1.75°, as shown in Figure 5.27. Based on the extrapolation, the soil resistance for the tributary areas from the depths of 2.08 m (82 in) to 3.07 m (121 in) and from 3.07 m (121 in) to 4.0 m (156 in) could have reached a fully-mobilized condition at a rotation of approximately 0.5°.

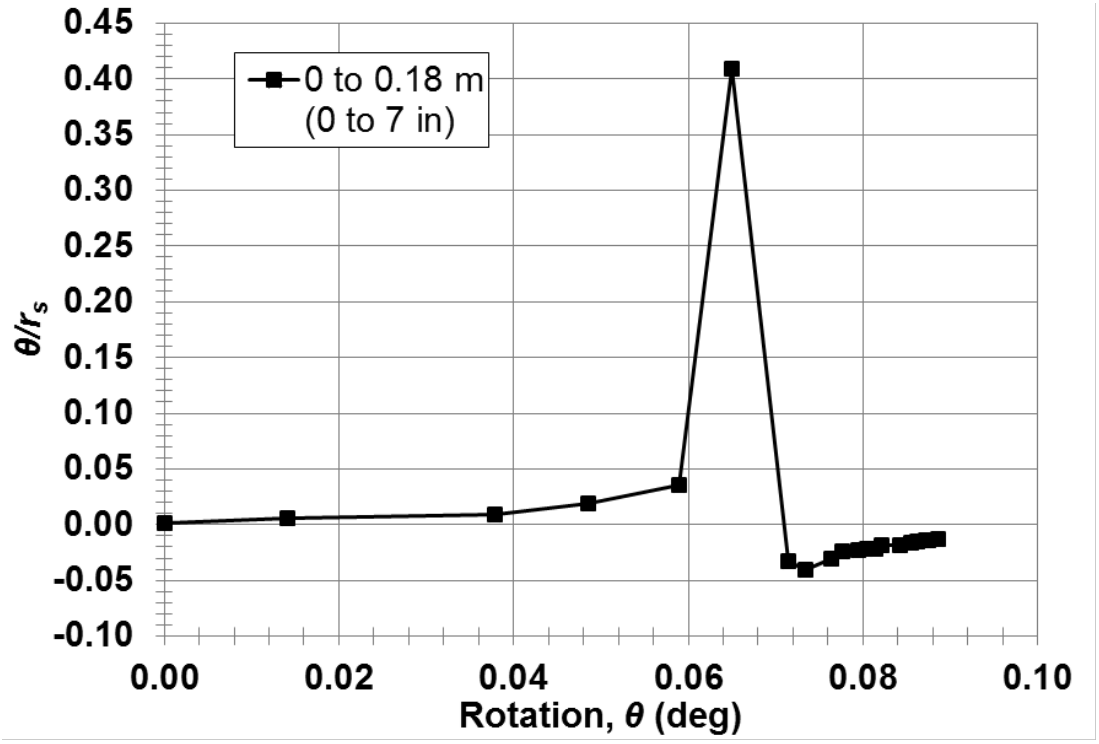

Figure 5.22: Observed τ–θ curve in hyperbolic space at depths from the ground surface to the depth of 0.18 m (7 in)

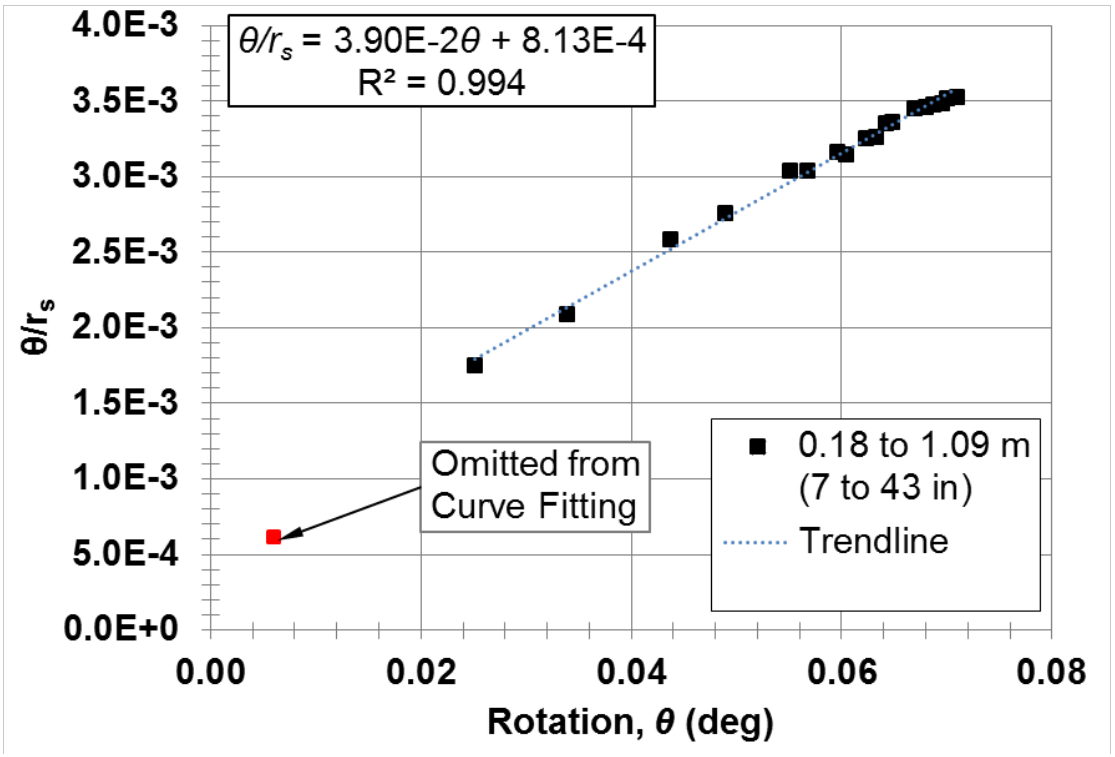

(a)

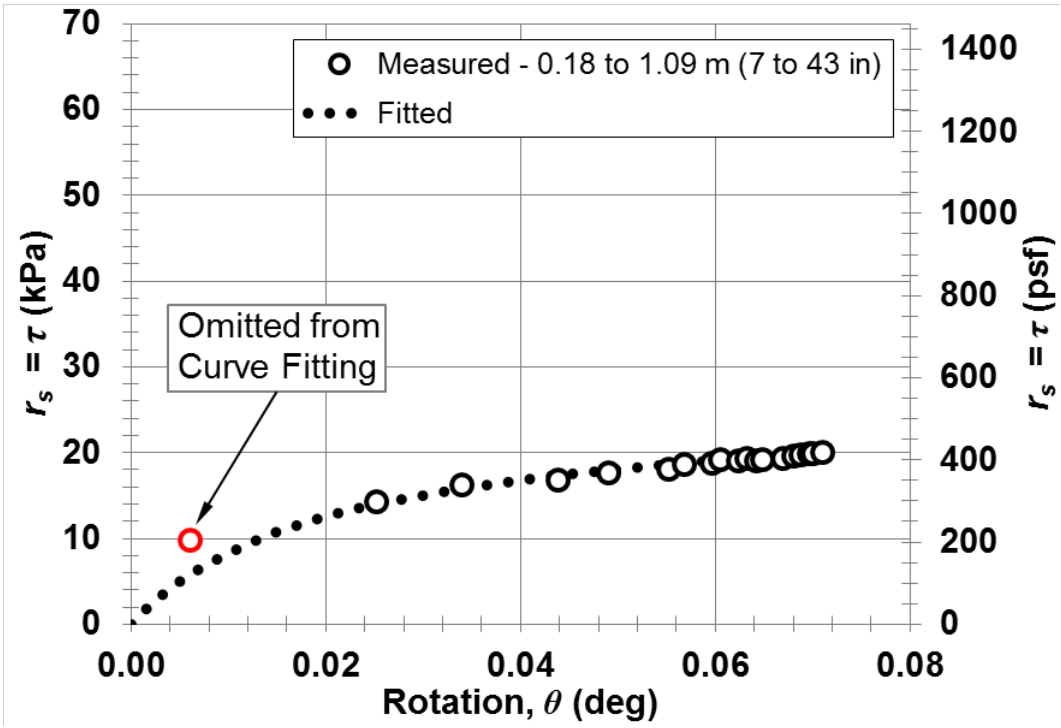

(b)

Figure 5.23: Hyperbolic model for TDS (a)observed τ–θ curve in hyperbolic space and fitted hyperbolic model and (b) comparison between fitted and measured response at depth from 0.18 to 1.09 m

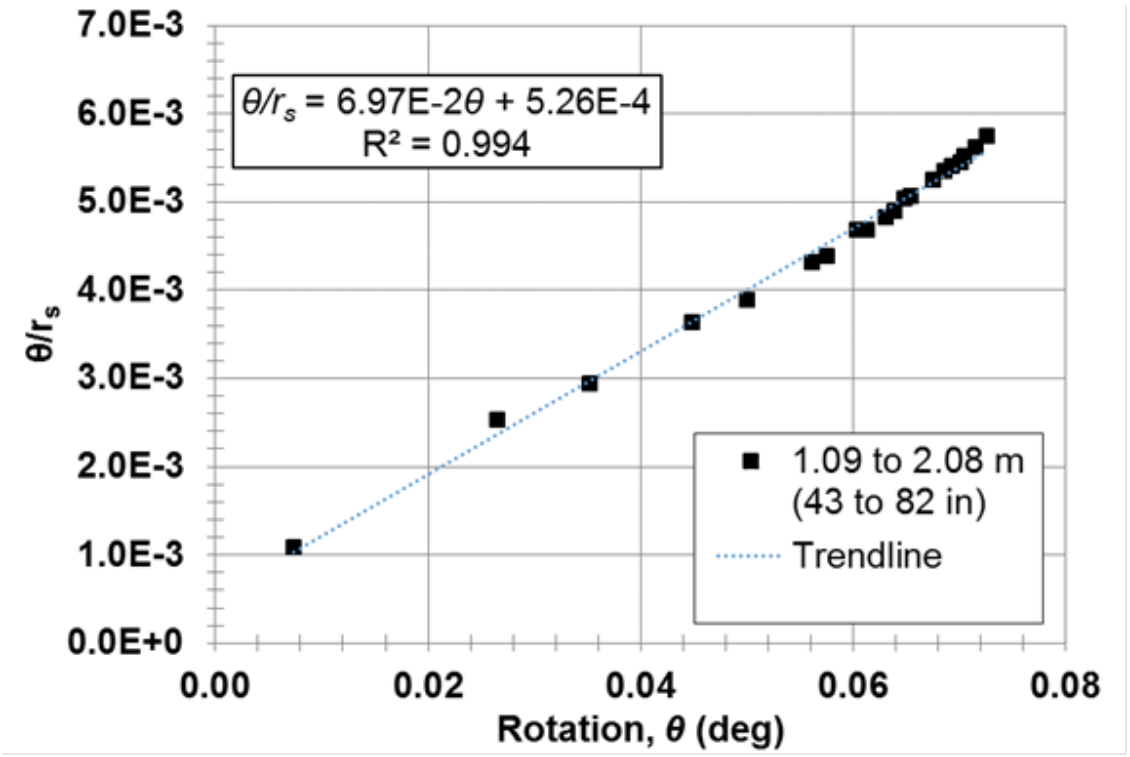

(a)

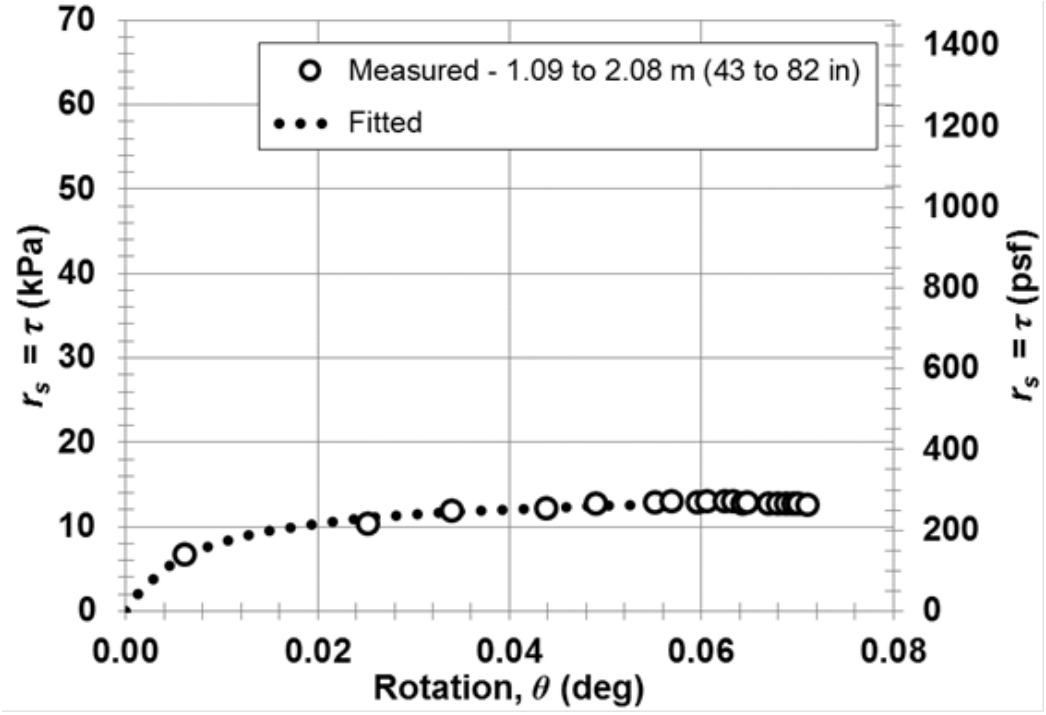

(b)

Figure 5.24: Hyperbolic model for TDS (a)observed τ–θ curve in hyperbolic space and fitted hyperbolic model and (b) comparison between fitted and measured response at depth from 1.09 to 2.08 m

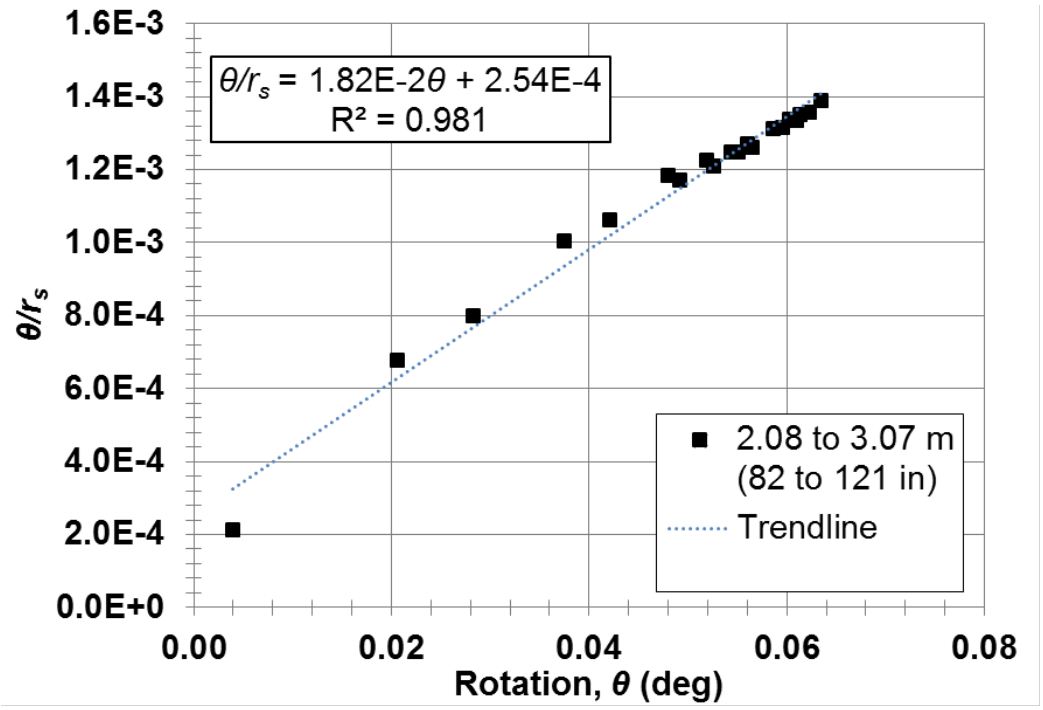

(a)

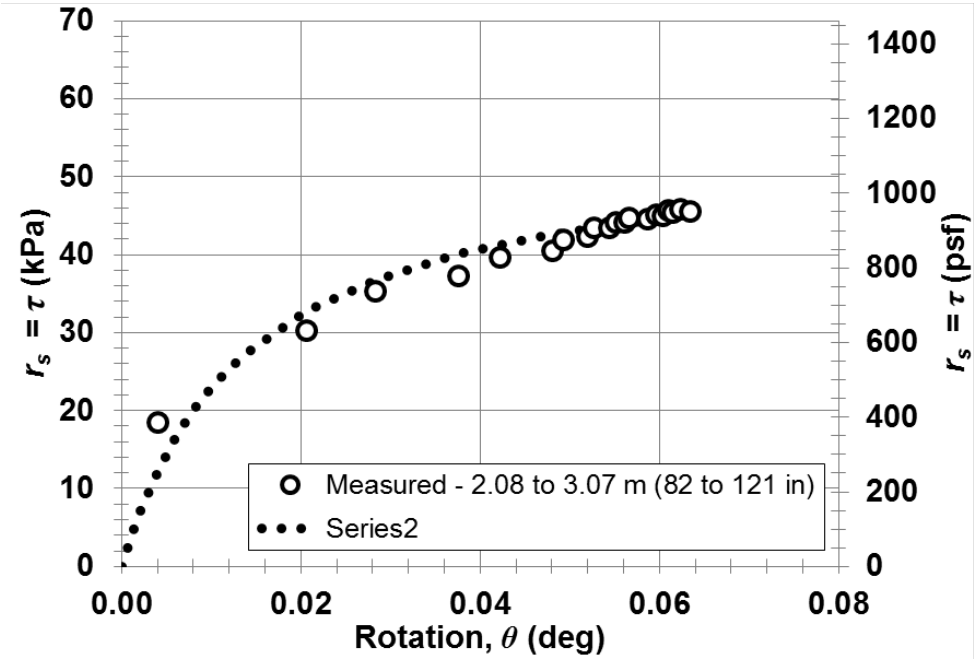

(b)

Figure 5.25: Hyperbolic model for TDS (a)observed τ–θ curve in hyperbolic space and fitted hyperbolic model and (b) comparison between fitted and measured response at depth from 2.08 to 3.07 m

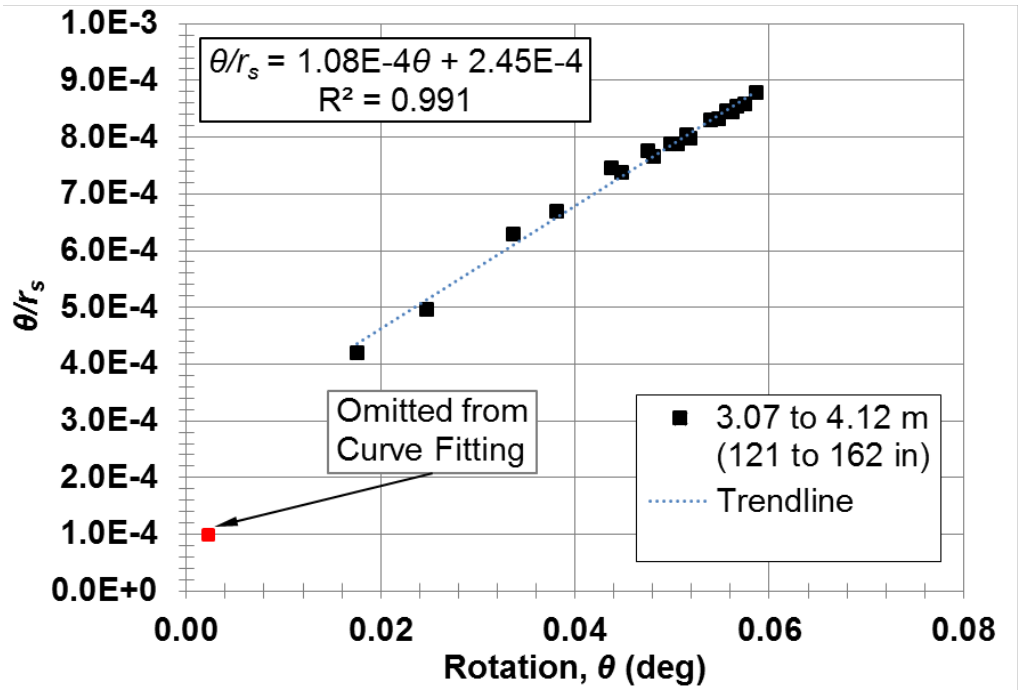

(a)

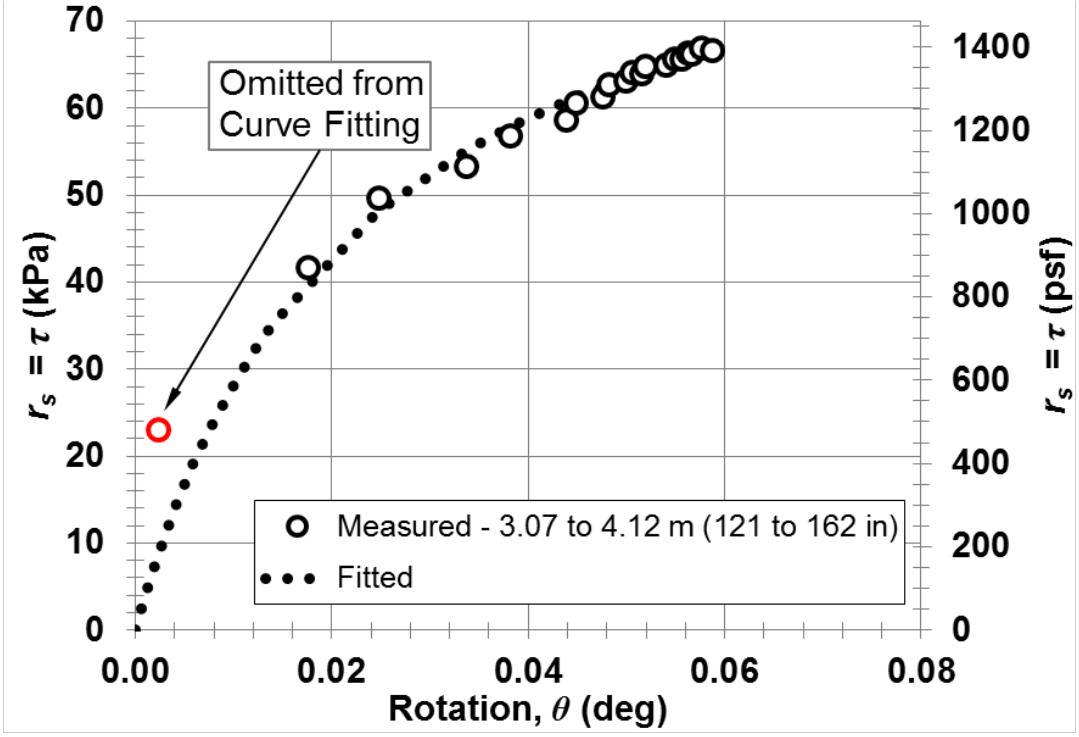

(b)

Figure 5.26: Hyperbolic model for TDS (a)observed τ–θ curve in hyperbolic space and fitted hyperbolic model and (b) comparison between fitted and measured response at depth from 3.07 to 4.12 m

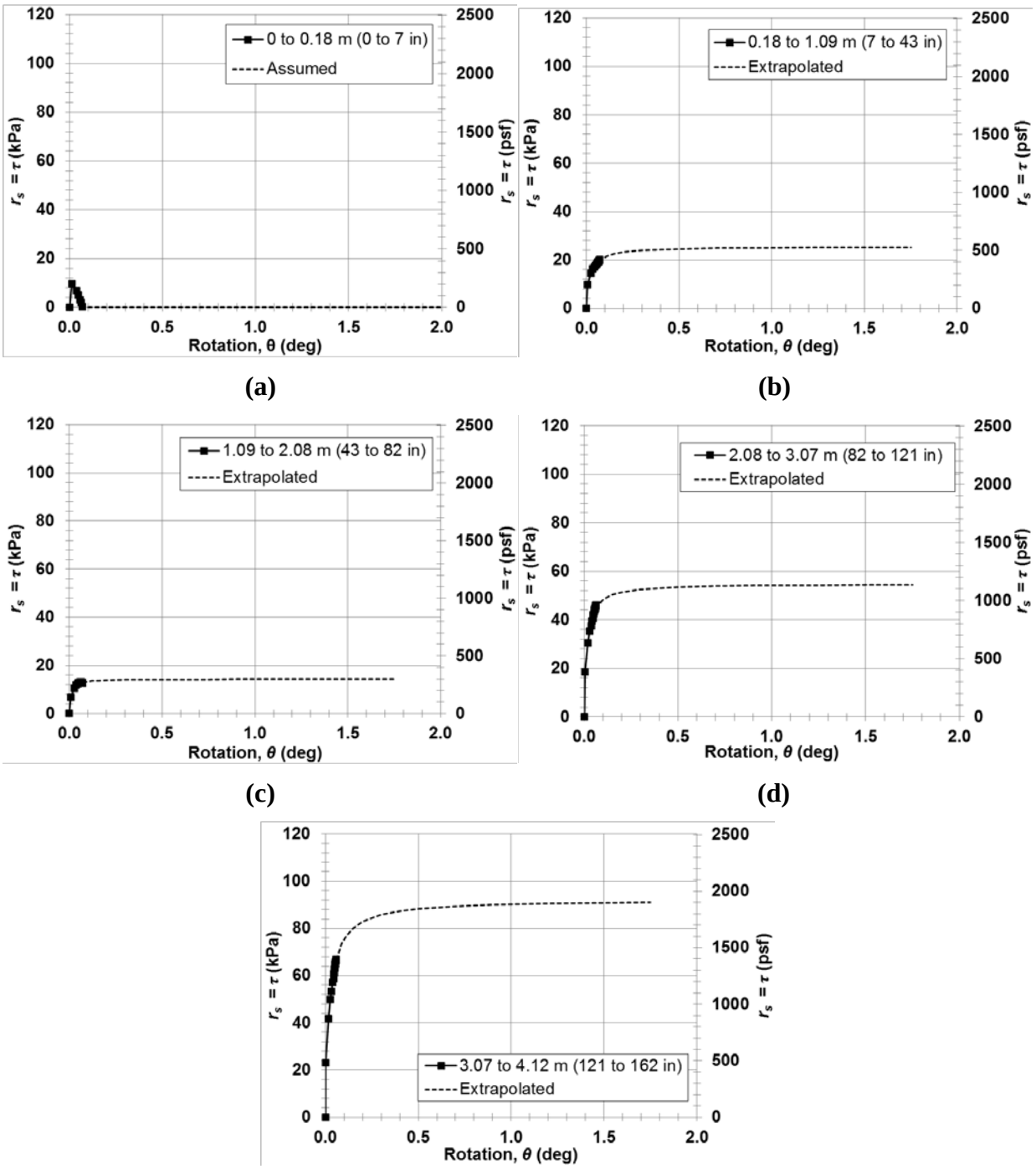

Figure 5.27: τ–θ curve for TDS at the depths of (a) 0 to 0.18 m (b) 0.18 to 1.09 m (c) 1.09 to 2.08 m, (d) 2.08 to 3.07 m, and (e) 3.07 to 4.12 m with the rotation up to 2°

The estimated ultimate unit torsional soil resistance, r_s, for TDS at the rotation of 1.75° and the mobilized unit torsional soil resistance for TDSFB at the rotation of 1.75° are shown in Figure 5.28 (with imperial units in Figure 5.29). Figure 5.30 shows the comparison between TDS and TDSFB in terms of the tip resistance (q_t) profile and the unit soil resistance (r_s) profile. The cone

tip resistance was included in this figure to correlate the soil strength and consistency with the shaft resistance. The estimated ultimate unit torsional soil resistance for TDS for each tributary area correlated well with the tip resistance profile, q_t. It is noted that the tributary area from the depth of 3.07 m (121 in) to 4.1 m (162 in) corresponding to the sand layer could contribute significant ultimate unit torsional soil resistance.

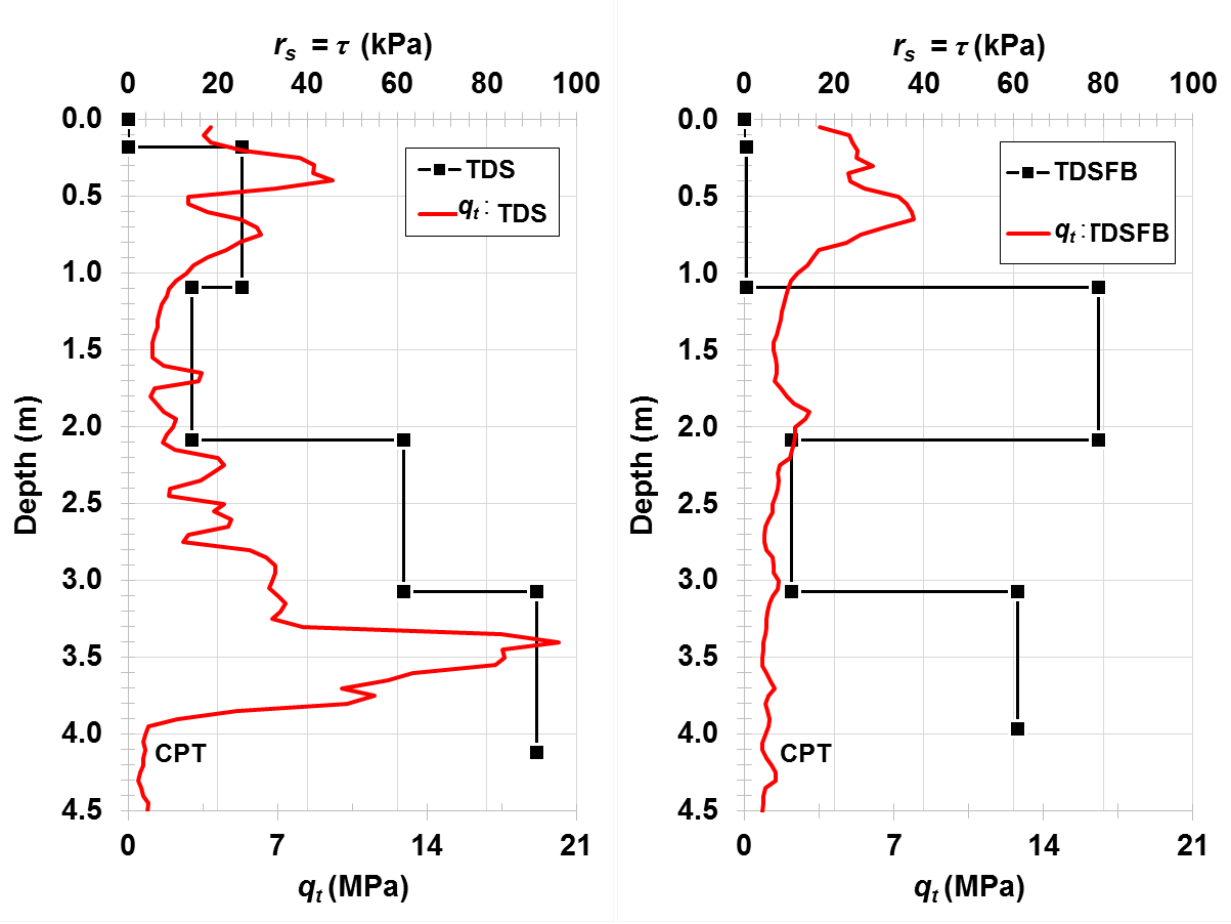

Figure 5.28: Unit soil resistance (r_s) profile and tip resistance (q_t) profile for (a) TDS and (b) TDSFB with metric units

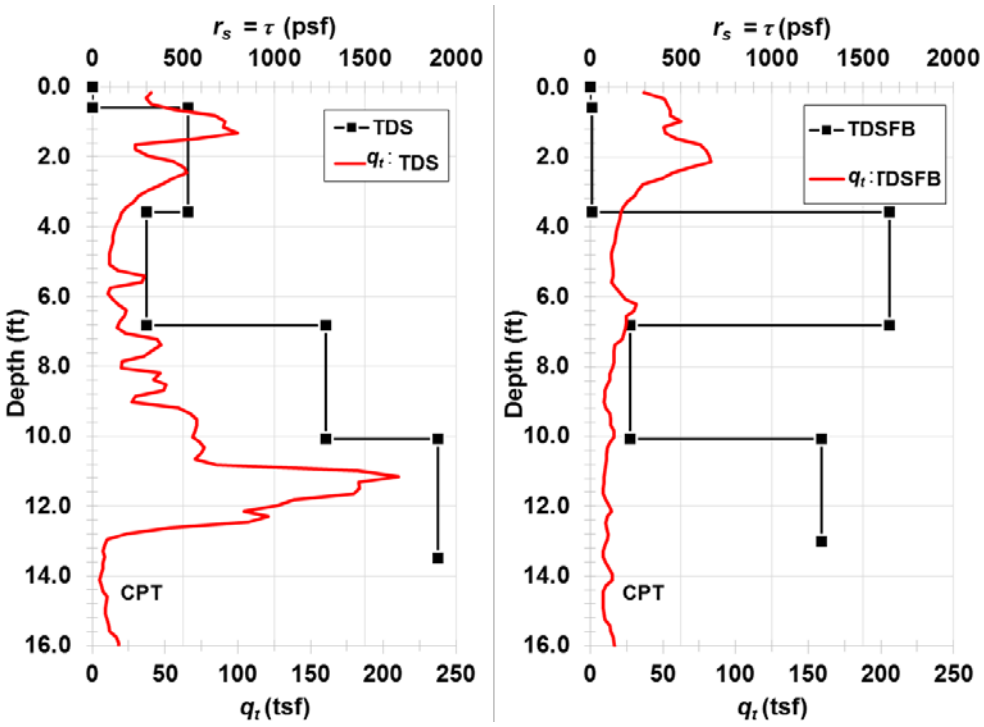

(a) **(b)**

Figure 5.29: Unit soil resistance (r_s) profile and tip resistance (q_t) profile for (a) TDS and (b) TDSFB with imperial units

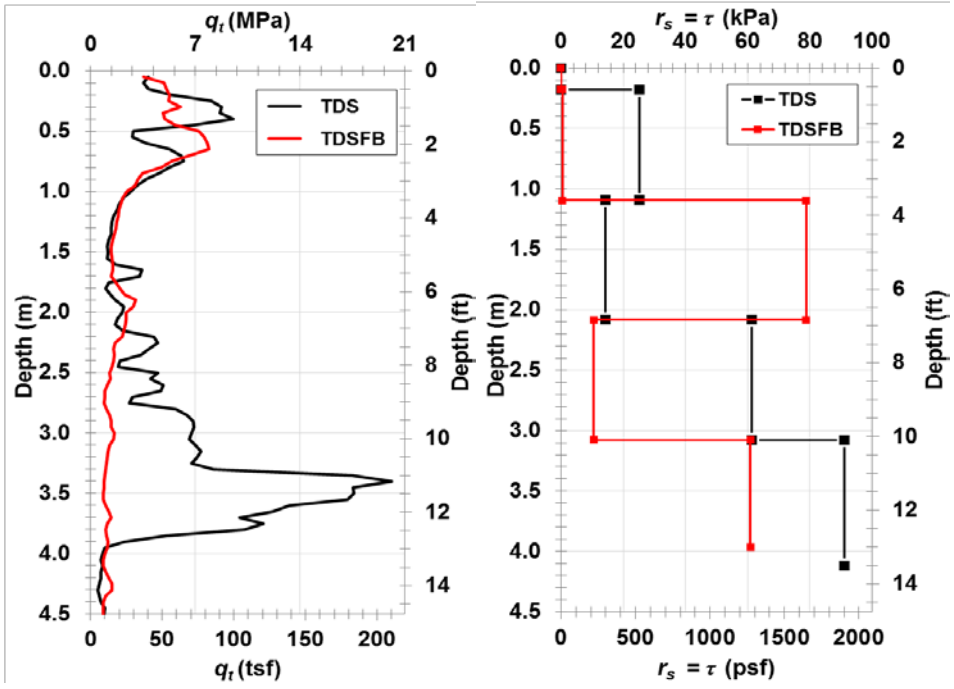

(a) **(b)**

Figure 5.30: Comparison for (a) tip resistance (q_t) profile and (b) unit soil resistance (r_s) profile

The torque at the shaft head was calculated using the extrapolated unit torsional soil resistance for each tributary area of shaft TDS and compared with the torque estimated and extrapolated using the load cell data, as shown in Figure 5.31. The two torque-rotation responses, which were obtained using two independent measurements (i.e., load cells and ESGs) and corresponding hyperbolic model, have a similar trend. The difference in the torsional capacity computed using the hyperbolic model extrapolations, is approximately 3%.

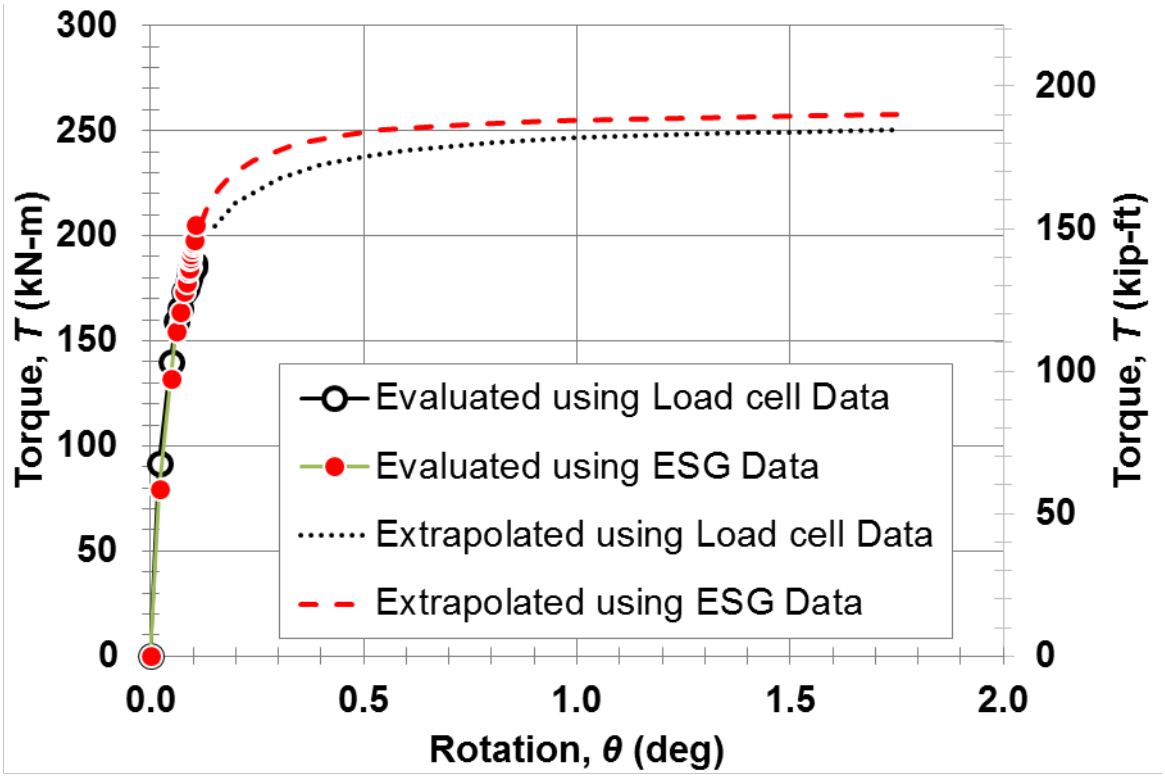

Figure 5.31: Comparison of the torque-rotation response using the load cells data and the ESGs data for shaft TDS

5.6.5 Lateral Loading and Flexure of Test Shafts during Testing

Over the course of rotating the shafts during the torsional loading test, the differential mobilized resistance at the soil-shaft interface resulted in the development of flexure in the shafts. The lateral load-deflection response for both test shafts is shown in Figure 5.32. The lateral load of each test shaft increased during the monotonic quasi-static loading. Softening was observed for the lateral load-deflection response during cyclic loading for each test shaft. The initial lateral stiffness of shaft TDS was larger than that of shaft TDSFB, due in part to the greater resistance provided by the granular layer. The lateral load that developed was quite small at the TDSFB shaft head rotation of 1.75° (corresponding to the shaft head rotation of 0.1° for TDS), the rotation prior to the increase in rotation rate, and equaled 4.9 kN (1.1 kips). However, this load increased substantially at larger rotations, as shown in Figure 5.32.

The curvature, ϕ, was computed at the instrumented depth z using the following equation and the flexural strains measured using the RSGs:

$$\phi(z) = \frac{\varepsilon_T(z) - \varepsilon_C(z)}{h} \quad \textbf{(5.15)}$$

where $\varepsilon_T(z)$ and $\varepsilon_C(z)$ = measured tensile and compressive strain at depth z, h = horizontal distance between the strain gauges. Then, bending moment at each depth was evaluated according to the moment-curvature relationship (Figure 5.33 in metric units and Figure 5.34 in imperial units) for the constructed shafts, estimated using the computer program LPile (http://www.ensoftinc.com). Figure 5.35 and Figure 5.36 show the bending moment profiles and the percentage of ultimate bending moment profiles for both test shafts, respectively. It appears that the base of shaft TDSFB was free to rotate due to the bentonite layer beneath the shaft, whereas the soils at the base of shaft TDS provided partial restraint in bending. The depth-to-maximum bending moment of shaft TDSFB is larger than that of shaft TDS. The maximum induced bending moment calculated from the longitudinal strains for TDS and TDSFB at 1.75° of shaft head rotation of TDSFB is 28.5 and 30.5 kN m (corresponding to 21.0 and 22.5 kips-ft), respectively, which is approximately 4.3 and 4.6% of the estimated ultimate bending resistance. The measured maximum bending moment at the end of the torsion test for TDS and TDSFB is 190 and 262 kN-m (corresponding to 140 and 193 kips-ft), respectively, which is approximately 28 and 39% of the ultimate bending moment. The differences between TDS and TDSFB can be attributed to the reduction of lateral resistance due to the excessive rotation of shaft TDSFB comparing to shaft TDS. Comparison of the estimated values of the maximum bending moment at the end of the torsion test with the moment-curvature diagram shown below, it is assumed that during the test, both of the shafts remained essentially elastic in flexure.

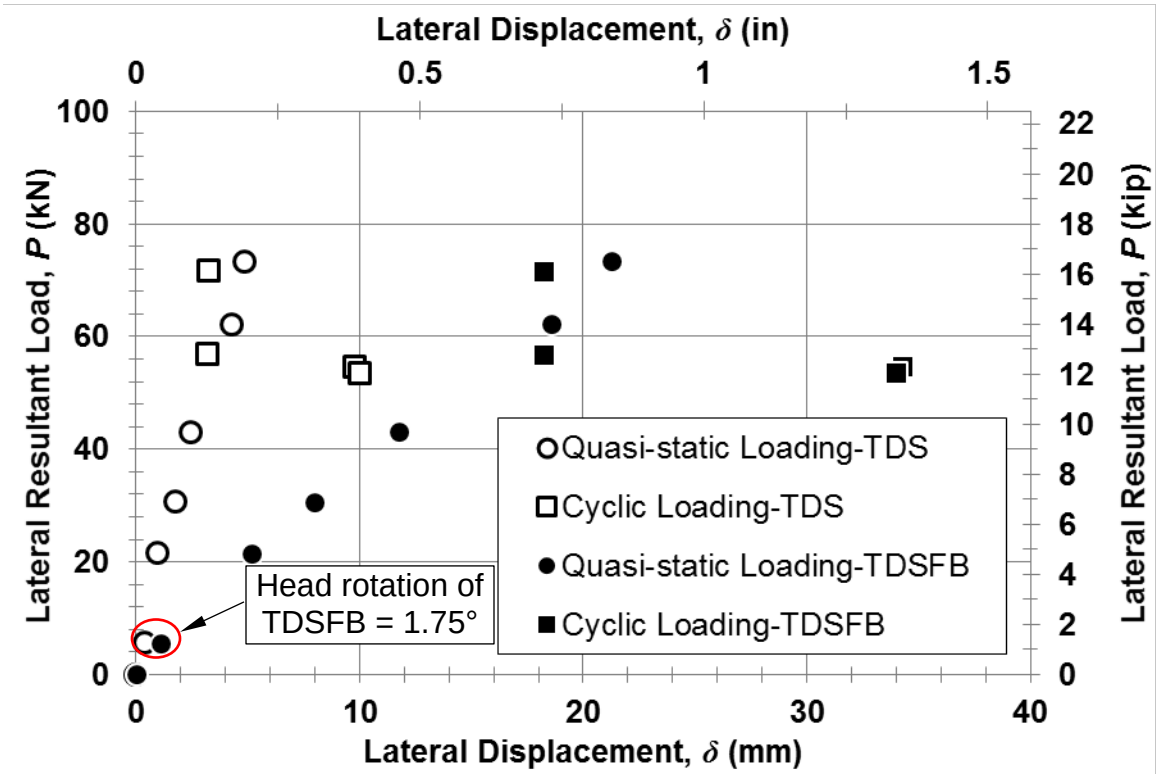

Figure 5.32: Lateral load-deflection response

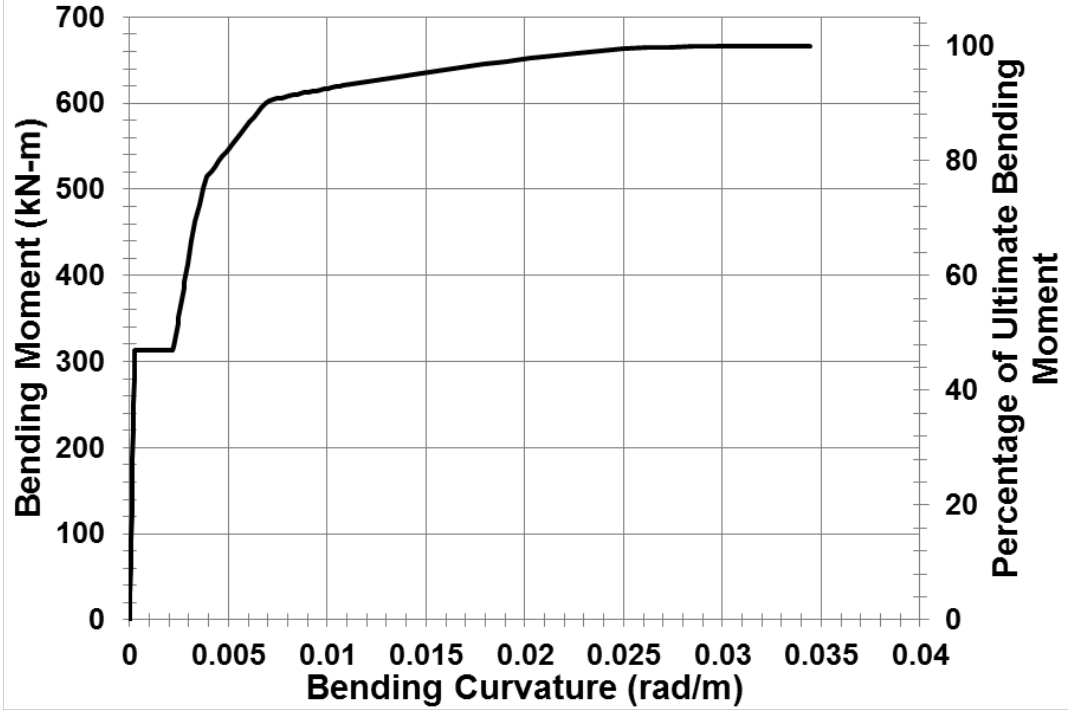

Figure 5.33: Moment-curvature relationship for the test shafts TDSFB with metric units

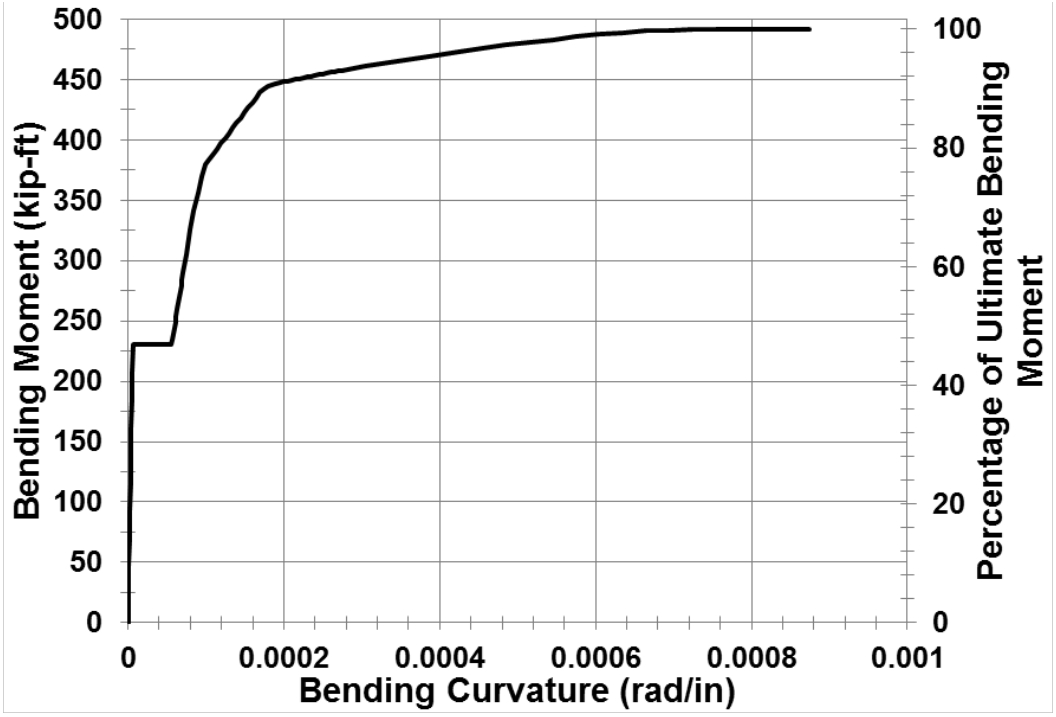

Figure 5.34: Moment-curvature relationship for the test shafts with imperial units

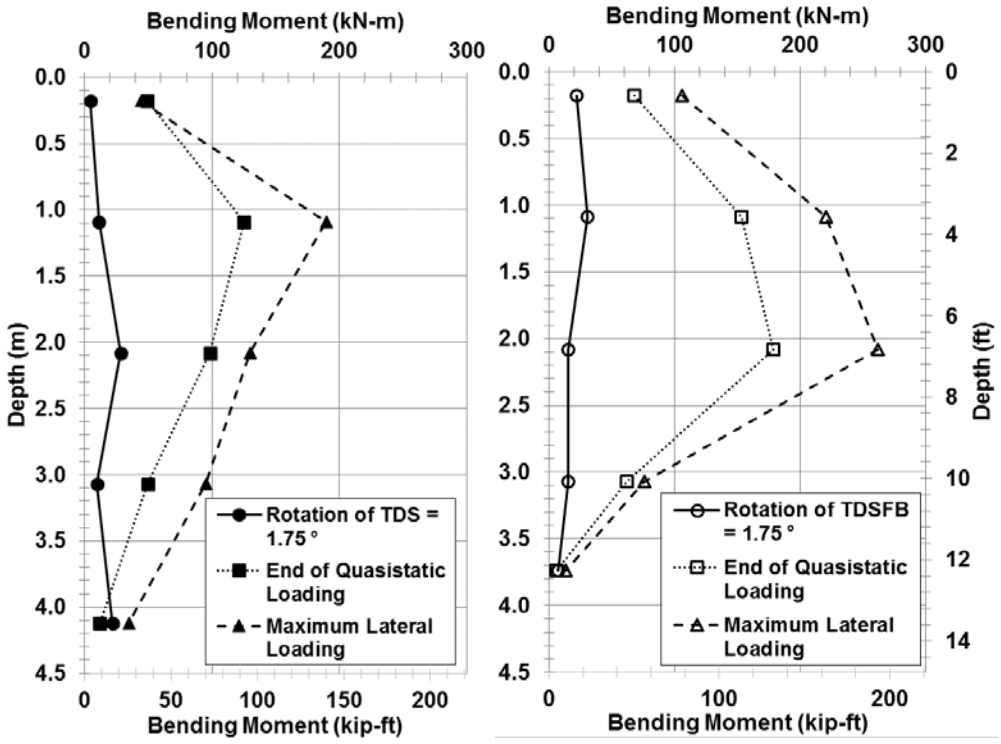

(a) **(b)**

Figure 5.35: Bending moment profiles for (a) TDS and (b) TDSFB

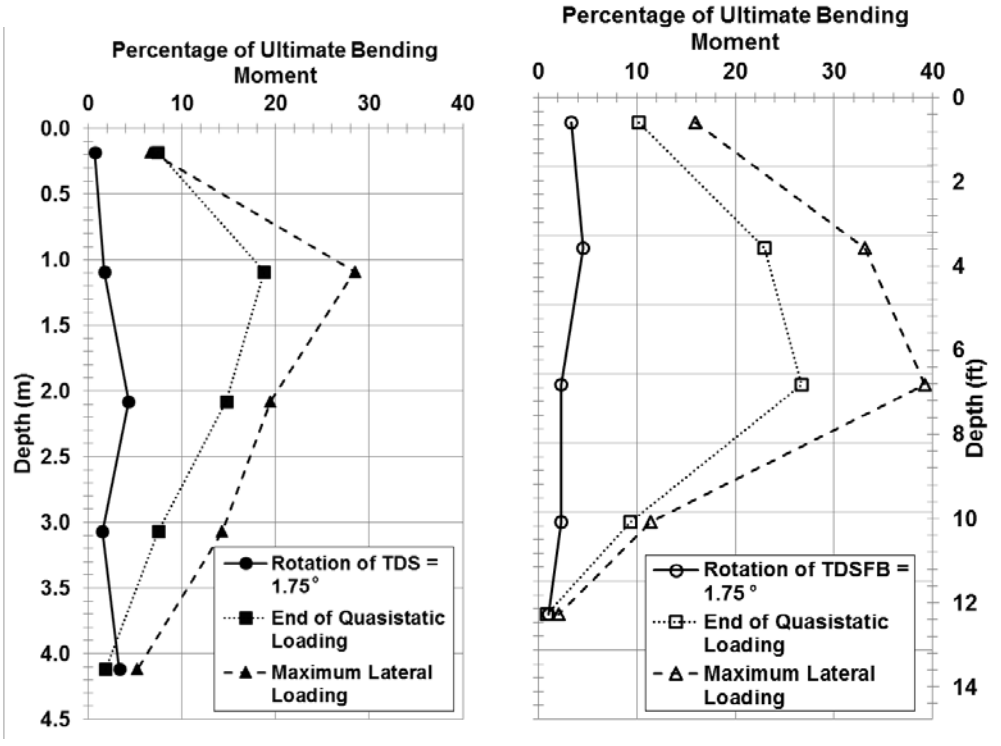

(a) **(b)**

Figure 5.36: Profiles of percent ultimate bending moment for (a) TDS and (b) TDSFB

5.7 ASSESSMENT OF DESIGN APPROACHES

5.7.1 Assessment on Torsional Capacity

In order to help establish the general accuracy of existing design methods, it is helpful to compare the ultimate torsional resistance of the shafts to those calculated with existing design approaches. The torsional capacities of TDS and TDSFB were estimated using the CDOT Design Method and the Florida District 7 Method, both of which can deal with layered soils (as is the case for TDS).

For TDS, the torsional resistance incorporates shaft and toe resistance. The soil stratigraphy around TDS was separated into four layers based on the soil properties: (1) the near-surface cohesive soils, to a depth of 0.9 m (3 ft), (2) the cohesive soils to a depth of 2.7 m (9 ft), (3) the granular soils at the depth from 2.7 m (9 ft) to 3.8 m (12 ft-6 in), and (4) the cohesive soils for the rest of the shaft from 3.8 m (12 ft-6 in) to 4.1 m (13 ft-6 in) as shown in Figure 3.4. Based on the CPT and grab samples from the shaft excavation, the base of TDS was considered to bear on cohesive soil (Figure 3.4).

For TDSFB, only shaft resistance was considered owing to its construction with a relatively frictionless base. The soils around TDSFB were separated into two layers based on the soil properties: (1) the near-surface cohesive soils, to a depth of 0.9 m (3 ft), and (2) the cohesive from 0.9 m (3 ft) to the bottom of the shaft, 4 m (13 ft).

As discussed above, the CDOT Method neglects the soil resistance for the top 1.5D of the shaft length; and the Florida District 7 Method neglects the soil resistance for the top 1.5 m (5 ft). The soil properties and torsional resistance for each soil layer using the aforementioned methods are summarized through Table 5.1 to Table 5.4. The calculated torsional capacities are summarized in Table 5.5 and compared to the measured capacity of TDSFB and extrapolated capacity of TDS. The CDOT Design Method over-predicted the torsional capacity, as quantified with the bias (ratio of measured to calculated capacity) less than 1.0; this is attributed to the use of the unfactored undrained shear strength to compute the unit shaft resistance with this method. On the other hand, the Florida District 7 Method under-predicted the torsional capacity as indicated with a bias greater than 1.0. Similar trends, as shown in Table 5.6, were identified for these design methods in consideration of the Stoll *(Stoll 1972)*, Tawfiq *(Tawfiq 2000)*, and McVay et al. *(McVay et al. 2014)* field test data and the Poulos *(Poulos 1975)* model test data. In general, the average bias and coefficient in variation (the ratio of standard deviation of point bias and average bias) for the CDOT and Florida District 7 Methods equaled 0.71 and 17.2% and 1.39 and 28.3%, respectively. Thus, it appears that the development of improved methods for assessing torsional capacity is desirable.

Table 5.1: Soil profile used for calculation of torsional resistance for TDS using the Florida District 7 Method

	Soil Type	Depth, m (ft)	Soil Unit Weight, kN/m^3 (pcf)	Average Cohesion, kPa (psf)	Adhesion Factor, α	Friction Angle, deg	Unit Friction, kPa (psf)	Torsional Resistance, kN-m (kips-ft)
Shaft	Clay to Clayey silt (CL-ML)	0 ~ 1.5 (0 ~ 5)	18 (115)	225 (4699)	-	-	-	-
	Clay to Clayey silt (CH-MH)	1.5 ~ 2.7 (5 ~ 8.9)	18 (115)	148 (3091)	0.55	-	81 (1700)	128 (95)
	Sand to Silty Sand	2.7 ~ 3.8 (8.9 ~ 12.5)	20 (130)	-	-	39	38 (791)	55 (40)
	Clay to Clayey silt (CH-MH)	3.8 ~ 4.1 (12.5 ~ 13.5)	18 (115)	39 (815)	0.55	-	21 (448)	8 (6)
Base	Clay to Clayey silt (CH-MH)	-	18 (115)	34 (710)	0.55	-	-	4 (3)
Total	-	-	-	-	-	-	-	**195 (144)**

Table 5.2: Soil profile used for calculation of torsional resistance for TDS using the CDOT Method

	Soil Type	**Depth, m (ft)**	**Soil Unit Weight, kN/m^3 (pcf)**	**Average Cohesion, kPa (psf)**	**Friction Angle, deg**	**Torsional Resistance, kN-m (kips-ft)**
Shaft	Clay to Clayey silt (CL-ML)	0 ~ 1.35 (0 ~ 4.5)	18 (115)	225 (4699)	-	-
	Clay to Clayey silt (CH-MH)	1.35 ~ 2.7 (4.5 ~ 8.9)	18 (115)	149 (3112)	-	264 (195)
	Sand to Silty Sand	2.7 ~ 3.8 (8.9 ~ 12.5)	20 (130)	-	39	59 (43)
	Clay to Clayey silt (CH-MH)	3.8 ~ 4.1 (12.5 ~ 13.5)	18 (115)	39 (815)	-	15 (11)
Base	Clay to Clayey silt (CH-MH)	-	18 (115)	34 (710)	-	7 (5)
Total	-	-	-	-	-	**345 (254)**

Table 5.3: Soil profile used for calculation of torsional resistance for TDSFB using the Florida District 7 Method

	Soil Type	**Depth, m (ft)**	**Soil Unit Weight, kN/m^3 (pcf)**	**Average Cohesion, kPa (psf)**	**Adhesion Factor, α**	**Friction Angle, deg**	**Unit Friction, kPa (psf)**	**Torsional Resistance, kN-m (kips-ft)**
Shaft	Clay to Clayey silt (CL-ML)	0 ~ 1.5 (0 ~ 5)	18 (115)	225 (4700)	-	-	-	-
	Clay to Clayey silt (CH-MH)	1.5 ~ 4.0 (5 ~ 13)	18 (115)	77 (1608)	0.55	-	42 (884)	139 (103)
Base	Clay to Clayey silt (CH-MH)	-	18 (115)	28 (585)	-	-	-	-
Total	-	-	-	-	-	-	-	**139 (103)**

Table 5.4: Soil profile used for Calculation of Torsional Resistance for TDSFB using the CDOT Method

	Soil Type	Depth, m (ft)	Soil Unit Weight, kN/m^3 (pcf)	Average Cohesion, kPa (psf)	Friction Angle, deg	Torsional Resistance, kN-m (kips-ft)
Shaft	Clay to Clayey silt (CL-ML)	0 ~ 1.35 (0 ~ 4.5)	18 (115)	242 (5054)	-	-
	Clay to Clayey silt (CH-MH)	1.35 ~ 4.0 (4.5 ~ 13)	18 (115)	77 (1608)	-	268 (198)
Base	Clay to Clayey silt (CH-MH)	-	18 (115)	28 (585)	-	-
Total	-	-	-	-	-	268 (198)

Table 5.5: Summary of calculated torsional capacities for TDS and TDSFB

		Field Test	Florida District 7 Method	CDOT Design Method
TDSFB	Torsional capacity, kN-m (kip-ft)	185 (136)	139 (103)	268 (198)
	Ratio of measured and computed capacity (Bias)	-	1.33	0.69
TDS	Extrapolated Torsional capacity, kN-m (kip-ft)	251 (185)	195 (144)	345 (254)
	Ratio of extrapolated and computed capacity (Bias)	-	1.29	0.73

Table 5.6: Comparison between estimated torsional capacity and test results *(modified from Nusairat et al. 2004)*

Tests		Capacity			Bias in Method	
		Test Results	**Florida District 7 Method**	**Colorado Dept. of Trans.**	**Florida District 7 Method**	**Colorado Dept. of Trans.**
Stoll *(Stoll1972)*, Field Tests ,kN-m (kip-ft)	A-3	29.2 (21.5)	19.5 (14.4)	47.7 (35.2)	1.50	0.61
	V-4	52.2 (38.5)	37.1 (27.4)	91.4 (67.4)	1.41	0.57
Poulos *(Poulos 1975)*, Model Tests N-m (lb-ft)	#1	1.86 (1.38)	1.63 (1.2)	2.85 (2.10)	1.14	0.65
	#2	2.20 (1.62)	1.80 (1.33)	3.63 (2.68)	1.22	0.61
	#3	0.91 (0.67)	0.81 (0.60)	1.71 (1.26)	1.12	0.53
Tawfiq *(Tawfiq 2000)*, Field Tests, kN-m (kip-ft)	#1 (Dry)	664 (490)	553 (408)	876 (646)	1.20	0.76
	#2 (polymer slurry)	569 (420)	488 (360)	773 (570)	1.17	0.74
	#3 (bentonite slurry)	380 (280)	368 (271.23)	583 (430)	1.03	0.65
McVay et al. *(McVay et al. 2014)*, Field Tests, kN-m (kip-ft)	TS1	95 (70)	73 (54)	117 (86)	1.30	0.81
	TS2	285 (210)	113 (84)	322 (238)	2.52	0.89
	TS3	232 (171)	130 (96)	246 (181)	1.78	0.94
This study kN-m (kip-ft)	TDSFB	185 (136)	139 (103)	268 (198)	1.33	0.69
	TDS	251* (185)	195 (144)	345 (254)	1.29	0.73
Average Bias					**1.39**	**0.71**
Coefficient of Variation in Point Bias (%)					**28.3**	**17.2**

* This is an extrapolated torsional capacity.

5.7.2 Assessment on Unit Soil Resistance

The previous section focused on the accuracy of design methods with regard to ultimate torsional resistance of drilled shafts. However, such a comparison could obscure the actual accuracy of components of the design methodology. For example, an underestimation of the resistance in one soil layer could be offset or canceled by an overestimation of the resistance in another soil layer. Thus, an investigation into the accuracy of the unit torsional resistance is of interest in this report. For the measured resistance, the representative tributary area used was selected based on the location of the embedded strain gages, whereas the representative tributary area used for the computed capacities was based on the stratigraphy as revealed in borings and CPTs.

Figure 5.37 (with metric units in Figure 5.38) shows the comparison of the computed unit soil resistance profiles of TDS and TDSFB to those developed from the torsional loading tests. Both of the design methods (e.g., the Florida District 7 Method and the CDOT Method.) underestimate the unit torsional soil resistance for the sand to silty sand layer near the base of TDS as shown in Figure 5.37a (with metric units in Figure 5.38a) from the depth of 2.7 m (8.9 ft) to 3.8 m (12.5 ft). The unit soil resistance for the sand to silty sand layer extrapolated from the torsional loading test is 91 kPa (1902 psf). However, the calculated unit soil resistance is 40 kPa (845 psf) and 38 kPa (786 psf) using the Florida District 7 Method and the CDOT Method, respectively. The CDOT method tended to overestimate the unit soil resistance, whereas the Florida District 7 Method tended to underestimate the unit soil resistance in the cohesive soils. This was also observed in Section 5.7.1 for the ultimate torsional resistance. This comparison indicates a need to further investigate and refine design methods for the torsional resistance of drilled shaft foundations.

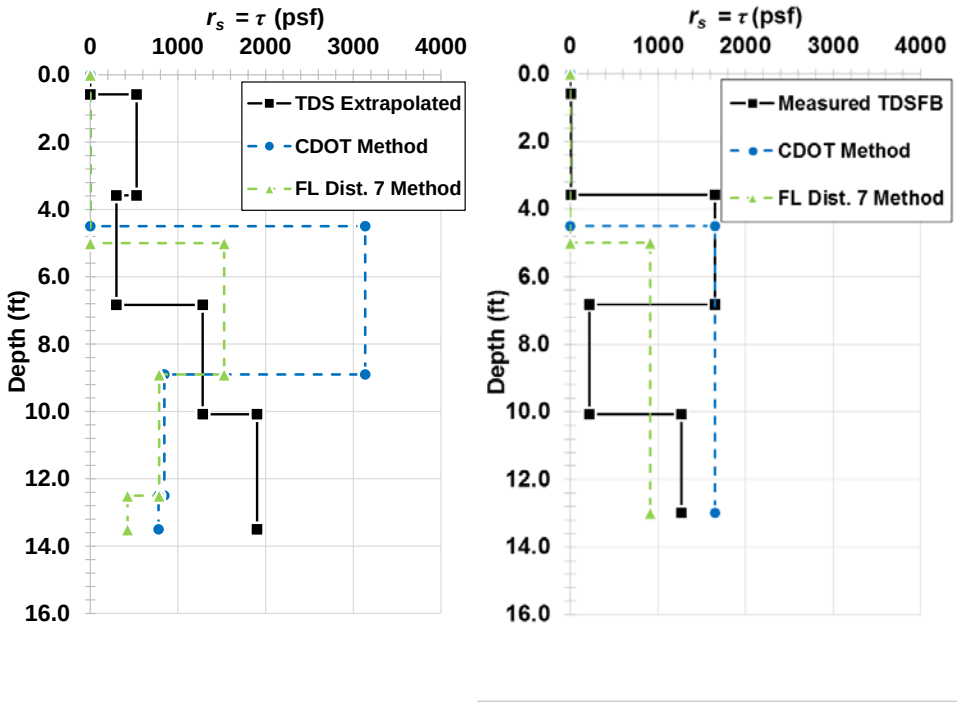

(a) **(b)**

Figure 5.37: Unit soil resistance (r_s) profile and tip resistance (q_t) profile for (a) TDS and (b) TDSFB with imperial units

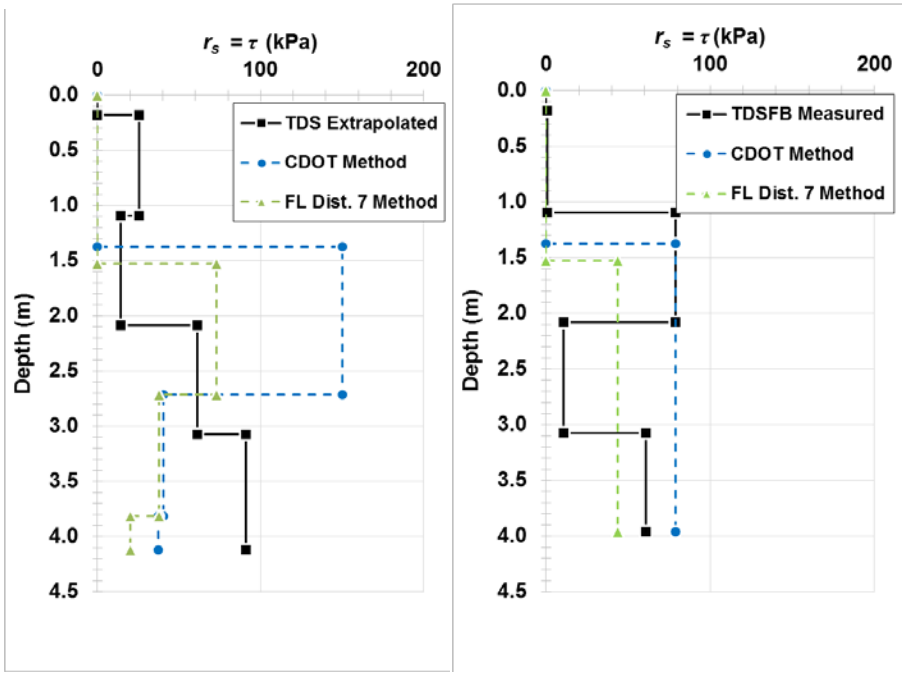

(a) **(b)**

Figure 5.38: Unit soil resistance (rs) profile and tip resistance (qt) profile for (a) TDS and (b) TDSFB with metric units

5.8 CYCLIC LOADING OF THE TEST SHAFTS

Owing to the potential for wind gusts to repeatedly load traffic sign and signal structures, the cyclic response of the drilled shaft foundations at the soil-shaft interface was of interest. Following the quasi-static loading of the drilled shafts, a cyclic loading test was initiated. When the the rotation of TDSFB achieved approximately 13°, the displacements were held for 5 minutes to record the large rotation ESG and RSG data. The displacements of the actuators, d_0, equal to 224 mm (8.8 in), was noted. Then, the shafts were unloaded to achieve a zero load condition, and the zero-load displacements of the actuators, d_1, equal to 218.5 mm (8.6 in) was noted. Then, 20 load-unload cycles between d_0 and d_1 were initiated. Due to a control issue, the actuators exceeded d_1 on the first unload cycle, and instead stopped at d_2 (220 mm or 8.65 in) instead of d_1, as shown in Figure 5.39. The difference of imposed displacements between the first cycle (d_1) and the remaining cycles (d_2) resulted in the difference in rotation between these cycles, as shown in Figure 5.40. Although the overall rotation of TDS after the quasi-static loading was quite small, the magnitude of cyclic change in rotation was similar between TDS and TDSFB.

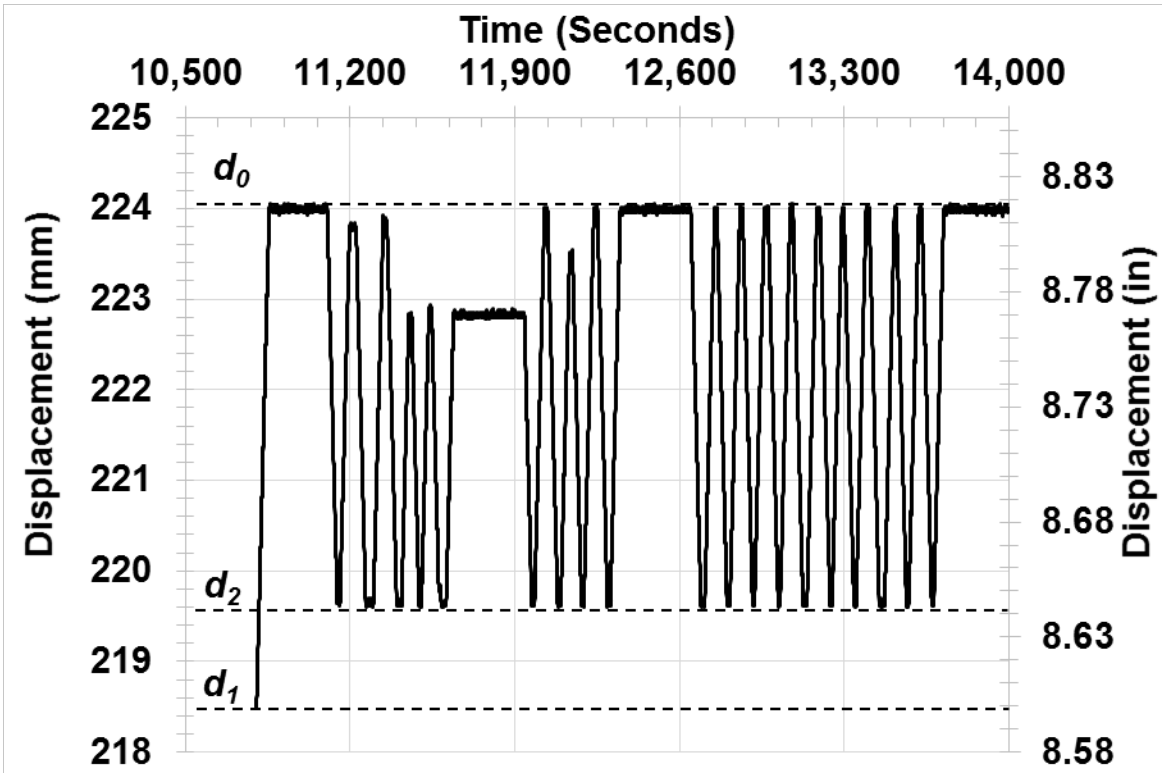

Figure 5.39: Actual displacement protocol used by actuators during the cyclic loading test

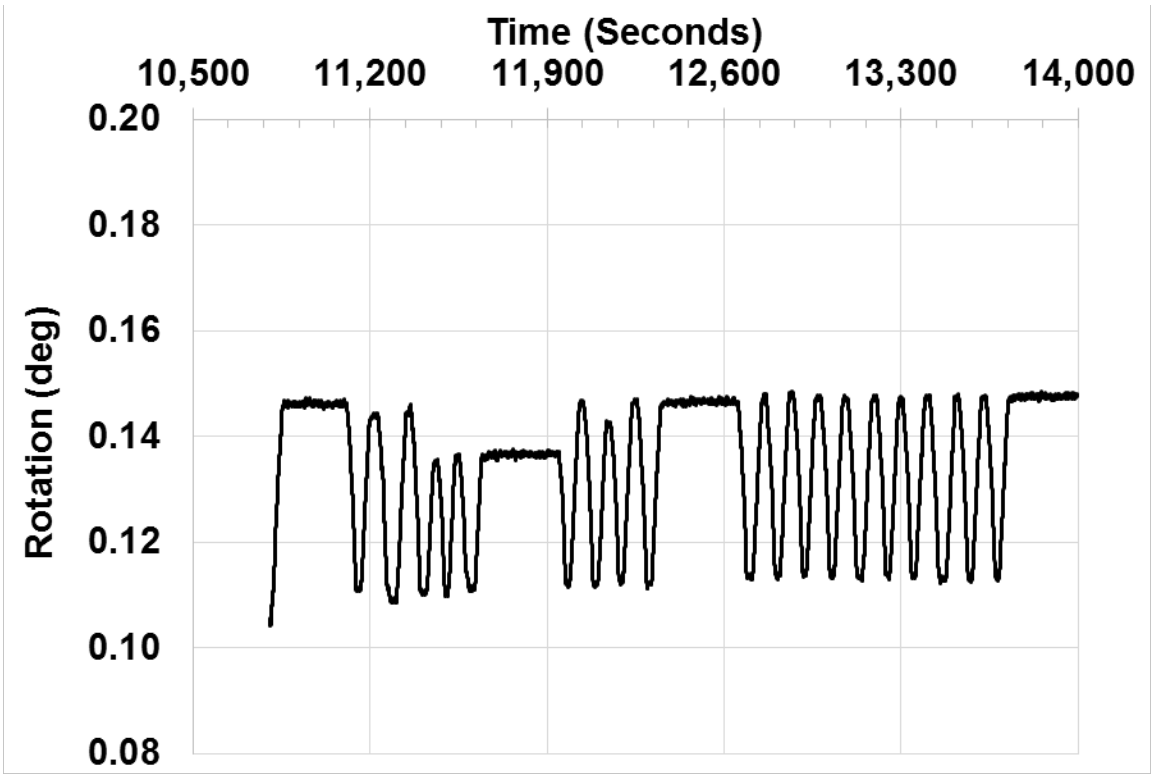

(a)

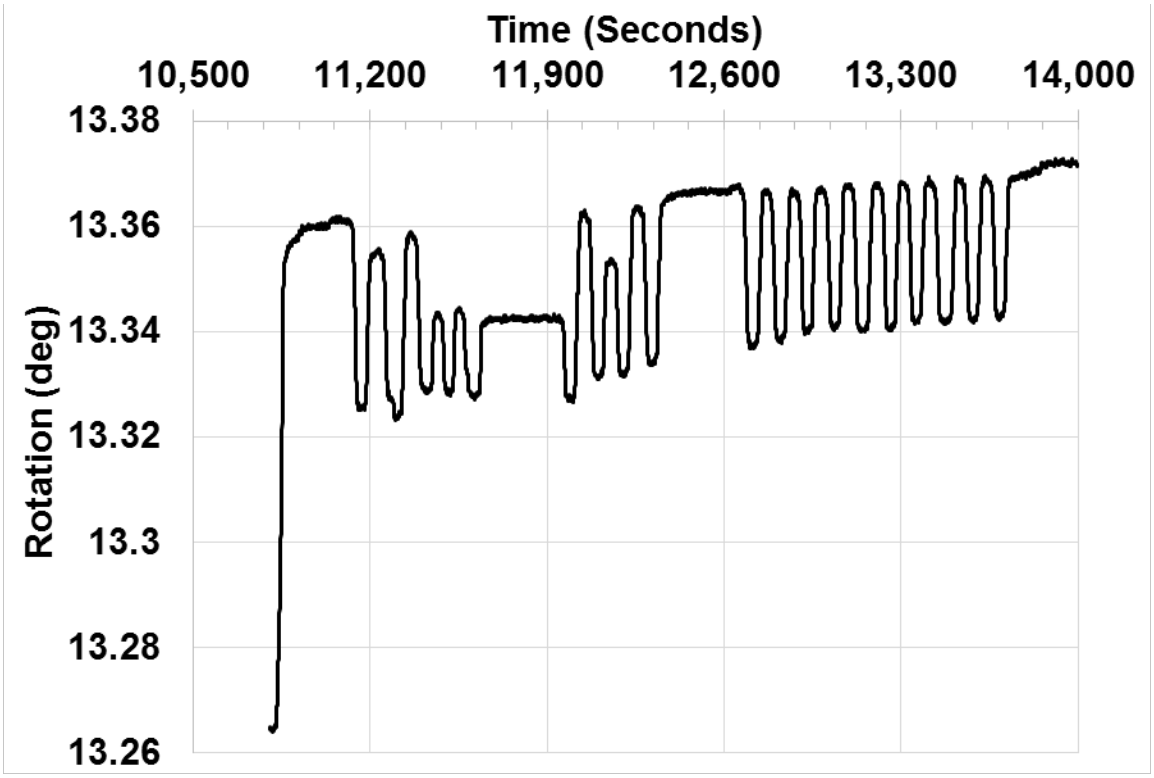

(b)

Figure 5.40: Rotation vs. time series for (a) TDS and (b) TDSFB

The relationship between the torque and the applied rotation for TDS and TDSFB under the cyclic loading protocol is shown in Figure 5.41. In this figure, every five cycles were grouped by color in the sequence of orange, purple, green, and blue. Based on Figure 5.41, the initial stiffness and post-yield slope of each cycle is similar for each shaft, indicating that no global degradation in the torsional response was observed. However, individual instrumented depths did show softening and hardening, as described below. The post-yield slope of TDS is larger than that of TDSFB, a function of the granular layer present for TDS. The average initial stiffness and post-yield stiffness are 9.2×104 kN-m/deg (6.7 ×104 kip-ft/deg) and 2288 kN-m/deg (1688 kip-ft/deg), respectively, for TDSFB, and 9.6×104 kN-m/deg (7.1 ×104 kip-ft/deg) and 4084 kN-m/deg (3012 kip-ft/deg), respectively, for TDS.

The unit soil resistance profiles at 1.75° of rotation (of TDSFB) and after the 1st, 10th and 20th cycle are shown in Figure 5.42. The soil around TDSFB provided negligible torsional resistance from the ground surface until the depth of 1.1 m (3.6 ft) for all of the cases. Compared to the case at 1.75° of rotation of TDSFB, the unit torsional soil resistance for cases under cyclic loading was smaller from the depth of 1.1 m (3.6 ft) to 2.1 m (6.8 ft), indicating that softening of about 36% had occurred by the 20th cycle. The unit torsional soil resistance increased with cycles at depths of 2.1 m (6.8 ft) and deeper, and indicated hardening of up to 111% occurred. Based on these observations, it appears that further investigation into the effect of cyclic torsional loading on the response of drilled shafts is warranted.

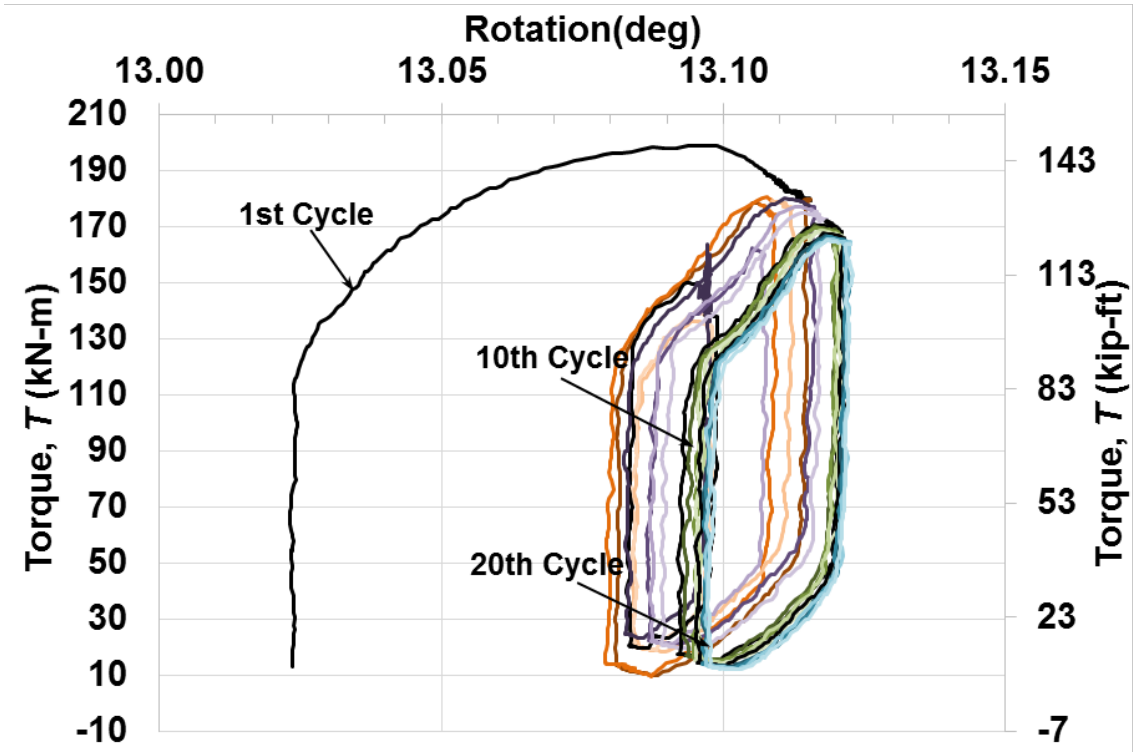

(a)

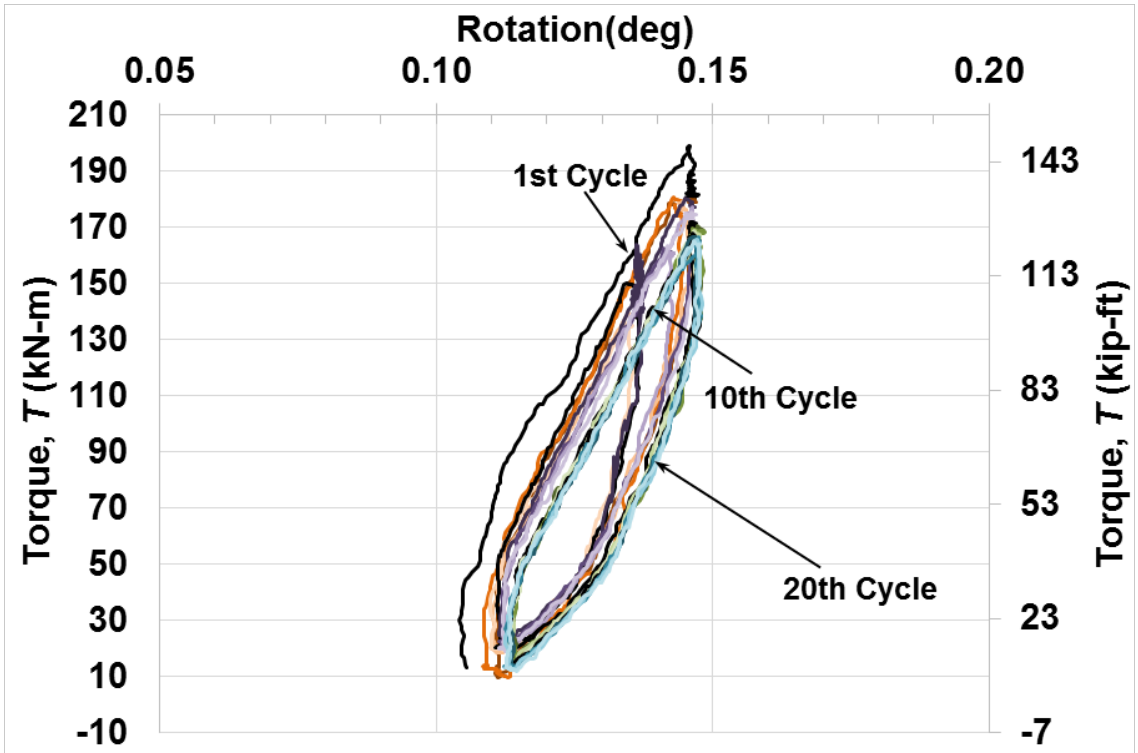

(b)

Figure 5.41: Relationship between torque and rotation under cyclic loading

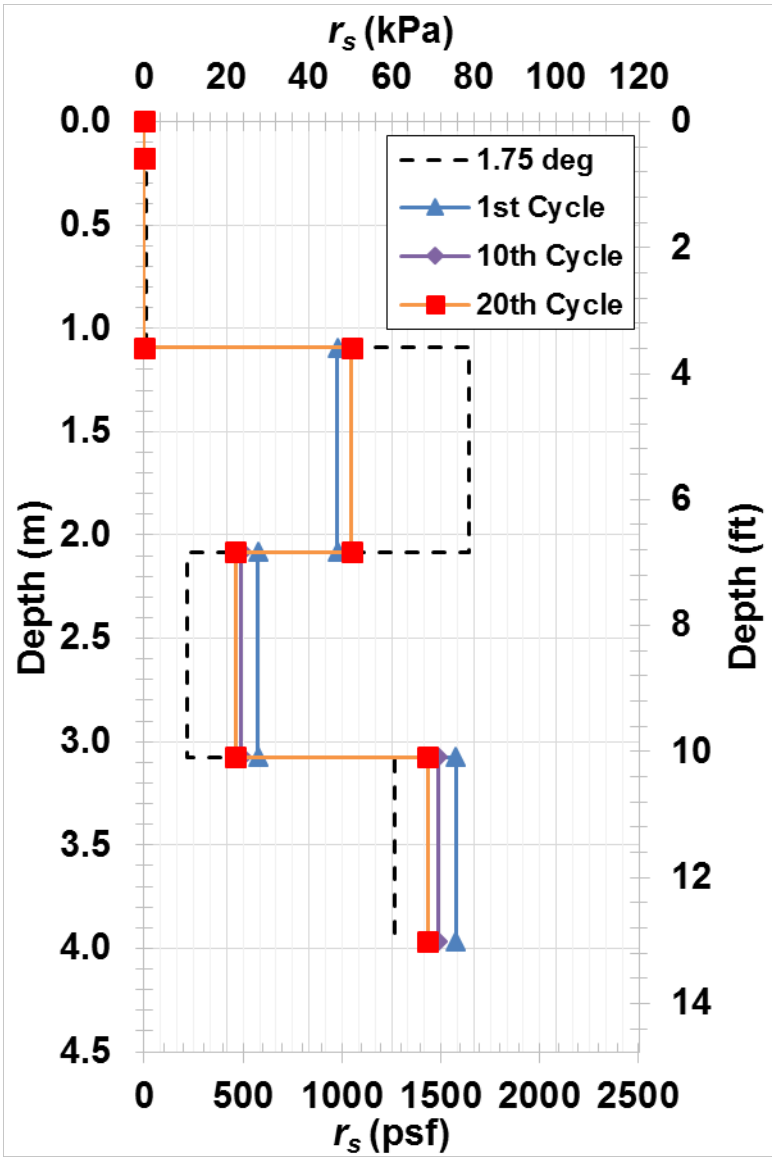

Figure 5.42: Unit soil resistance profile at selected loading cycles for shaft TDSFB

5.9 SUMMARY

Torsional loading tests were conducted at Oregon State University during a strong storm, ideal conditions for evaluating the performance traffic signal and sign foundations. Two shafts were evaluated: one with a production base (TDS) and one with a simulated near-frictionless base (TDSFB). This chapter presented the approaches used for processing and interpreting the recorded data, including: (1) the weighted smoothing function to reduce noise in the string-potentiometer data, (2) the methodology for estimating the internal torque using the recorded torsional strains, and (3) the hyperbolic model to extrapolate the load transfer behavior of TDS. The behavior of TDS and TDSFB under quasi-static torsional loading was evaluated in terms of: (1) the relationship between applied rotation and observed torque at shaft head, (2) torsional load

transfer along the test shafts (i.e., τ–θ curves), (3) the unit torsional soil resistance profiles, and (4) the lateral loading and flexure of test shafts during testing. The measured torsional capacity of TDSFB was 185 kN-m (136 kip-ft) at the rotation of 1.75°; and the extrapolated torsional capacity of TDS was 250 kN-m (184 kip-ft) at the rotation of 1.75°. The ultimate unit torsional soil resistance was in the range of 10 to 100 kPa (corresponding to 209 to 2089 psf). Based on the τ–θ curves for each tributary area of each test shaft, the unit torsional soil resistance under quasi-static loading maintained a near-constant following mobilized of full resistance. The maximum induced lateral load for each test shaft was 73.4 kN (16.5 kips); and the maximum bending moment for TDS and TDSFB estimated using the measured flexural strain was 190 and 262 kN-m (corresponding to 140 and 193 kips-ft), respectively.

The CDOT Design Method and the Florida District 7 Method, both of which can treat layered cohesive and cohesionless soils, were selected to estimate the torsional capacities of the test shafts and compared with the test results. However, these design methods appeared to over- and under-predict the torsional capacity, respectively, and the development of modified design approaches is recommended. Cyclic loading of the shafts was performed following completion of the quasi-static test. No global degradation of the initial and post-yield stiffness was observed for each loading cycle; however, individual instrumented depths did show softening and hardening, indicating that additional research on the cyclic response of torsional shafts is warranted.

6.0 SUMMARY, CONCLUSIONS, AND SUGGESTIONS FOR FURTHER RESEARCH

6.1 SUMMARY AND CONCLUSIONS

Despite the prevalence of the use of drilled shafts for the support of traffic signal and signs along state highways, relatively little is known about the torsional load transfer between the structure and soil providing its support. Some scale model and centrifuge loading tests investigated the torsional load transfer by measuring the shear strains along the test shafts. However, there are only three full-scale torsional loading test series reported in the literature, and these did not report the observation of the torsional load transfer.

To help address this gap in knowledge, two instrumented test shafts, which were designed to support signal pole type SM3 based on ODOT Standard Drawing TM653, were constructed to evaluate the torsional capacity and load transfer of these shafts at full-scale at the Oregon State University (OSU) Geotechnical Engineering Field Research Site (GEFRS). To help evaluate the magnitude of torsional toe resistance, one shaft designated as the torsion test drilled shaft with production base (TDS) was constructed using the dry method, whereas another shaft designated as the torsional drilled shaft with frictionless base (TDSFB) was constructed by placing bentonite chips the bottom of the cavity to create near-zero base shear condition. Both monotonic, quasi-static and cyclic loading tests were performed using two hydraulic actuators and a displacement couple. The imposed rotation and corresponding torque was monitored using string-potentiometers and load cells, respectively. Embedded strain gages were installed on both test shafts over five depths to measure shear strains and reveal the load transfer of the drilled shafts in torsion. After the torsion tests were completed, the test shafts were exhumed andpressure-washed so that the as-built dimensions of the shafts were measured and recorded to accurately investigate the torsional load transfer.

At the end of the quasi-static, monotonic loading test, TDSFB shaft rotated approximately 13°, whereas TDS shaft only rotated about 0.1°. Based on the measured torque-rotation response, the torsional resistance of the TDSFB shaft was fully mobilized at a rotation of the shaft head of about 0.5°. However, the torsional resistance of TDS shaft was not fully mobilized during the test due to the difference in the soil profile. Since the measured torque-rotation response of TDSFB shaft showed an approximate hyperbolic relationship, a hyperbolic model was used to estimate the torque-rotation response of TDS shaft at larger rotations. The measured torsional capacity of TDSFB shaft was 185 kN-m (136 kip-ft) at the rotation of 1.75°, and the extrapolated torsional capacity of TDS was 250 kN-m (184 kip-ft) at the rotation of 1.75°. The maximum induced lateral load for each test shaft was 73.4 kN (16.5 kips); and the measured maximum bending moment for TDS and TDSFB was 190 and 262 kN-m (corresponding to 140 and 193 kips-ft), respectively.

Existing design procedures for predicting torsional capacity of drilled shafts were investigated. The CDOT Design Method and the Florida District 7 Method, both of which can treat layered

cohesive and cohesionless soils, were selected to estimate the torsional capacities of the test shafts and compared with the test results. However, these design methods appeared to over- and under-predict the torsional capacity, respectively, indicating the need for the development of improved methods for assessing torsional capacity.

The torsional load transfer along the test shafts was evaluated with the consideration of the angle of internal twist and τ–θ curves generated. Based on the back-calculated τ–θ curves of TDSFB shaft, the unit torsional soil resistance, r_s (equivalent to τ) was fully-mobilized for each tributary area. Hyperbolic models were used to extrapolate the τ–θ curves of TDS shaft for the tributary areas. The observed ultimate unit torsional soil resistance for TDSFB shaft was in the range of 10 to 80 kPa (corresponding to 209 to 1671 psf); and the extrapolated ultimate unit torsional soil resistance for TDS shaft was in the range of 18 to 100 kPa (corresponding to 376 to 2089 psf).

For the cyclic loading test, no global degradation of the initial and post-yield stiffness with increasing cycle was observed for each test shaft; however, individual instrumented depths did show softening and hardening. The average initial stiffness of TDS shaft was slightly larger than that of TDSFB shaft (9.6×10^4 kN-m/deg or 7.1×10^4 kip-ft/deg, 9.2×10^4 kN-m/deg or 6.7×10^4 kip-ft/deg). The post-yield slope of TDS shaft (4,084 kN-m/deg or 3,012 kip-ft/deg) was approximately 78% larger than that of TDSFB shaft (2,288 kN-m/deg or 1,688 kip-ft/deg).

6.2 SUGGESTIONS FOR FURTHER RESEARCH

The full-scale torsion tests conducted herein revealed the torsional capacity and torsional load transfer mechanisms of two drilled shafts designed to support signal poles. Furthermore, the back-calculated τ–θ curves provide the first full-scale data for use in numerical models of torsional loading. Nonetheless, the understanding of torsional load transfer for drilled shafts and the design of drilled shafts for supporting mast arm traffic signs and signal poles could be further improved by conducting the following additional research:

- The effect of installation method, for example dry, mineral slurry-, or polymeric slurry-supported shaft cavity construction, on load transfer and the τ–θ curves could be explored.

- Improvements in the design methods for the unit torsional resistance of drilled shaft foundations appear warranted based on the assessments conducted herein.

- The available correlations between CPT measurements and the shaft resistance under axial loading could be examined and assessed for use with assessment of the torsional capacity.

- Generalized τ–θ curves related with the soil type, deposition characteristics, construction method, and depth could be developed based on the data from this test and previously reported literature. Then, finite difference models implementing these τ–θ curves could be constructed to perform parametric studies of torsional loading of drilled shafts in uniform, layered, and heterogeneous soil conditions.

- Three-dimensional finite-element analysis of drilled shafts under torsional and combined loading could be conducted to improve the understanding of combined loads on geotechnical performance.

- The impact of the cracking of concrete in torsion on the response of drilled shafts could also be investigated, to improve our understanding on the concrete shear modulus to be used to estimate stiffness and strength of concrete core of the drilled shafts, which is important also for combined torsion and flexural loading.

7.0 REFERENCES

AASHTO. *Standard Specifications for Structural Supports for Highway Signs, Luminaires and Traffic Signals*, 4th Edition, American Association of State Highway and Transportation Officials, Washington, D.C., 2001.

ACI Committee 318. *Building Code Requirements for Structural Concrete (ACI 318-05) and Commentary* (318R-05), American Concrete Institute, Farmington Hills, MI, 2005.

Bizaliele, M.M. Torsional Cyclic Loading Response of a Single Pile in Sand. Dissertation, Presented to Schriftenreihe des Instituts fur Grundbau, Ruhr-Univ., Bochum, Germany, 1992.

Broms, B.B. Lateral Resistance of Piles in Cohesive Soil. *ASCE Journal for Soil Mechanics and Foundation Division*, Vol. 90, No. 2, 1964, pp. 27-63.

Broms, B.B. and J.O. Silberman. Skin Friction Resistance for Piles in Cohesionless Soils. *Sols-Soils*, 1964, pp.10-23.

Brown, D.A., J.P. Turner, and R.J. Castelli. *Drilled Shafts: Construction Procedures and LRFD Design Methods*. Publication FHWA-NHI-10-016. U.S. Department of Transportation, Federal Highway Administration, Washington, D.C., 2010.

Chow, Y. Torsional Response of Piles in Nonhomogeneous Soil. *Journal of Geotechnical Engineering*, Vol. 111, No.7 (942), 1985, pp. 942-947.

Dickenson, S. *Characterization of the Geotechnical Engineering Field Research Site at Oregon State University*. 3rd Edition, 2006.

Dutt, R.N. *Torsional Response of Piles in Sand.* Ph.D. Thesis, Presented to University of Houston, Houston, Texas, 1976.

Dutt, R.N., and M.W. O'Neill. Torsional Behavior of Model Piles in Sand. *Geotechnical Practice in Offshore Engineering*, ASCE, New York, 1983, pp. 315-334.

Geokon, Inc. www.geokon.com. Accessed September 28, 2015.

Gere, J.M., and S.P. Timoshenko. *Mechanics of Materials*, PWS PublishingCompany, Boston, 1997.

Hibbeler, R.C. *Mechanics of Materials*. 9th Edition. Upper Saddle River (NJ): Pearson Prentice Hall, 2013, pp. 181-243.

Hu, Z. *Determining the Optimum Depth of Drilled Shafts Subject to Combined Torsion and Lateral Loads in Saturated Sand from Centrifuge Testing*. Master's Dissertation, University of Florida, Gainesville, FL, 2003.

Laue, J., and T. Sonntag. Pile Subjected to Torsion. *Proceedings of Centrifuge '98*, Balkema, Rotterdam, the Netherlands, 1998, pp. 187–192.

McVay, M.C., D. Bloomquist, and S. Thiyyakkandi. *Field Testing of Jet-Grouted Piles and Drilled Shafts*. Report BDK75-977-41, 91977. Florida Department of Transportation, Tallahassee, FL, 2014.

McVay, M.C., R. Herrera, and Z. Hu. *Determine Optimum Depths of Drilled Shafts Subject to Combined Torsion and Lateral Loads using Centrifuge Testing*. Report No. BC-354, RPWO #9. Florida Department of Transportation, Tallahassee, FL, 2003.

McVay, M.C., and Z. Hu. *Determine Optimum Depths of Drilled Shafts Subject to Combined Torsion and Lateral Loads from Centrifuge Testing (using KB Polymer Slurry)-Supplemental Research*. Report No. BC-545, WO #4. Florida Department of Transportation, Tallahassee, FL, 2003.

Nusairat, J., R. Liang, R. Engel, D. Hanneman, N. AbuHejleh, and K. Yang. *Drilled Shaft Design for Sound Barrier Walls, Signs, and Signals*. Report No. CDOT-DTD-R-2004-8, Colorado Department of Transportation, Denver, CO, 2004.

ODOT. *Geotechnical Design Manual*. Oregon Department of Transportation (ODOT), Salem, OR, 2014.

ODOT. ODOT *Traffic Structures Design Manual*, 2015 Edition. Oregon Department of Transportation (ODOT), Salem, OR, 2015a.

ODOT. *Oregon Standard Specifications for Construction*. Oregon Department of Transportation (ODOT), Salem, OR, 2015b.

O'Neill, M.W. *Determination of the Pile-Head, Torque-Twist Relationship for a Circular Pile Embedded in a Clay Soil*. Master's Thesis Presented to the University of Texas, at Austin, TX, 1964.

O'Neill, M.W., and K.M. Hassan. Drilled Shafts: Effects of Construction on Performance and Design Criteria. Proceedings of the International Conference on Design and Construction of Deep Foundations, December 1994, Vol. 1, 1994, pp. 137-187.

O'Neill, M.W., and L.C. Reese. *Drilled Shafts: Construction Procedures and Design Methods.* Publication FHWA-IF-99-025, Federal Highway Administration, Office of Implementation, McLean, VA, 1999.

Poulos, H.G. Torsional Response of Piles. *Journal of the Geotechnical Engineering Division*, Vol. 101, No. 10, 1975, pp. 1019-1035.

Randolph, M.F. Design Consideration for Offshore Piles. *Geotechnical Practices in Offshore Engineering*, ASCE, Austin, 1983, pp. 422–439.

Randolph, M.F. Piles Subjected to Torsion. *Journal of the Geotechnical Engineering Division*, American Society of Civil Engineers, Vol.107, Issue 8, 1981, pp. 1095-1111.

Reiter, M. *December 1–4, 2007 Storm Events Summary*. Weyerhaeuser Company, Federal Way, WA, 2008.

Sheahan, T., C. Ladd, and J. Germaine. Rate-Dependent Undrained Shear Behavior of Saturated Clay. *Journal of Geotechnical Engineering*, Vol. 122, No. 2, 1996, pp. 99–108.

Stoll, U.W. Torque Shear Test of Cylindrical Friction Piles. *Civil Engineering*, Vol. 42, No. 4, 1972, pp. 63-65.

Tawfiq, K. *Drilled Shafts Under Torsional Loading Conditions*. Report No. B-9191, Florida Department of Transportation, Tallahassee, FL, 2000.

Tokyo Sokki Kenkyujo Co. www.tml.jp. Accessed September 28, 2015.

USGS. *The National Map Viewer*. Available: http://viewer.nationalmap.gov/viewer/. Accessed September 2, 2015.

Zhang, L.M., and L.G. Kong. Centrifuge Modeling of Torsional Response of Piles in Sand. *Canadian Geotechnical Journal*, Vol. 43, No. 5, 2006, pp. 500-515.

APPENDIX A

CONE PENETRATION TEST RESULTS AND

BORING LOG

Appendix A.1 Cone Penetration Test Results

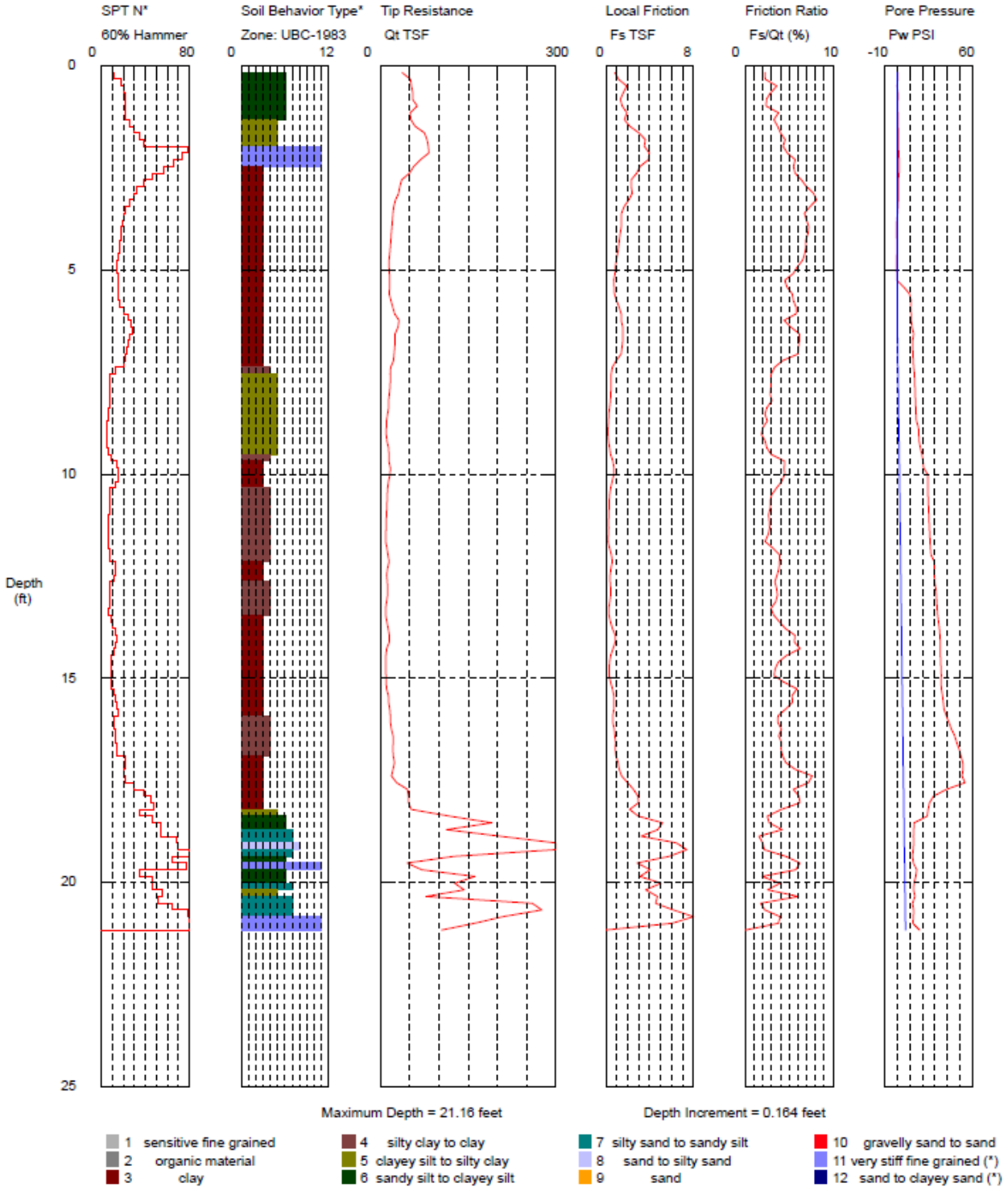

Figure A-1 Cone penetration test results of CPT1 performed at the GEFRS

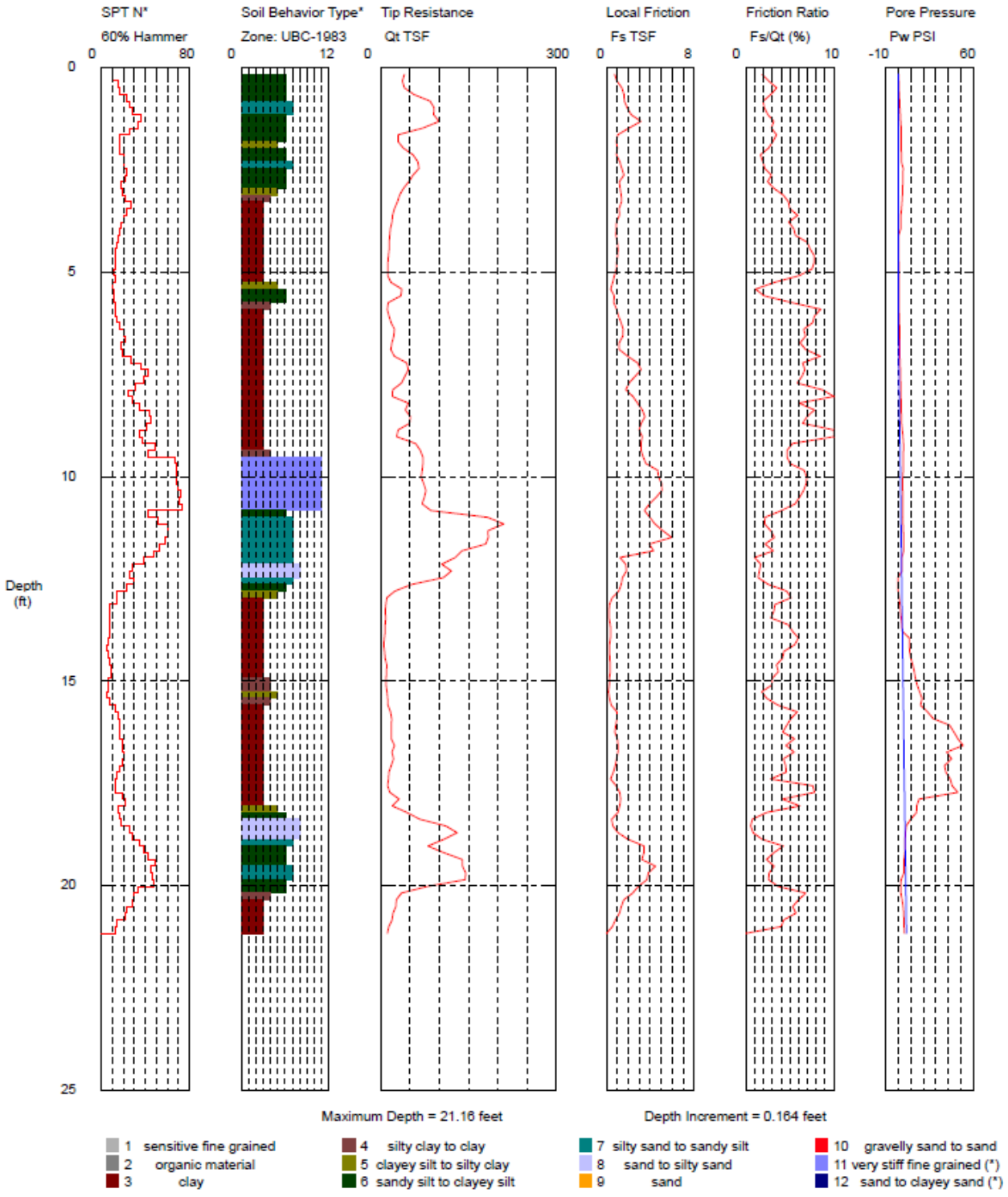

Figure A-2 Cone penetration test results of CPT2 performed at the GEFRS

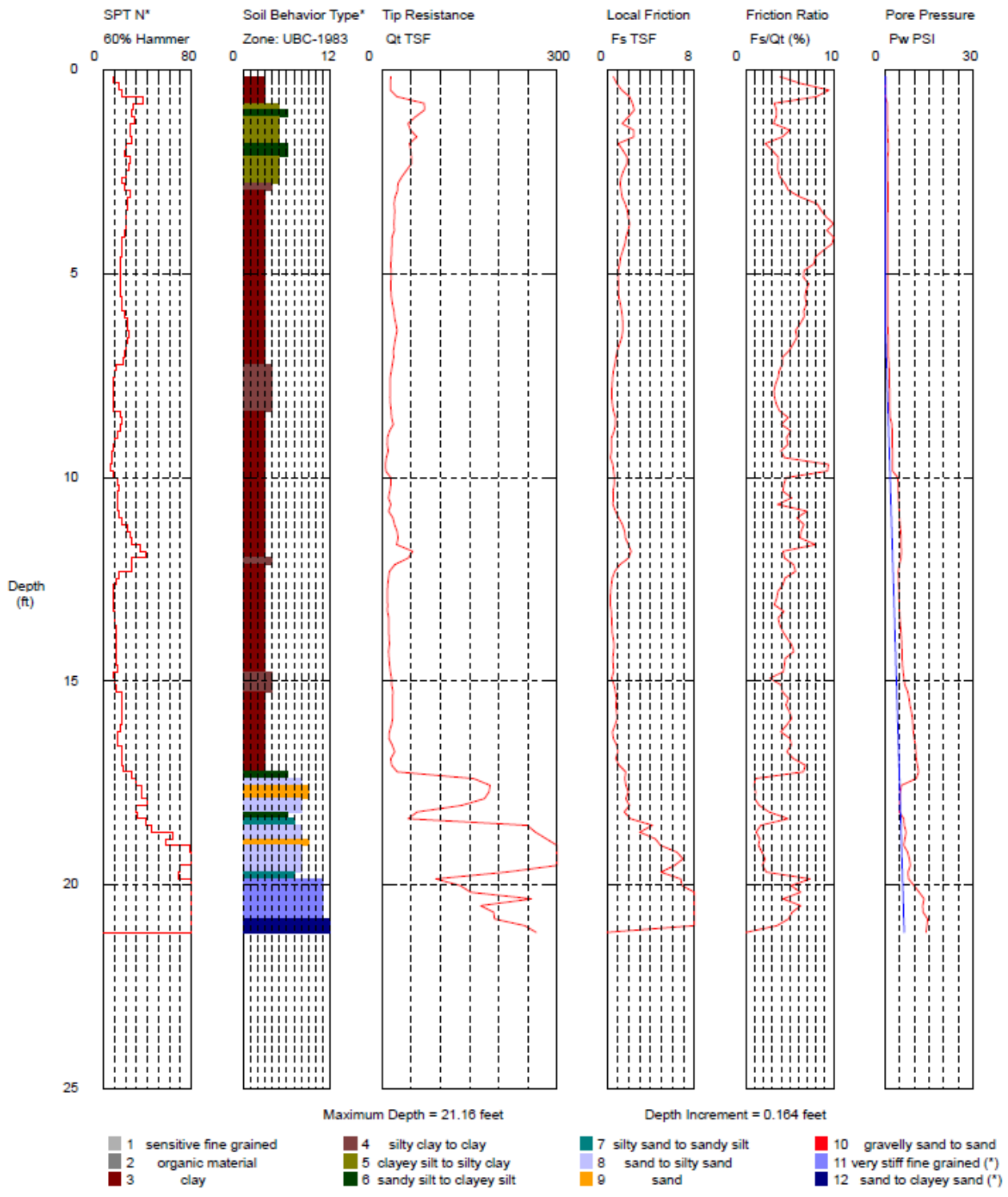

Figure A-3 Cone penetration test results of CPT3 performed at the GEFRS

Appendix A.2 Standard Penetration Test Boring Log

Date: 10/6/2014
Drill Equipment: Truck-mounted, mud-rotary, CME 75 HT Drill Rig
Hammer Type: automatic hammer
Drilled By: Western States Soil Conservation, Inc.
Logged By: Qiang Li

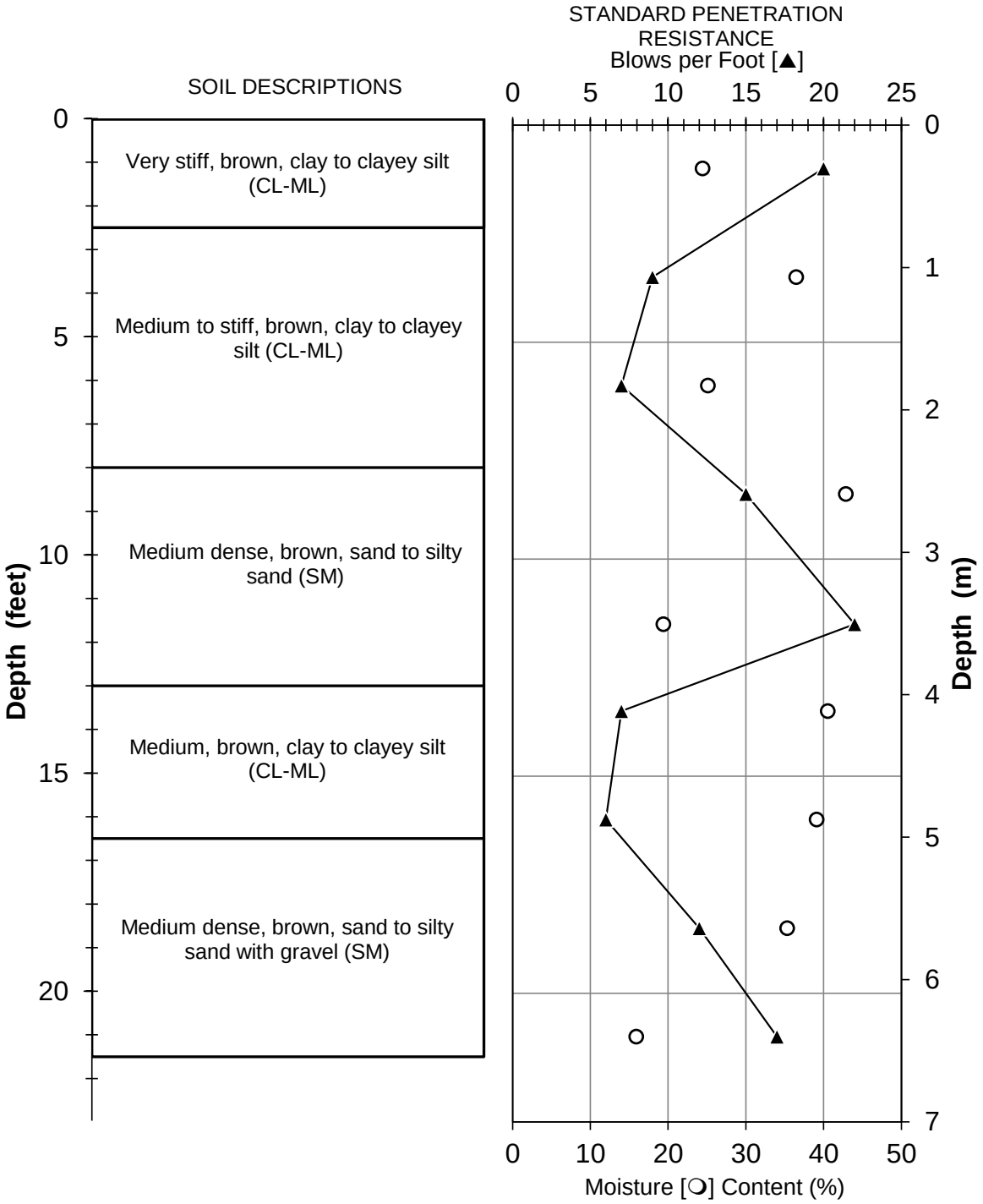

Appendix A.3 Undisturbed Sampling Log

Date: 10/6/2014
Drill Equipment: Truck-mounted, mud-rotary, CME 75 HT Drill Rig
Drilled By: Western States Soil Conservation, Inc.
Logged By: Qiang Li

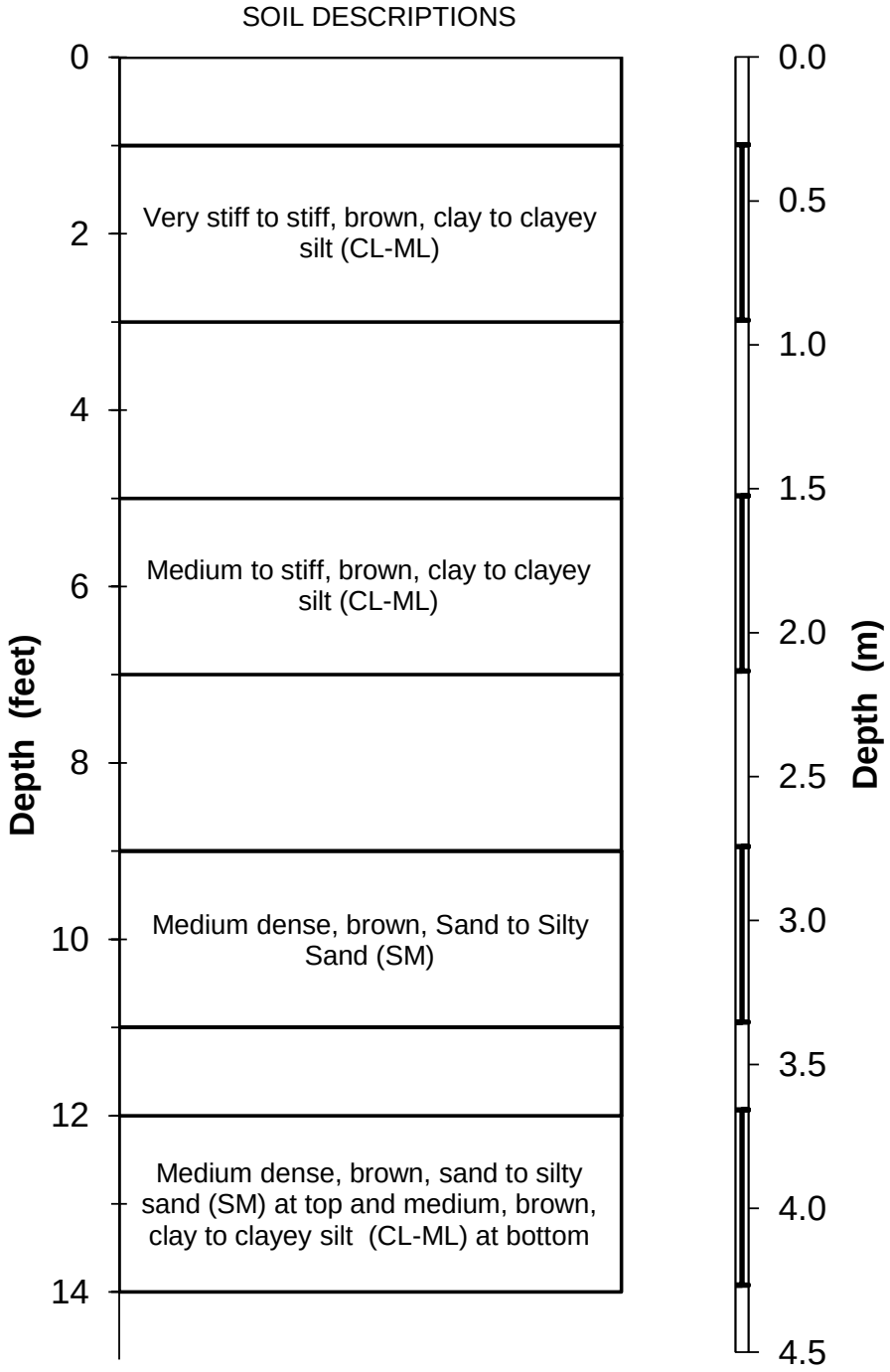

APPENDIX B

TRAFFIC SIGNAL SUPPORTS

STANDARD DRAWINGS

STANDARD SIGNAL ARM LOADS							
Signal Pole Type	Signal Arm Length	Signals			Sign		DS Max. for S2
		4L Qty.	2 Qty.	5 * Qty.	S1 Qty.	S2 * Qty.	
SM1 or SM1L	15'	1	0	1	2	0	N/A
SM2 or SM2L	20'	1	1	1	3	0	N/A
	25'	1	1	1	3	0	
SM3 or SM3L	30'	1	1	1	3	1	9'-1"
	35'	1	1	1	3	1	
SM4 or SM4L	40'	1	2	1	4	1	11'-1"
	45'	1	2	1	4	1	
SM5 or SM5L	50'	1	2	1	4	1	21'-1"
	55'	1	2	1	4	1	

* - Load location is the closest sign or signal of that type to the vertical post.

1. Camera mounted on 6 ft arm placed at any location on signal arm.
2. Fire Pre-Emption may be placed at any location along the mast arm.
3. Loads stated in the table produce reactions as shown in tables on TM651. Modifications to the loading shown require analysis to verify the structural adequacy of the pole.
4. Physical fit of the loading must be verified.

SIGNAL ARMS DEFLECTION		
Signal Arm Length "SA"	Allowable Dead Load Deflection	Allowable Total Load Deflection
15' or less	0.01"SA"	0.05"SA"
20'	2 1/2"	12"
25'	3 1/2"	15"
30'	5"	21"
35'	7"	29"
40'	9 1/2"	38"
45'	1'-1/2"	48"
50'	1'-4"	60"
55'	1'-8"	74"

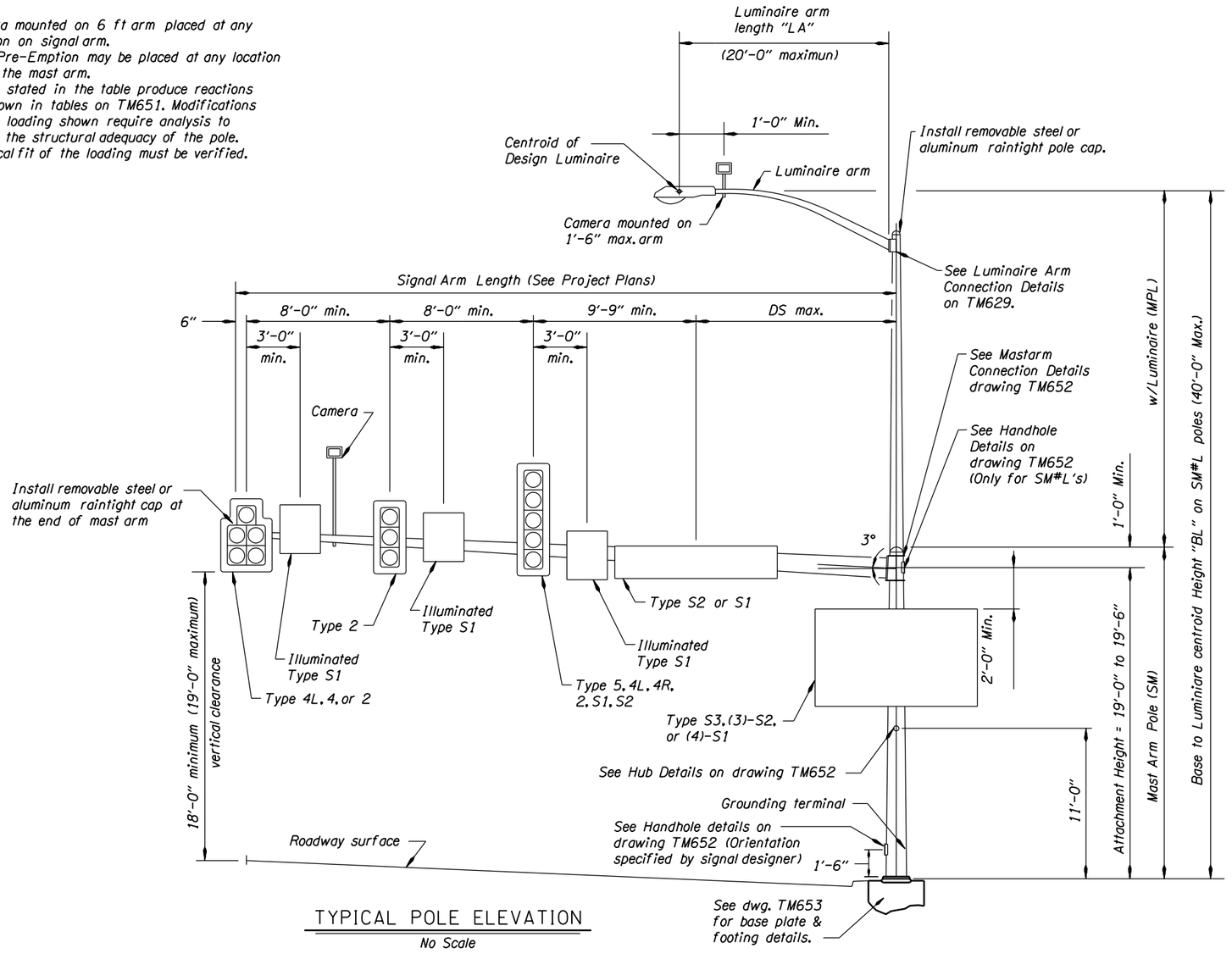

TYPICAL POLE ELEVATION

No Scale

VERTICAL POST LOADS								
Description	Maximum Centerline Elevation	Height (Each)	Width (Each)	Depth (Each)	Area Front (sq. ft)	Area Side (sq. ft)	Area Bottom (sq. ft)	Weight 0" Ice (lbs)
2-Ped. Push Buttons	3'-6"	7 3/4"	5"	3 3/8"	0.27	0.18	0.12	3.0
Controller Cabinet	5'-9"	46"	24"	22"	7.67	7.03	3.67	300
2-Pedestrian Signals	8'-3 1/2"	18 3/4"	19"	19"	2.47	2.47	2.51	25.0
Terminal Cabinet	10'-9"	18 1/8"	6 3/4"	8 3/8"	0.85	1.05	0.39	25.0
Guide Sign (S3)	15'-0"	72"	120"	8 3/8"	60.0	1.00	1.67	395
Photoelectric Cell	38'-4"	2 1/4"	3 1/4"	3 1/4"	0.05	0.05	0.07	5.0

1. Physical fit of the loading must be verified.

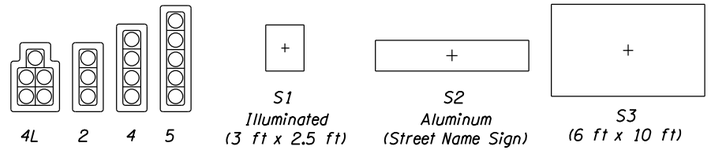

SIGNAL POLE APPURTENANCE TYPES

APPURTENANCE LOADS				
Type	Area Front (sq. ft)	Area Side (sq. ft)	Area Bottom (sq. ft)	Weight 0" Ice (lbs)
4L	12.4	6.61	3.64	145
2	8.67	6.61	1.95	85.0
4	11.0	8.49	1.95	97.0
5	13.3	10.36	1.95	142
S1	7.50	2.38	1.72	71.0
S2	21.0	0.00	1.67	105

CALC. BOOK NO.	BASELINE REPORT DATE	ACCOMPANIED BY DWGS.	SHEET
5301	07-JAN-2011	TM651, TM652, TM653, TM679	1 OF 4

NOTE: All material and workmanship shall be in accordance with the current Oregon Standard Specifications

The selection and use of this Standard Drawing, while designed in accordance with generally accepted engineering principles and practices, is the sole responsibility of the user and should not be used without consulting a Registered Professional Engineer.

OREGON STANDARD DRAWINGS
TRAFFIC SIGNAL SUPPORTS
GENERAL DETAILS & DESIGN CRITERIA

2015

DATE	REVISION DESCRIPTION

tm650.dgn 11-JUL-2014

TM650

tm651.dgn 11-JUL-2014

GENERAL NOTES:

1. Signal supports shall be designed in accordance with the AASHTO Standard Specifications for Structural Supports for Highway Signs, Luminaires and Traffic Signals 4th edition, 2001, 2002, and 2003 interim revisions.
2. All traffic signal supports shall conform to the design criteria and details shown on these drawings except as approved by the Engineer.
3. The design basic wind speed (3 second gust) shall be 110 mph, gust factor G = 1.14, Ir = 1.0 (50 yr recurrence interval), Fatigue Category II, no galloping, and truck speed = 55 mph.
4. Signal poles from this standard are not allowed over highways I-5, I-84, I-205, I-405, US 26 (Sunset Hwy) between mile points 64.3 - 73.0, I-105, and I-82. Signal poles on these highways require a Fatigue Category I.
5. Pole and arm shafts may be either round, hexdecagonal, dodecagonal, or octagonal but shapes shall not be mixed on a project. Dimensional tolerances of ASTM A595 shall apply to all tapered steel tubing members. Additionally, the diameter of round tapered steel tubing members or the dimensions across the flats of octagonal tapered steel tubing members shall not vary more than 2% from specified dimension. Two ply and fluted poles or arms are not permitted.
6. Pole taper shall be equal to .0117 in/in.
7. Anchor rods shall conform to ASTM Specification F1554 Gr. 55, Supplemenetary Requirement "S2" that include grade and manufacturer's identification.
8. High strength bolts shall conform to ASTM Specification A325 Type 1.
9. Nuts for high strength bolts shall be heavy hex and conform to ASTM A563 Grade DH with supplmentary requirements "S1" and "S2".
10. Hardened steel washers shall conform to ASTM F436 Type 1.
11. Direct Tension Indicators (DTI) shall be the compressible-washer type, mechanically galvanized, conforming to ASTM F959.
12. Steel sheet for poles and arm shall conform ASTM A595, Grades A or B, ASTM A572 Gr. 50, or approved equal. All other steel sheet and plate shall conform to AASHTO specification M223 (ASTM A572), or approved equal. Supplement S18 of ASTM A6 regarding maximum tensile strength shall apply.
13. All structural steel including fasteners shall be hot dip galvanized after fabrication unless otherwise noted.
14. Galvanize-Control Silicon, typical. Silicon content of the base metal shall be in the range of 0 to 0.04% or 0.15 to 0.25%.
15. Footing concrete shall be Commercial Grade Concrete (fc=3000 psi) per Specification Section 440. Grout in grout pad shall be non-shrink high early strength grout (non-ferrous) with a minimum strength of 5000 psi. Footing concrete may be used as an alternate to grout.
16. Reinforcing steel shall conform to AASHTO M31, Grade 60 (ASTM A615 or A706). A min. lap splice length of 32 bar diameters shall be used unless shown otherwise.
17. Computed deflection of these poles at full design loading shall be limited to 5% of the pole length. Computed dead load deflection of the poles shall be limited to 1% of the pole length. Pole shall be raked to offset the computed dead load deflection. Computed deflection (ignoring pole bending and/or rotation) of signal arms shall not exceed that listed in the Signal Arm Deflection Table on TM650. Additionally, the amplitude (maximum up to maximum down as measured at the tip of the arm) of wind induced vertical oscillations shall not exceed 1.5% of the signal arm length. Luminaire arms and pole extensions to support luminaire arms shall meet requirements of drawing TM629.
18. Hubs for cabinets and/or other appurtenances shall be welded into the pole prior to galvanizing. Poles may be tapped for up to 1" galvanized bolts after pole has been galvanized.
19. Longitudinal seam welds within 6" of a cirumferential weld shall be complete penetration welds. Weld inspection shall be in accordance with AWS D1.1 and the special provisions. Inspect seam welds using cyclically loaded criteria. Hubs shall be 3000# threaded forged carbon steel flat weld hubs by Anvil Products Inc., Phoenix Forging Co., Bonney Forge & Tool Works or approved equal.
20. Grounding terminal shall be ½" UNC x 1½" Type 308, 309 or 310 threaded stainless steel weld studs.
21. Tighten 4 bolt arm connection bolts and tighten anchor rods in accordance with 962.46(j)(2).
22. Tighten 8 bolt arm connection bolts in accordance with 930.40(d).
23. Round and smooth all edges along electrical way.
24. The Minimum arm flange thickness shall be equal to the value where prying action is not included in the bolt calculation.

Standard Maximum Base Reactions								
Signal Pole Type	Signal Arm Lengths	Wind Load Case II				Controlling Fatigue		
		Axial (Kips)	Shear (Kips)	Moment (Kip-ft)	Torque (Kip-ft)	Shear (Kips)	Moment (Kip-ft)	Torque (Kip-ft)
SM1	15′	2.10	5.15	80.39	16.95	0.68	10.39	2.13
SM2	20′, 25′	2.66	6.23	105.41	42.54	0.82	13.35	5.37
SM3	30′, 35′	3.49	7.77	138.43	82.87	1.00	17.10	10.31
SM4	40′, 45′	4.51	9.00	173.46	132.72	1.16	20.54	16.50
SM5	50′, 55′	5.69	9.23	190.91	181.60	1.18	21.62	22.55
SM1L	15′	2.96	6.09	113.28	23.22	0.79	14.08	2.84
SM2L	20′, 25′	3.69	7.23	139.41	48.81	0.94	17.17	6.08
SM3L	30′, 35′	4.39	8.80	176.51	87.88	1.14	21.43	11.02
SM4L	40′, 45′	5.94	10.14	215.11	136.97	1.31	25.27	17.21
SM5L	50′, 55′	7.34	10.56	241.17	187.96	1.34	26.49	23.26

Standard Maximum Mast Arm Reactions						
Signal Pole Type	Signal Arm Lengths	Wind Load Case II			Controlling Fatigue	
		Axial (Kips)	Shear (Kips)	Moment (Kip-ft)	Shear (Kips)	Moment (Kip-ft)
SM1, SM1L	15′	0.06	1.98	18.44	0.23	2.18
SM2, SM2L	20′, 25′	0.10	3.14	46.20	0.37	5.48
SM3, SM3L	30′, 35′	0.15	4.51	89.42	0.53	10.51
SM4, SM4L	40′, 45′	0.23	5.91	146.67	0.67	16.82
SM5, SM5L	50′, 55′	0.34	6.78	211.94	0.70	22.99

Luminaire Arm Reactions					
Arm Lengths	Wind Load Case II			Controlling Fatigue	
	Axial (Kips)	Shear (Kips)	Moment (Kip-ft)	Shear (Kips)	Moment (Kip-ft)
6′	0.03	0.31	1.49	0.03	0.15
10′	0.06	0.38	2.85	0.04	0.29
15′	0.08	0.47	4.96	0.05	0.51
20′	0.05	0.55	7.24	0.06	0.74

CALC. BOOK NO.	BASELINE REPORT DATE	ACCOMPANIED BY DWGS.	SHEET
5301	07-JAN-2011	TM650, TM652, TM653	2 OF 4

NOTE: All material and workmanship shall be in accordance with the current Oregon Standard Specifications

The selection and use of this Standard Drawing, while designed in accordance with generally accepted engineering principles and practices, is the sole responsibility of the user and should not be used without consulting a Registered Professional Engineer.

OREGON STANDARD DRAWINGS

TRAFFIC SIGNAL SUPPORTS NOTES AND REACTIONS

2015

DATE	REVISION DESCRIPTION

TM651

Effective Date: February 1, 2015 - May 31, 2015

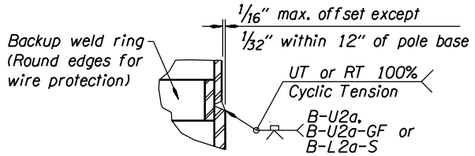

POLE AND ARM SPLICE
WELD DETAILS
No Scale

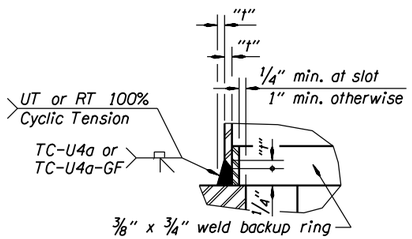

TC-U4a WELD DETAIL
No Scale

Mast arm Connection				
Signal Arm Lengths	N Number	D Bolt Diam.	BC Bolt Circle	V Bolt Spacing
15'	4	1"	9 1/2"	——
20', 25'	4	1 1/4"	14"	——
30', 35'	4	1 1/2"	15 1/2"	——
40', 45'	8	1 "	——	5"
50', 55'	8	1 1/4"	——	6"

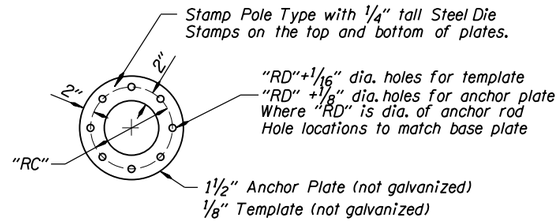

ANCHOR PLATE AND TEMPLATE DETAIL
No Scale

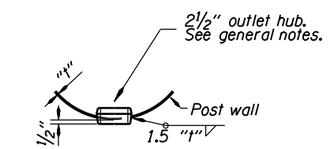

HUB WELD DETAIL
No Scale

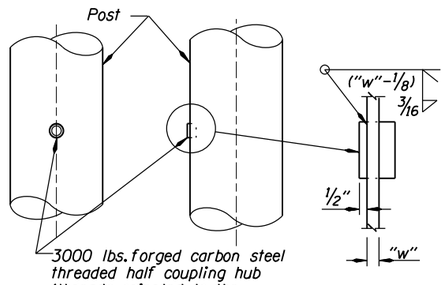

3000 lbs. forged carbon steel threaded half coupling hub (threads oriented to the outside of post) by "Bonney Forge", "Phoenix Forge" or approved equal. Inside edge of conduit hub shall be smooth

HUB WELD DETAIL
No Scale

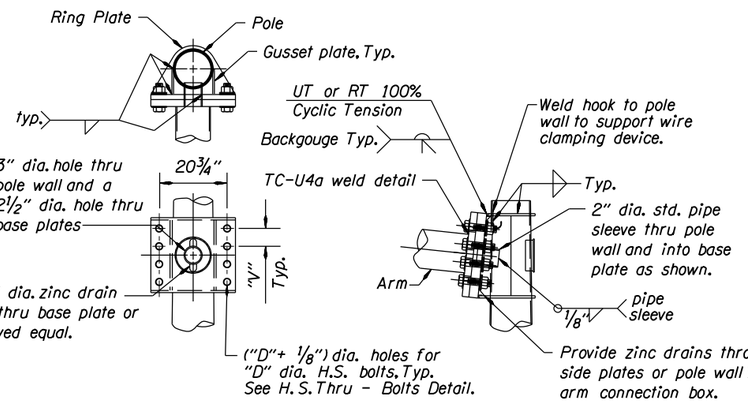

8 BOLT ARM CONNECTION DETAILS
No Scale

ARM CONNECTION NOTES:
Gusset plates are 1/4" min. thickness.
Ring plates are 3/8" min. thickness.
See general notes on TM651 for bolt tightening.

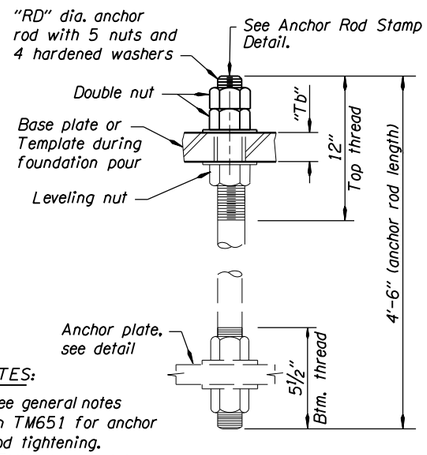

NOTES:
- See general notes on TM651 for anchor rod tightening.
- "Tb" determined by manufacturer.

ANCHOR ROD DETAIL
No Scale

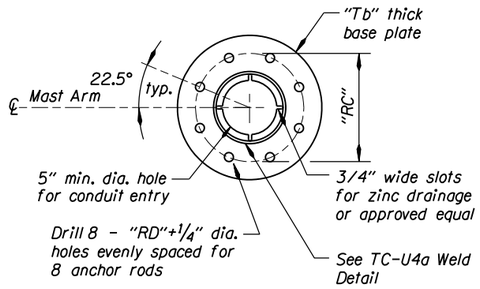

PLAN - BASE PLATE
No Scale

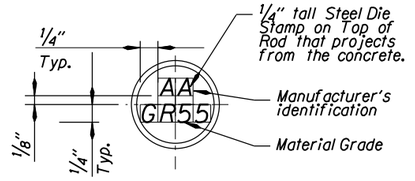

Note: The end of each anchor rod shall be color coded yellow.

ANCHOR ROD STAMP DETAIL
No Scale

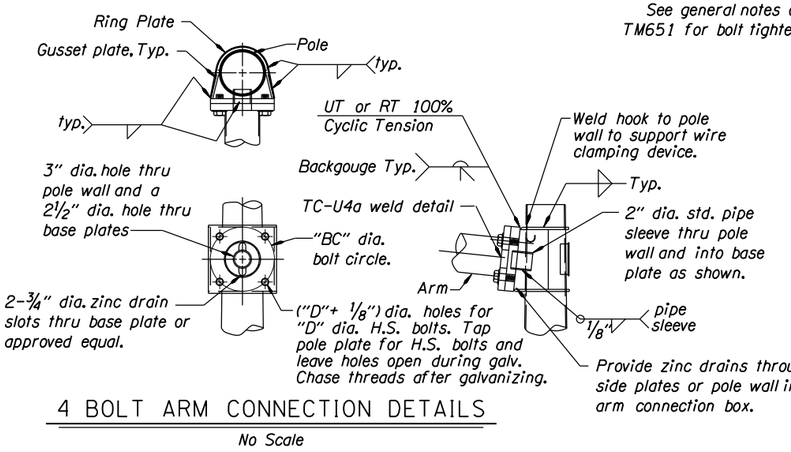

4 BOLT ARM CONNECTION DETAILS
No Scale

Anchor Rods and Base Plate Data			
Mastarm Pole Type	Strain Pole Type	RD Rod Diam.	RC Rod Circle
SM1	-----	1 1/4"	16 1/2"
SM2, SM1L	-----	1 1/2"	17"
SM3, SM2L	STP1, STP1L, STP2, STP2L	1 1/2"	20"
SM4, SM3L	STP3, STP3L, STP4, STP4L	1 3/4"	22"
SM5, SM4L	-----	1 3/4"	23"
SM5L	STP5, STP5L, STP6, STP6L, STP7, STP7L	2"	23 1/2"

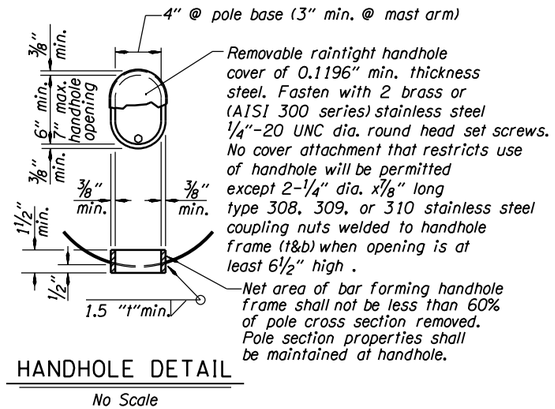

HANDHOLE DETAIL
No Scale

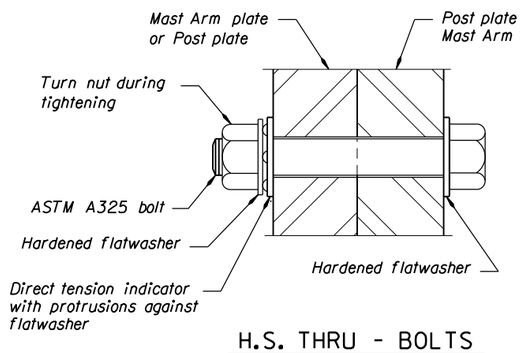

H.S. THRU - BOLTS
No Scale

CALC. BOOK NO.	BASELINE REPORT DATE	ACCOMPANIED BY DWGS.	SHEET
5301	10-JAN-2014	TM650, TM651, TM653	3 OF 4

NOTE: All material and workmanship shall be in accordance with the current Oregon Standard Specifications

The selection and use of this Standard Drawing, while designed in accordance with generally accepted engineering principles and practices, is the sole responsibility of the user and should not be used without consulting a Registered Professional Engineer.

OREGON STANDARD DRAWINGS

TRAFFIC SIGNAL SUPPORTS STEEL DETAILS

2015

DATE	REVISION DESCRIPTION

Standard Foundations						
Foundation Number	Mastarm Pole Types	Strain Pole Types	"FD" Diameter Min.	Vertical Rebar	Hoop Size and Spacing	Hoop Lap Length
1	SM1	-----	36"	8-#8	#4 at 6"	18"
2	SM2,SM1L	-----	36"	8-#8	#4 at 6"	18"
3	SM3, SM2L	STP1, STP1L	36"	8-#8	#4 at 6"	18"
4	SM4, SM3L	STP2, STP2L	42"	10-#8	#5 at 6"	21"
5	SM5, SM4L	STP3, STP3L	42"	10-#9	#5 at 6"	21"
6	SM5L	STP4, STP4L	42"	10-#9	#5 at 6"	21"
7	-----	STP5, STP5L	42"	TBD	TBD	TBD
8	-----	STP6, STP6L	42"	TBD	TBD	TBD
9	-----	STP7, STP7L	42"	TBD	TBD	TBD

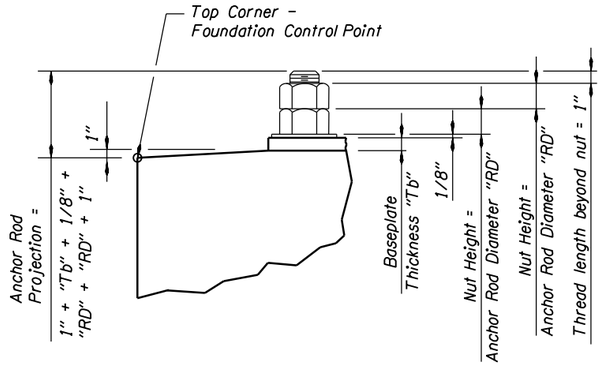

PROJECTION DETAIL

No Scale

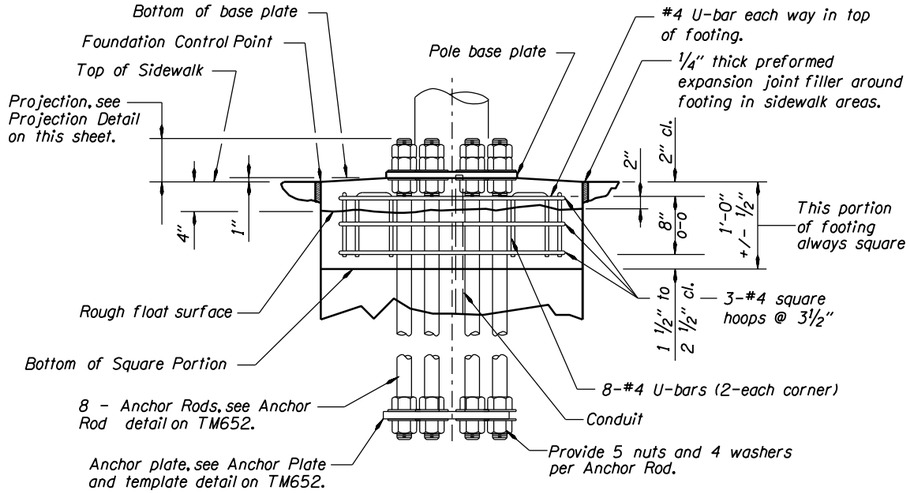

ELEVATION - TOP OF FOOTING

No Scale

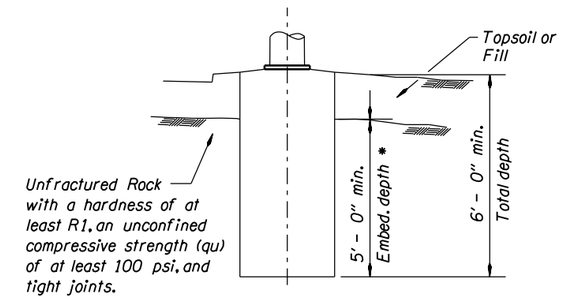

* - or embed to a total depth that is at least equal to the required footing depth.

ROCK INSTALLATION REQUIREMENTS

No Scale

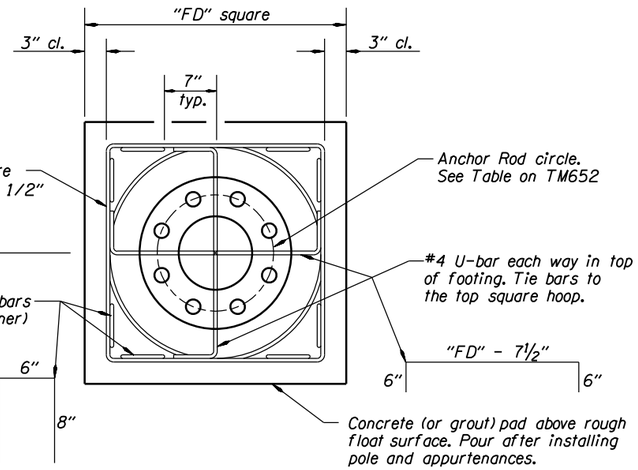

PLAN - TOP OF FOOTING

No Scale

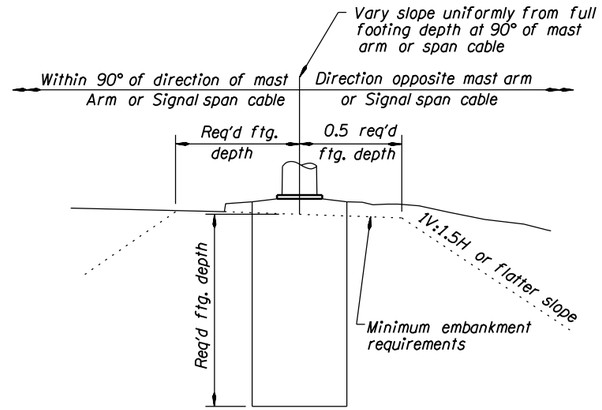

MINIMUM EMBANKMENT REQUIREMENTS

No Scale

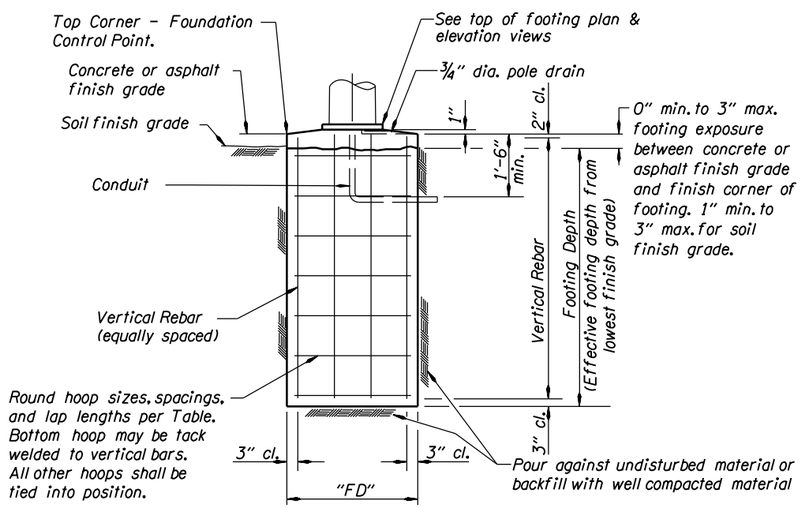

TYPICAL FOOTING ELEVATION

No Scale

NOTES:

See TM651 for general notes.
The pier torsional forces have been designed according to the ACI 318.
Shafts 7,8, and 9 do not include torsion rebar.

CALC. BOOK NO.	BASELINE REPORT DATE	ACCOMPANIED BY DWGS.	SHEET
5323	10-JAN-2014	TM650, TM651, TM652	4 OF 4

NOTE: All material and workmanship shall be in accordance with the current Oregon Standard Specifications

The selection and use of this Standard Drawing, while designed in accordance with generally accepted engineering principles and practices, is the sole responsibility of the user and should not be used without consulting a Registered Professional Engineer.

OREGON STANDARD DRAWINGS

TRAFFIC SIGNAL SUPPORTS FOUNDATION REQUIREMENTS

2015

DATE	REVISION DESCRIPTION

tm653.dgn 11-JUL-2014

TM653

APPENDIX C

DESIGN EXAMPLES

Spreadsheet C. 1 – Brom's Method for Foundation Embedment Length - Cohesionless (Sand)

Date: October 7, 2010

See Section 13.6.1.1 commentary of the 5th Edition AASHTO code

Input:

Moment =	176.51	kip-ft	(Allowable Stress Design)
Shear =	8.8	Kip	(Allowable Stress Design)
Diameter =	3.5	ft	round
Stress Increase Factor =	1.33		Section 13.5.1 ------> Section 3 "Loads"
phi =	30		25 for low side of average soil, 35 for good soil
K_p =	3.690172		Eq. C 13-8 --- Kp = tan^2(45 + phi/2)
Bulk Weight =	110	pcf	Full weight of soil
	☐ In water?		Check Box when in water
Eff_Weight =	125	pcf	This is the weight of soil minus the weight of water
U-C Factor =	0.7		Under-capacity factor
O-F Factor =	2		Overload Factor - 2 used because the loads are well defined.
SF =	2.15		Safety Factor = Overload Factor / under-capacity factor
M_f =	379.18	kip-ft	Factored applied Moment to the shaft at ground level including safety factor
V_f =	18.90	Kip	Factored applied Shear to the shaft at ground level including safety factor
H = M_f / V_f	20.06	ft	Eq. C 13-4
M_{f_max} =	414.12	kip-ft	Factored Maximum Moment in the shaft
Depth_M_{f_max} =	2.81	ft	Depth of Mf_max below the surface

Results:

L^3 - (2 * V_f * L)/(K_p * Eff_Density * D) - (2 * M_f)/(K_p * Eff_Density * D) = 0

	0.00		This value must equal zero
Length =	**10**	**ft**	<======== Calculate

Spreadsheet C. 2– Brom's Method for Foundation Embedment Length - Cohesive (Clay)

October 7, 2010

See Section 13.6.1.1 commentary of the 5th Edition AASHTO code

Input:

Moment =	176.51	kip-ft	(Allowable Stress Design)
Shear =	8.8	Kip	(Allowable Stress Design)
Diameter =	3.5	ft	round
Stress Increase Factor =	1.33		Section 13.5.1 ------> Section 3 "Loads"
c =	1	ksf	
U-C Factor =	0.7		Under-capacity factor
O-F Factor =	2		Overload Factor - 2 used because the loads are well defined.
SF =	2.15		Safety Factor = Overload Factor / under-capacity factor
M_f =	379.18	kip-ft	Factored applied Moment to the shaft at ground level including safety factor
V_f =	18.90	Kip	Factored applied Shear to the shaft at ground level including safety factor
H = M_f / V_f	20.06	ft	Eq. C 13-4
q = V_f / (9*c*D)	0.60014		
M_{f_max} =	484.10	kip-ft	Factored Maximum Moment in the shaft
Depth_M_{f_max} =	5.85014	ft	Depth of Mf_max below the surface

Results:

L = 1.5* D + q * (1 + sqrt(2 + (4*H +6*D)/q)) Eq. C 13-3

Length = **14** **ft**

Appendix C. Evaluation of Torsional Capacity

Appendix C. 1 Drilled shafts in Sand Deposit

(1) FDOT structural Design Office Method

(Rational Method, Hu 2003; Brown et al. 2010)

Drilled shaft and soil Properties

Length of drilled shaft:

$$L := 10\ ft$$

Drilled shaft diameter:

$$D := 42\ in$$

Unit weight of reinforced concrete:

$$\gamma_{shaft} := 150\ pcf$$

Weight of drilled shaft:

$$W := \pi \cdot \frac{D^2}{4} \cdot L \cdot \gamma_{shaft} = 14.4\ kip$$

Friction angle of the sand:

$$\phi := 30\ °$$

Unit weight of the sand:

$$\gamma := 110\ pcf$$

Calculation of Torsional Capacity

Effective vertical stress at middle of this layer:

$$\sigma_v' := \frac{1}{2}\ \gamma \cdot L = 550\ psf$$

Effective friction between soil and shaft:

$$\delta := \phi = 30\ deg$$

Coefficient of lateral earth pressure:

$$K_0 := 1 - \sin(\phi) = 0.5$$

Unit shaft resistance:

$$r_s := \sigma_v' \cdot K_0 \cdot \tan(\delta) = 158.8 \ \textbf{psf}$$

Shaft resistance:

$$T_s := r_s \cdot \pi \cdot \frac{D^2}{2} \cdot L = 30.6 \ \textbf{kip} \cdot \textbf{ft}$$

Toe resistance:

$$T_b := \frac{D}{3} W \cdot \tan(\delta) = 9.7 \ \textbf{kip} \cdot \textbf{ft}$$

Torsional capacity:

$$T := T_s + T_b = 40.3 \ \textbf{kip} \cdot \textbf{ft}$$

(2) Florida District 5 Method

(BETA Method, Brown et al. 2010)

Drilled shaft and soil Properties

Length of drilled shaft:

$$L := 10\ \textbf{ft}$$

Drilled shaft diameter:

$$D := 42\ \textbf{in}$$

Unit weight of reinforced concrete:

$$\gamma_{shaft} := 150\ \textbf{pcf}$$

Weight of drilled shaft:

$$W := \pi \cdot \frac{D^2}{4} \cdot L \cdot \gamma_{shaft} = 14.4\ \textbf{kip}$$

Friction angle of the sand:

$$\phi := 30\ °$$

Unit weight of the sand:

$$\gamma := 110\ \textbf{pcf}$$

STP blow count:

$$N := 10$$

Axial load applied on drilled shafts:

$$Q_a := 4.39\ \textbf{kip} \cdot 2.15 = 9.4\ \textbf{kip}$$

where 2.15 = the safety factor

Calculation of Torsional Capacity

Effective vertical stress at middle of this layer:

$$\sigma_v' := \frac{1}{2}\ \gamma \cdot L = 550\ \textbf{psf}$$

Effective friction between soil and shaft:

$$\delta := \phi = 30 \ \textbf{deg}$$

Load transfer ratio:

$$\beta := \frac{N}{15}\left(1.5 - 0.135 \cdot \sqrt{\frac{L}{2 \cdot \textbf{ft}}}\right) = 0.8$$

Unit shaft resistance:

$$r_s := \sigma_v' \cdot \beta = 439.3 \ \textbf{psf}$$

Shaft resistance:

$$T_s := r_s \cdot \pi \cdot \frac{D^2}{2} \cdot L = 84.5 \ \textbf{kip} \cdot \textbf{ft}$$

Toe resistance:

$$T_b := \frac{D}{3}\left(W + Q_a\right) \cdot \tan(\delta) = 16.1 \ \textbf{kip} \cdot \textbf{ft}$$

Torsional capacity:

$$T := T_s + T_b = 100.6 \ \textbf{kip} \cdot \textbf{ft}$$

(3) Florida District 7 Method

(Rational Method, Brown et al. 2010)

Drilled shaft and soil Properties

Length of drilled shaft:

$$L := 10\ \textbf{ft}$$

Drilled shaft diameter:

$$D := 42\ \textbf{in}$$

Unit weight of reinforced concrete:

$$\gamma_{shaft} := 150\ \textbf{pcf}$$

Weight of drilled shaft:

$$W := \pi \cdot \frac{D^2}{4} \cdot L \cdot \gamma_{shaft} = 14.4\ \textbf{kip}$$

Friction angle of the sand:

$$\phi := 30\ \textbf{°}$$

Unit weight of the sand:

$$\gamma := 110\ \textbf{pcf}$$

Axial load applied on drilled shafts:

$$Q_a := 4.39\ \textbf{kip} \cdot 2.15 = 9.4\ \textbf{kip}$$

Calculation of Torsional Capacity

Effective vertical stress at middle of this layer:

$$\sigma_v' := \frac{1}{2}\ \gamma \cdot L = 550\ \textbf{psf}$$

Effective friction between soil and shaft:

$$\delta := \phi = 30\ \textbf{deg}$$

Coefficient of lateral earth pressure:

$$K_0 := 1 - \sin(\phi) = 0.5$$

Unit shaft resistance:

$$r_s := \sigma_v' \cdot K_0 \cdot \tan(\delta) = 158.8 \ \textbf{psf}$$

Shaft resistance:

$$T_s := r_s \cdot \pi \cdot \frac{D^2}{2} \cdot L = 30.6 \ \textbf{kip} \cdot \textbf{ft}$$

Toe resistance:

$$T_b := \frac{4 \cdot D}{9} \left(W + Q_a\right) \cdot \tan(\delta) = 21.4 \ \textbf{kip} \cdot \textbf{ft}$$

Torsional capacity:

$$T := T_s + T_b = 52 \ \textbf{kip} \cdot \textbf{ft}$$

(4) CDOT Method

(Nusairat et al., 2004)

Drilled shaft and soil Properties

Length of drilled shaft:

$$L := 10\ \textbf{ft}$$

Drilled shaft diameter:

$$D := 42\ \textbf{in}$$

Unit weight of reinforced concrete:

$$\gamma_{shaft} := 150\ \textbf{pcf}$$

Weight of drilled shaft:

$$W := \pi \cdot \frac{D^2}{4} \cdot L \cdot \gamma_{shaft} = 14.4\ \textbf{kip}$$

Friction angle of the sand:

$$\phi := 30\ \textbf{°}$$

Unit weight of the sand:

$$\gamma := 110\ \textbf{pcf}$$

Axial load applied on drilled shafts:

$$Q_a := 4.39\ \textbf{kip} \cdot 2.15 = 9.4\ \textbf{kip}$$

Calculation of Torsional Capacity

Effective vertical stress at middle of this layer:

$$\sigma_v' := \frac{1}{2}\ \gamma \cdot L = 550\ \textbf{psf}$$

Effective friction between soil and shaft:

$$\delta := \phi = 30\ \textbf{deg}$$

Coefficient of lateral earth pressure

$$K := \frac{2\ L}{3\ D} \cdot (1 - \sin(\phi)) = 0.95$$

Unit shaft resistance:

$$r_s := \sigma_v' \cdot K \cdot \tan(\delta) = 302.4\ \textbf{psf}$$

Shaft resistance:

$$T_s := r_s \cdot \pi \cdot \frac{D^2}{2} \cdot L = 58.2\ \textbf{kip} \cdot \textbf{ft}$$

Toe resistance:

$$T_b := \frac{D}{3}\ W \cdot \tan(\delta) = 9.7\ \textbf{kip} \cdot \textbf{ft}$$

Torsional capacity:

$$T := T_s + T_b = 67.9\ \textbf{kip} \cdot \textbf{ft}$$

Appendix C.2. Drilled shafts in Clay Deposit

(1) Florida District 7 Method

(Rational Method, Brown et al. 2010)

Drilled shaft and soil Properties

Length of drilled shaft:

$$L := 14\ \textit{ft}$$

Drilled shaft diameter:

$$D := 42\ \textit{in}$$

Unit weight of reinforced concrete:

$$\gamma_{shaft} := 150\ \textit{pcf}$$

Weight of drilled shaft:

$$W := \pi \cdot \frac{D^2}{4} \cdot L \cdot \gamma_{shaft} = 20.2\ \textit{kip}$$

Undrained shear strength:

$$s_u := 1000\ \textit{psf}$$

Axial load applied on drilled shafts:

$$Q_a := 4.39\ \textit{kip} \cdot 2.15 = 9.4\ \textit{kip}$$

Calculation of Torsional Capacity

Atmospheric pressure:

$$P_a := 2115.7\ \textit{psf}$$

Adhesion factor:

$$\alpha := \begin{cases} 0.55 & \text{if } \frac{s_u}{P_a} \le 1.5 \\ 0.55 - 0.1 \cdot \left(\frac{s_u}{P_a} - 1.5 \right) & \text{else} \end{cases} = 0.55$$

Shaft resistance:

$$T_s := \pi \cdot D \cdot (L - 5\ \mathit{ft}) \cdot \alpha \cdot s_u \cdot \frac{D}{2} = 95.2\ \mathit{kip} \cdot \mathit{ft}$$

Toe resistance:

$$T_b := \frac{\pi \cdot D^3}{12} \cdot \alpha \cdot s_u = 6.2\ \mathit{kip} \cdot \mathit{ft}$$

Torsional capacity:

$$T := T_s + T_b = 101.4\ \mathit{kip} \cdot \mathit{ft}$$

(2) CDOT Method

(Nusairat et al., 2004)

Drilled shaft and soil Properties

Length of drilled shaft:

$$L := 14\ \textbf{ft}$$

Drilled shaft diameter:

$$D := 42\ \textbf{in}$$

Unit weight of reinforced concrete:

$$\gamma_{shaft} := 150\ \textbf{pcf}$$

Weight of drilled shaft:

$$W := \pi \cdot \frac{D^2}{4} \cdot L \cdot \gamma_{shaft} = 20.2\ \textbf{kip}$$

Undrained shear strength:

$$s_u := 1000\ \textbf{psf}$$

Axial load applied on drilled shafts:

$$Q_a := 4.39\ \textbf{kip} \cdot 2.15 = 9.4\ \textbf{kip}$$

Calculation of Torsional Capacity

Shaft resistance:

$$T_s := \pi \cdot D \cdot (L - 1.5\ D) \cdot s_u \cdot \frac{D}{2} = 168.4\ \textbf{kip} \cdot \textbf{ft}$$

Toe resistance:

$$T_b := \frac{\pi \cdot D^3}{12}\ s_u = 11.2\ \textbf{kip} \cdot \textbf{ft}$$

Torsional capacity:

$$T := T_s + T_b = 179.6\ \textbf{kip} \cdot \textbf{ft}$$

Appendix C.3 Drilled shafts in Granular Fill (Sandy Gravel) Over Clay Soil

(1) Florida District 7 Method

(Rational Method, Brown et al. 2010)

Drilled shaft and soil Properties

Length of drilled shaft:

$$L := 12.5\ \textit{ft}$$

Drilled shaft diameter:

$$D := 42\ \textit{in}$$

Unit weight of reinforced concrete:

$$\gamma_{shaft} := 150\ \textit{pcf}$$

Weight of drilled shaft:

$$W := \pi \cdot \frac{D^2}{4} \cdot L \cdot \gamma_{shaft} = 18\ \textit{kip}$$

Friction angle of the first layer (sandy gravel):

$$\phi := 35\ °$$

Unit weight of the sand:

$$\gamma := 125\ \textit{pcf}$$

Undrained shear strength of the second layer (clay):

$$s_u := 1000\ \textit{psf}$$

Axial load applied on drilled shafts:

$$Q_a := 4.39\ \textit{kip} \cdot 2.15 = 9.4\ \textit{kip}$$

where 2.15 = the safety factor

Calculation of Torsional Capacity

First Layer (0~5ft)

Shaft Length in this layer:

$$L_1 := 5\ \textbf{ft}$$

Effective vertical stress at middle of this layer:

$$\sigma_v` := \frac{1}{2}\gamma \cdot L_1 = 312.5\ \textbf{psf}$$

Effective friction between soil and shaft:

$$\delta := \phi = 35\ \textbf{deg}$$

Coefficient of lateral earth pressure:

$$K_0 := 1 - \sin(\phi) = 0.4$$

Unit shaft resistance:

$$r_s := \sigma_v` \cdot K_0 \cdot \tan(\delta) = 93.3\ \textbf{psf}$$

Shaft resistance from this layer:

$$T_{s1} := r_s \cdot \pi \cdot \frac{D^2}{2} \cdot L_1 = 9\ \textbf{kip} \cdot \textbf{ft}$$

Second Layer (5~12.5ft)

Shaft Length in this layer:

$$L_2 := 7.5\ \textbf{ft}$$

Atmospheric pressure:

$$P_a := 2115.7\ \textbf{psf}$$

Adhesion factor:

$$\alpha := \begin{cases} \text{if } \frac{s_u}{P_a} \le 1.5 \\ \quad 0.55 \\ \text{else} \\ \quad 0.55 - 0.1 \cdot \left(\frac{s_u}{P_a} - 1.5 \right) \end{cases} = 0.55$$

Shaft resistance:

$$T_{s2} := \pi \cdot D \cdot L_2 \cdot \alpha \cdot s_u \cdot \frac{D}{2} = 79.4 \ \textbf{kip} \cdot \textbf{ft}$$

Toe resistance:

$$T_b := \frac{\pi \cdot D^3}{12} (\alpha \cdot s_u) = 6.2 \ \textbf{kip} \cdot \textbf{ft}$$

Torsional capacity:

$$T := T_{s1} + T_{s2} + T_b = 94.5 \ \textbf{kip} \cdot \textbf{ft}$$

(2) CDOT Method

(Nusairat et al., 2004)

Drilled shaft and soil Properties

Length of drilled shaft:

$$L := 12.5\ \textit{ft}$$

Drilled shaft diameter:

$$D := 42\ \textit{in}$$

Unit weight of reinforced concrete:

$$\gamma_{shaft} := 150\ \textit{pcf}$$

Weight of drilled shaft:

$$W := \pi \cdot \frac{D^2}{4} \cdot L \cdot \gamma_{shaft} = 18\ \textit{kip}$$

Friction angle of the first layer (sandy gravel):

$$\phi := 35\ °$$

Unit weight of the sand:

$$\gamma := 125\ \textit{pcf}$$

Undrained shear strength of the second layer (clay):

$$s_u := 1000\ \textit{psf}$$

Axial load applied on drilled shafts:

$$Q_a := 4.39\ \textit{kip} \cdot 2.15 = 9.4\ \textit{kip}$$

where 2.15 = the safety factor

Calculation of Torsional Capacity

First Layer (0~5ft)

Shaft Length in this layer:

$$L_1 := 5\ \textbf{ft}$$

Effective vertical stress at middle of this layer:

$$\sigma_v` := \frac{1}{2}\gamma \cdot L_1 = 312.5\ \textbf{psf}$$

Effective friction between soil and shaft:

$$\delta := \phi = 35\ \textbf{deg}$$

Coefficient of lateral earth pressure:

$$K := \frac{2\ L}{3\ D} \cdot (1 - \sin(\phi)) = 1.02$$

Unit shaft resistance:

$$r_s := \sigma_v` \cdot K \cdot \tan(\delta) = 222.2\ \textbf{psf}$$

Shaft resistance from this layer:

$$T_{s1} := r_s \cdot \pi \cdot \frac{D^2}{2} \cdot L_1 = 21.4\ \textbf{kip} \cdot \textbf{ft}$$

Second Layer (5~12.5ft)

Shaft Length in this layer:

$$L_2 := 7.5\ \textbf{ft}$$

Shaft resistance:

$$T_{s2} := \pi \cdot D \cdot L_2 \cdot s_u \cdot \frac{D}{2} = 144.3\ \textbf{kip} \cdot \textbf{ft}$$

Toe resistance:

$$T_b := \frac{\pi \cdot D^3}{12} s_u = 11.2 \ \textbf{kip} \cdot \textbf{ft}$$

Torsional capacity:

$$T := T_{s1} + T_{s2} + T_b = 176.9 \ \textbf{kip} \cdot \textbf{ft}$$